ÉCOLE DE TECHNOLOGIE SUPÉRIEURE
UNIVERSITÉ DU QUÉBEC

THÈSE PAR ARTICLES PRÉSENTÉE À
L'ÉCOLE DE TECHNOLOGIE SUPÉRIEURE

COMME EXIGENCE PARTIELLE
À L'OBTENTION DU
DOCTORAT EN GÉNIE
Ph.D.

PAR
KECHROUD, Riyad

UNE MÉTHODE DE COUPLAGE ÉLÉMENTS FINIS- CONDITIONS ABSORBANTES DE TYPE-PADÉ POUR LES PROBLÈMES DE DIFFRACTION ACOUSTIQUE

MONTRÉAL, LE 16 JANVIER 2008

CETTE THÈSE A ÉTÉ ÉVALUÉE

PAR UN JURY COMPOSÉ DE :

Professeur, Azzeddine Soulaïmani, directeur de thèse
Département de génie mécanique à École de technologie supérieure

Professeur, Ammar B. Kouki, président du jury
Département de génie électrique à École de technologie supérieure

Professeur, Marius Paraschivoiu, examinateur externe
Département de génie mécanique à l'Université Concordia

Professeur, Frédéric Laville, examinateur
Département de génie mécanique à École de technologie supérieure

ELLE A FAIT L'OBJET D'UNE SOUTENANCE DEVANT JURY ET PUBLIC

LE 7 JANVIER 2008

À L'ÉCOLE DE TECHNOLOGIE SUPÉRIEURE

UNE MÉTHODE DE COUPLAGE ÉLÉMENTS FINIS- CONDITIONS ABSORBANTES DE TYPE-PADÉ POUR LES PROBLÈMES DE DIFFRACTION ACOUSTIQUE

KECHROUD, Riyad

SOMMAIRE

Nous nous intéressons aux problèmes harmoniques de diffraction acoustique en milieu infini régis par l'équation de Helmholtz. La simulation numérique de ces phénomènes est complexe notamment lorsqu'il est question de fréquences élevées et d'obstacles de forme allongée tel qu'un sous-marin. Les codes éléments finis commerciaux sont incapables de cerner tous les aspects liés à ce type de problèmes. De plus, ce genre d'applications fait appel à de grandes ressources de calcul. En effet, la taille du système d'équations à résoudre (plusieurs millions de ddl) engendre souvent l'épuisement des ressources des calculateurs traditionnels.

Notre objectif est de solutionner ce type de problèmes avec une précision pratique en utilisant le minimum de ressources. Nous proposons ainsi une méthode de couplage éléments finis de type Lagrange et à base d'ondes planes avec les conditions absorbantes d'ordre élevé basées sur les approximants complexes de Padé. A travers une série d'expériences numériques, nous montrons l'efficacité de ces conditions absorbantes en comparaison avec les conditions absorbantes de Bayliss-Gunzburger-Turkel d'ordre deux implémentées dans les codes commerciaux. La méthodologie proposée permet non seulement une réduction de la taille du domaine de calcul sans dégradation de la précision mais conduit également à la résolution de systèmes d'équations de taille relativement réduite.

A FINITE ELEMENT METHOD COUPLED TO A HIGHER ORDER PADÉ-TYPE ABSORBING BOUNDARY CONDITIONS FOR ACOUSTIC SCATTTERING PROBLEM

KECHROUD, Riyad

ABSTRACT

We address problems of acoustic diffraction in infinite medium governed in the harmonic regime by the Helmholtz equation. The simulation of these phenomena is complex especially when it involves higher frequency and elongated scatterers such as a submarine. The finite element commercial codes are unable to deal with all the aspects related to this kind of problems. Moreover, this kind of applications requires a huge amount of computational resources. Indeed, the size of the system of equations to be solved (several million ddl) often overwhelm the resources of the most available calculators.

Our goal is to solve this kind of problems with an engineering accuracy using the minimum of resources. We thus propose a method coupling plane wave and Lagrange finite elements with higher order Padé-type absorbing boundary conditions. Through a series of numerical experiments, we show the effectiveness of these absorbing conditions in comparison with the second order Bayliss-Gunzburger-Turkel absorbing boundary conditions implemented in the commercial codes. This methodology allows us not only to reduce the size of the computational domain without degrading the precision but also lead us to the solution of systems of reduced size.

REMERCIEMENTS

Je remercie toutes les personnes de prés ou de loin qui m'ont aidé à l'aboutissement de cette thèse.

Je voudrais exprimer ma gratitude au Professeur Azzeddine Soulaïmani pour m'avoir proposé ce thème de recherche et d'en avoir assumé la direction. Ses conseils éclairés m'ont permis de progresser mais surtout d'apprendre, merci pour la patience et pour le support inconditionnel.

Je voudrais également remercier le Professeur Ammar B. Kouki, pour avoir accepté d'être président de ce jury de thèse, et les Professeurs Marius Paraschivoiu et Frédéric Laville pour avoir accepté d'évaluer ce travail.

Je tiens aussi à remercier les Professeurs Youssef Saad et Xavier Antoine pour la collaboration fructueuse que nous avons eu.

Je tiens également à remercier tous les membres du groupe GRANIT, où j'ai trouvé un environnement humain idéal pour la recherche. Que mes amis et collègues Amine Benhaj Ali, Riadh Ata, Youcef Bouchera, Youcef Loukili, Nizar El-Houssaïni, Jack Feng, Simon Nicolas Roth, Adile et Jean-Marie trouvent ici l'expression de ma gratitude.

Je ne saurais oublier l'appui inconditionnel de toute ma famille. Je voudrais remercier en particulier ma conjointe Nassima et ma petite fille Aya. Je vous dédie ce travail.

Je voudrais reconnaître l'appui financier de mon directeur de thèse et celui de l'École de Technologie Supérieure.

TABLE DES MATIÈRES

Page

LISTE DES TABLEAUX

Page

LISTE DES FIGURES

Page

LISTE DES ABRÉVIATIONS ET SIGLES

a	Forme bilinaire symétrique définie sur $H_1(\Omega) \times H_1(\Omega)$
a_{GLS}	Forme bilinaire et symétrique associée à la méthode GLS et définie sur $H_1(\Omega) \times H_1(\Omega)$
b	Forme linéaire définie sur $L_2(\Omega)$
b_{GLS}	Forme linéaire associée à la méthode GLS
d	Dimension de l'espace (d=1,2 ou 3)
k	Nombre d'onde
u	Champ de pression diffracté
u_{inc}	Champ de pression incident
h	Pas du maillage
n_λ	Nombre d'éléments par longueur d'onde
$\mathcal{A}$	forme variationnelle symétrique définie sur $H^1(\Omega) \times H^1(\Omega)$
$\mathcal{B}_j$	est une forme variationnelle symétrique définie sur $H^1(\Sigma) \times H^1(\Sigma)$
$\mathcal{C}$	est une forme variationnelle symétrique définie sur $H^1(\Sigma) \times H^1(\Sigma)$
$\mathcal{D}$	est une forme variationnelle symétrique définie sur $H^1(\Sigma) \times H^1(\Sigma)$
$\mathcal{A}_{\text{GLS}}$	forme variationnelle associée à la méthode GLS
$\mathbf{d}$	Vecteur unitaire de direction du champ incident
$\mathbf{n}_\Gamma$	Vecteur unitaire normale sortant de Ω^- à la frontière Γ
$[A]$	Matrice carrée bande, symmetrique, non hermitienne, à coefficients et à diagonale non dominante
$H^1(\Omega)$	Espace de Sobolev définie sur Ω
$H^1(\Sigma)$	Espace de Sobolev définie sur Σ
ILU	Factorisation incomplète LU

$ILUC$	Factorisation incomplète LU du type Crout
$[K_e]$	Matrice rigidité élémentaire
$[L]$	Matrice triangulaire inférieure
$[M]$	Matrice carrée de préconditionnement
$[M_e]$	Matrice masse élémentaire
$[U]$	Matrice triangulaire supérieure
DtN	Opérateur pseudodifférentiel (Dirichlet to Neumann), relation reliant l'inconnue physique à sa dérivée normale
$\mathcal{H}$	Opérateur différentiel de Helmholtz $\Delta + k^2$
M_i	Opérateur différentiel d'ordre i approximant l'opérateur DtN
Δ	Opérateur de Laplace
Δ_Σ	Opérateur différentiel de Laplace-Beltrami
Γ	Frontière externe de l'obstacle
Γ_{art}	Frontière artificielle
κ	Courbure en un noeud donnée
λ	longueur d'onde
Ω_e	Domaine extérieur
Ω^{ext}	Domaine extérieure associée à Ω^-
Ω^-	Obstacle de frontière Γ
Σ	Frontière artificielle
τ	Paramètre de la méthode Galerkin-Moindres Carrés (GLS)
BGT-2	Conditions aux limites absorbantes de Bayliss-Gunzburger-Turkel du second ordre
NRBC	Conditions aux limites non-réfléchissantes (Non- Reflecting Boundary Conditions)

INTRODUCTION GÉNÉRALE

La modélisation numérique des problèmes d'ondes demeure un domaine où la recherche est très active depuis près d'un demi-siècle. Cette activité est poussée en partie par l'importance des applications telles que le sonar, le radar, l'exploration géophysique, l'imagerie médicale, les tests non-destructifs et récemment la météorologie. En dépit des progrès réalisés, ce domaine de recherche est toujours considéré comme un des plus difficiles en calcul scientifique notamment lorsqu'il est question d'ondes courtes.

Nous nous intéressons dans ce travail à la résolution des problèmes harmoniques de diffraction acoustique en milieu infini, régis par l'équation de Helmholtz (ou équation réduite des ondes), avec une condition de radiation à l'infini dite condition de Sommerfeld, par la méthode des éléments finis (MEF). Nous considérons les problèmes directs liés aux applications du type sonar où une onde de pression incidente (harmonique) rentre en interaction avec un obstacle donné donnant ainsi naissance à un champ de pression diffracté caractérisé en champ lointain par la section équivalente (ou image) sonar (ou radar) (radar cross section, RCS).

Les premières applications de la technologie MEF se sont concentrées sur les problèmes dits intérieurs (Thompson,2006) où les structures mécaniques ayant une géométrie complexe sont couplées de façon directe avec des cavités acoustiques afin soit d'analyser la réponse fréquentielle de telles structures lorsqu'elle sont soumises à des vibrations forcées ou afin d'effectuer une analyse modale pour déterminer les modes résonants.

Toutefois, les énormes progrès réalisés ces dernières années dans le développement de la technologie éléments finis a permis d'étendre ses applications aux problèmes dits extérieurs où le domaine d'étude est non-borné. De nombreux travaux démontrant les potentialités de la MEF sont publiés régulièrement qu'ils s'agissent de problèmes dits directs (Djellouli et *al.*,2000; Tezaur et *al.*,2002; Farhat and Hetmaniuk,2002) ou inverses (Farhat et *al.*,2002). Des méthodes MEF d'analyse par bandes de fréquences sont éga-

lement proposées (Djellouli et *al.*,2001).

Revue de la littérature et position du problème

La résolution des problèmes extérieurs hautes fréquences demeure un défi pour la MEF standard (Zienkiewicz,2000). En effet, cette méthode exige des ressources de calcul considérables afin de solutionner de tels problèmes notamment lorsqu'il est question d'ondes courtes. A titre d'exemple, résoudre un problème de diffraction acoustique tridimensionnel (Tezaur et *al.*,2000) en utilisant des éléments finis quadratiques conduit à la résolution d'un système d'équations à nombres complexes ayant une dizaine de millions d'inconnues pour un nombre d'onde adimensionnel kD=10 où k est le nombre d'onde et D une dimension caractéristique du sous-marin. Les applications industrielles et militaires reliées au sonar requièrent la résolution de tels problèmes pour kD beaucoup plus important avoisinant 200 (Gillman,2006). Ceci indique clairement que la méthode des éléments finis standard est incapable d'adresser des problèmes dans la gamme des moyennes et hautes fréquences.

Ainsi, les recherches se sont orientées notamment vers l'amélioration de la technologie éléments finis par entre-autres l'incorporation du comportement ondulatoire de la solution (autrement dit de la nature physique du problème) de ce type de problèmes dans la base d'approximation locale combinée à une décomposition de domaine et une résolution itérative parallèle. Ces améliorations devront permettre d'étendre ses applications à des fréquences encore plus élevées.

Habituellement, pour les moyennes et hautes fréquences, ce sont les méthodes analytiques ou numériques telles que méthodes asymptotiques (Molinet et *al.*,2005), la méthode des conditions de radiation sur le bord (On surface radiation condition, OSRC) (Antoine et al.,1999 ; Antoine et al.,2006) et la méthode des équations intégrales de frontière (Burton and Miller,1971 ; Colton and Kress,1983 ; Nédélec,2001) qui sont traditionnellement uti-

lisées. Les méthodes analytiques restent limitées aux obstacles de formes géométriques simples alors que les méthodes asymptotiques ne sont pas précises dans le cas où la longueur d'onde en question est du même ordre de grandeur que les dimensions caractérisant l'obstacle. La méthode des conditions de radiation sur le bord bien que rapide par rapport à la méthode des équations intégrales de frontière reste malheureusement dépendante de la forme géométrique de l'obstacle qui doit être convexe.

Harari et Hughes (Harari and Hughes,1992) montrent que la méthode des éléments finis est compétitive avec la méthode des équations intégrales de frontière standard. En effet, contrairement à la méthode des éléments finis, cette technique est limitée aux problèmes linéaires, isotropes et homogènes. La présence de fréquences de résonances parasites (qui n'ont pas d'origine physique) reliées au problème intérieur associé forcent l'adoption de formulations intégrales, souvent complexes, alternatives telles que celles de Burton-Miller (Burton and Miller,1971) et la méthode CHIEF (Combined Helmholtz Integral Equation Formulation) de (Schenck,1968). Ne nécessitant que la discrétisation des surfaces en 3D, elle conduit, cependant, à des systèmes d'équations denses exigeant ainsi un espace mémoire considérable lorsqu'il s'agit de problèmes 3D où les fréquences en jeu sont relativement élevées. Ces systèmes sont de plus mal-conditionnés compliquant leur résolution par des méthodes de résolution itératives et augmentant ainsi les temps de calcul. Toutefois, cette compétitivité éléments finis- méthode intégrale devient moins évidente lorsque cette dernière est associée à la méthode rapide des multipôles (Fast Multipole Method, FMM) (Chew et *al.*,2001; Darve,2000) et à des solveurs rapides (Darve,2000; Rokhlin,1990; Bruno,2004)

Problématique liée au domaine non-borné

Contrairement à la méthode des équations intégrales de frontière, les méthodes d'approximation par sous domaines telles que la méthode des éléments finis (Zienkiewicz,2000) ou des différences finies (MDF) (Harari and Turkel,1992) sont conçues pour des applications

où les domaines de calcul sont bornés. Cependant, la nature non-bornée des domaines de calcul du problème extérieur de Helmholtz, due à l'imposition d'une condition de radiation à l'infini (condition de Sommerfeld) assurant l'unicité de la solution, pose un autre défi à ces méthodes.

L'application de la MEF ou la MDF nécessite avant tout la définition d'un domaine de calcul borné. Cette opération est réalisée pratiquement en entourant l'obstacle par une frontière artificielle positionnée à une distance, généralement mesurée en multiple de la longueur d'onde correspondant à la fréquence en question (Mittra et *al.*,1989), de la surface extérieure de l'obstacle.

Le comportement de la solution dans le domaine complémentaire est alors représenté par des conditions aux limites imposées sur la frontière artificielle ou par une interpolation spécifique. La première approche est associée aux conditions non-réfléchissantes ou absorbantes (Givoli,1999; Givoli,2004) alors que la seconde est associée aux éléments infinis (Astley,2000; Gerdes,2000). Pour ces éléments, la précision dépend entre autres du choix des fonctions d'interpolation, leur ordre dans la direction radiale et du choix de la formulation variationnelle adoptée (conjuguée ou non). Dans ces deux approches, l'idée est de minimiser les réflexions parasites dues à l'introduction de la frontière artificielle.

Une alternative consiste à remplacer la frontière artificielle par une couche parfaitement adaptée (Bérenger,1994)(ou Perfectly Matched Layer, PML) conçue pour amortir toutes les ondes qui y pénètrent. Dans ce cas, la taille du domaine de calcul est élargie par celle de cette couche. L'épaisseur de cette couche peut rapidement accroître l'espace mémoire et les temps de calcul en 3D (Turkel,2007). Cette technique, facile à implémenter dans un code élément fini, semble bien fonctionner en coordonnées cartésiennes et favorise ainsi les couches rectangulaires. Toutefois, la précision des résultats reste sensible à l'amortissement (fictif) caractérisant cette couche. De plus, Il n'existe pas à notre connaissance de

règle générale permettant, pour une fréquence donnée, de spécifier la valeur de cet amortissement et l'épaisseur adéquate de cette couche (Turkel,2007; Turkel,1998).

Dans toutes ces approches (conditions absorbantes, éléments infinis et couche parfaitement adaptée), le problème aux limites reste bien posé au sens de Hadamard et admet ainsi une solution unique.

Conditions absorbantes non-locales

Les conditions absorbantes peuvent être non-locales comme c'est le cas de la technique Dirichlet à Neumann (Dirichlet to Neumann, DtN) introduite par Keller et Givoli (Keller and Givoli,1989). Cette technique permet grâce à une expansion en série de Fourier de l'opérateur DtN (opérateur qui relie l'inconnue physique et sa dérivée normale) d'imposer des conditions dites transparentes (sans réflexions) sur des frontières artificielles de formes simples telles qu'un cercle et une ellipse en 2D ou une sphère et une ellipsoïde en 3D (Thompson et *al.*,2000). Dans l'implémentation de cette technique, la série de Fourier est tronquée à un ordre m tel que m soit supérieur à kR où R le rayon de la frontière artificielle sans pour autant introduire des fréquences de résonance parasites dans la solution éléments finis (Harari,1991). L'ordre m peut devenir rapidement trop élevé s'il s'agit de fréquences élevées et/ou de structures allongées.

L'emploi de cette technique conduit à une sous-matrice symétrique mais pleine étant donné que tous les degrés de liberté sur la frontière artificielle sont tous liés entre eux via la condition aux limites DtN. Son stockage peut devenir très vite problématique en 3D lorsque les fréquences en jeu sont élevées. De plus, son utilisation pratique se limite aux frontières de formes circulaire et sphérique, ce qui conduit à de grands domaines de calcul (en termes de longueurs d'onde) lorsqu'il s'agit de problèmes de diffraction mettant en jeu des obstacles de forme allongée. L'implémentation de cette technique dans un solveur

itératif parallèle est démontrée dans la référence (Thompson et *al.*,2000).

Conditions absorbantes locales

Alternativement, des conditions locales préservant la structure bande et la symétrie des matrices EF peuvent être construites comme des approximations de l'opérateur DtN (Givoli,2004 ; Turkel,2007 ; Tsynkov,1998). Antoine, Barucq et Bendali (Antoine et *al.*,1999) présentent une procédure générale et rigoureuse d'approximation de l'opérateur DtN, basée sur la théorie des opérateurs pseudodifférentiels, dans le cadre de la méthode des conditions de radiation sur le bord (On surface radiation conditions, OSRC). Cette procédure permet de construire des conditions absorbantes d'ordre élevé et donc plus précises. En particulier, elle permet non seulement de retrouver entre-autres les conditions absorbantes développées par Enquist et Majda (Engquist and Majda,1977), Bayliss et Turkel (Bayliss and Turkel,1980) et Bayliss, Gunzburger et Turkel (Bayliss et *al.*,1982) pour les frontières circulaires et sphériques mais également de généraliser leurs applications à des frontières artificielles de formes générales convexes. Les conditions absorbantes d'ordre supérieur à deux sont rarement utilisées dans la pratique à cause des difficultés liées à leur implémentation avec des éléments finis linéaires et quadratiques par d'exemple.

Une étude de comparaison de la précision conditions absorbantes *versus* éléments infinis a été menée par (Shirron and Babuška,1998) dans le cas du problème de diffraction de la sphère. Celle-ci montre que la précision des résultats obtenus avec les éléments infinis est supérieure à celle avec les conditions absorbantes de Bayliss-Gunzburger-Turkel pour un nombre d'onde adimensionnel égal à kR=10. L'inverse est constatée pour kR=1. Toutefois, les systèmes d'équations obtenus en utilisant les éléments infinis sont moins bien conditionnés que ceux avec les conditions absorbantes.

Une alternative prometteuse concernant les conditions absorbantes locales consiste à utiliser des fonctions auxiliaires pour implémenter les conditions absorbantes d'ordre élevé

dans les codes éléments finis (Givoli,2004) et obtenir ainsi des conditions plus précises dont l'ordre peut être augmenté à volonté.

Problématique liée au problème de pollution numérique de la MEF

La résolution de l'équation de Helmholtz par la méthode des éléments finis soulève une autre problématique liée à la perte du caractère elliptique de cette équation et sa solution fortement oscillante lorsque le nombre d'onde k augmente (Harari,1991). Ainsi, une dégradation rapide de la précision des résultats éléments finis est constatée à mesure que le nombre d'onde augmente et ce même si le nombre d'éléments par longueur d'onde est gardé constant (la règle heuristique de dix éléments finis linéaires par longueur d'onde s'avère dans la pratique insuffisante) à l'opposé de la méthode intégrale de frontière (Gerdes,2000). Outre donc l'erreur de discrétisation, il existe une autre erreur désignée dans la référence (Ihlenburg and Babuška,1995) par l'erreur de pollution.

Il est possible de quantifier cette erreur soit par une analyse d'erreur ou de dispersion où l'on montre que le nombre d'onde du système discret k^h diffère du nombre d'onde k du système continu. Ceci se traduit par un retard (un déphasage) entre la solution numérique et la solution exacte. Ihlenburg et Babuška (Ihlenburg and Babuška,1997) ont montré, pour un problème monodimensionnel que l'erreur relative e de la solution éléments finis hp au sens la semi-norme H_1 satisfait pour un kh suffisamment petit : $e \leq C_1(k\mathrm{h}/(2p))^p + C_2(k\mathrm{h}/(2p))^{2p}kL$ avec C_1 et C_2 des constantes indépendantes de k, L désigne la taille du domaine, h le pas de discrétisation et p l'ordre du polynôme. Le terme $C_1(k\mathrm{h}/(2p))^p$ représente l'erreur d'approximation qui peut être contrôlée en maintenant le produit kh constant pour un p donné. Le deuxième terme $C_2(k\mathrm{h}/(2p))^{2p}kL$ est lié à la pollution. Pour des nombres d'onde adimensionnels kL élevés, l'erreur due à la pollution devient prépondérante et affecte la précision des schémas éléments finis hp standards. Il est clair aussi qu'on peut contrôler l'effet de pollution soit en utilisant un maillage très fin (kh très petit donc des systèmes d'équations très grands) pour un p fixe, ou au contraire en

augmentant p (éléments finis d'ordre élevé) tout en maintenant la résolution du maillage fixe.

Pour les problèmes bidimensionnels et tridimensionnels, la taille du domaine de calcul mesurée en termes de longueur d'onde est dans la pratique importante à cause des contraintes imposées par les conditions absorbantes lorsque les fréquences en jeu sont élevées. En effet, celles-ci sont plus précises lorsqu'elles sont placées suffisamment loin de l'obstacle. La réduction du problème de la pollution numérique implicitement par la réduction de la taille du domaine est donc limitée par cette contrainte. Les remèdes au phénomène de pollution ou de dispersion se sont donc orientés vers la minimisation explicite.

Différentes méthodes ont été développées afin de contrer le phénomène de pollution et stabiliser la méthode de Galerkin; citons à titre d'exemple : les éléments finis hp (Ihlenburg and Babuška,1997), les éléments finis spectraux (Karniadakis and Sherwin,1999 ; Gary,2002 ; Mehdizadeh and Paraschivoiu,2003), la méthode des éléments finis généralisés (Ilhenburg,1998) (generalized finite element method, GFEM) où l'on retrouve entreautres la méthode Galerkin-Moindes carrés (Galerkin least- squares, GLS)(Harari,1991) et la méthode des éléments finis quasi-stabilisés (quasi-stabilized finite element)(Babuška and Sauter,1997)

Dans les revues de littérature récentes de Thompson (Thompson,2006) et de Harari (Harari,2006), sont citées d'autres méthodes de stabilisation telles que la méthode PUFEM (the partition of unity finite element), la méthode RFB (residual free bubble), la méthode de Galerkin discontinue et enrichie (the discontinuous enrichment methods, DEM), la méthode de Galerkin discontinue (the discontinuous Galerkin method, DGM), la méthode de l'élément faible (weak element method), la méthode variationnelle ultra-faible (ultra weak variational formulation, UWVF) ou récemment la méthode des éléments finis oscillants (Gillman et *al.*,2007; Gillman,2006) (Oscillated FEM).

Plusieurs de ces techniques peuvent être regroupées dans le cadre plus générale de l'analyse variationnelle multi-échelle (variational multiscale, VMS) (Thompson,2006) . D'autres comme les méthodes PUFEM et DGM incluent le comportement ondulatoire de la solution dans l'approximation locale (au niveau élémentaire) par le biais d'ondes planes ayant des directions spécifiques. Ces méthodes peuvent être regroupées sous le thème des éléments finis avec ondes planes (plane wave finite element, PWFEM).

Problématique liée à la résolution directe et itérative du système discret de Helmholtz

Un autre domaine où la recherche demeure active est celui de la résolution du système d'équations de Helmholtz issu d'une discrétisation par la méthode des éléments finis. En effet, bien que ce système à coefficients complexes, soit linéaire, creux et symétrique (dans le cas où la formulation variationnnelle adoptée est bilinéaire), il est non-Hermitien, à diagonale non-dominante, indéfini et peut être de grande taille.

Les applications pratiques conduisent souvent à plusieurs millions d'inconnues (même en 2D). Les méthodes directes de résolution telles que la méthode d'élimination de Gauss ou la factorisation LU , bien que robustes en comparaison avec les méthodes itératives, peuvent devenir excessivement chères en termes de mémoire et temps de calcul dès qu'il s'agit de problèmes tridimensionnels où les fréquences en jeu sont élevées. Généralement, la résolution itérative se fait dans l'ensemble des nombres complexes. En effet, la résolution dans l'ensemble des nombres réels bien que possible (Mehdizadeh et Paraschivoiu,2003), le conditionnement du système à résoudre est mauvais en comparaison avec celui du système original (Zebic,1992). Dans la pratique, les méthodes itératives de résolution utilisées sont celles dites de projection dans l'espace de Krylov (Saad,1996) telles que GMRES (generalized minimal residual method)(Kechroud et *al.*,2004), BiCG-Stab (stabilized biconjugate gradient method) (Thompson,2006), et QMR (quasi-minimal residual method) (Thompson et *al.*,2000). Le choix d'un solveur dépend du problème traité

(Thompson,2006) du moment qu'il n'existe pas de solveur itératif universel pour ce type de problèmes.

Pour accélérer la convergence, ces solveurs sont munis soit de préconditionneurs spécialisés dits préconditionneurs analytiques (Gander and Nataf,2001) ou de préconditionneurs algébriques standards à usage général (Kechroud et *al.*,2004). Ces derniers sont basés sur les méthodes directes du type factorisation LU, tels que ILUT (décomposition incomplète LU avec seuil) (Saad,1994) , ILU0 ou ILUTC (ILU version Crout) (Li et *al.*,2002) ou de préconditionneurs modifiés (perturbés) (Mardochée,2001) où avant la factorisation incomplète de Cholesky, la partie réelle de la matrice de préconditionnement est modifiée de façon à la rendre moins indéfinie ou définie positive ce qui permet d'accélérer la convergence de GMRES. Une autre technique similaire à cette dernière baptisée *shifted Laplace Preconditioners* (Erlangga et *al.*,2004) consiste à construire le préconditionneur à partir d'un opérateur de Helmholtz modifié en considérant un nombre d'onde complexe.

D'autres techniques de résolutions sont basées sur la méthode de décomposition de domaine (domain decomposition method, DDM), technique qui favorise le traitement parallèle, avec toutefois la nécessité de stabiliser les problèmes posés dans les sous-domaines. Le solveur FETI-H (Djellouli et *al.*,2000; Tezaur et *al.*,2000) en est un exemple. Il y a lieu aussi de citer également les méthodes de résolution basées sur les transformations rapides de Fourier (Elman and O'Leary,1998) et la méthode des domaines fictifs (fictitious domain method,FDM) (Farhat and Hetmaniuk,2002; Hetmaniuk and Farhat,2003).

Objectifs de la thèse

Nous nous proposons dans cette thèse de solutionner les problèmes de diffraction acoustique hautes fréquences en milieu non-borné. Notre objectif principal est de développer une méthodologie simple et efficace de résolution itérative de ces problèmes basée sur une méthode de couplage éléments finis (de Lagrange, GLS, et à base d'ondes planes)

-conditions absorbantes généralisées d'ordre élevé basées sur les approximants complexes de Padé. Notre but est d'atteindre des résultats probants aussi bien en champ proche qu'en champ lointain en particulier lors du calcul de la surface équivalente radar ou sonar,(radar cross section, RCS)) qui a un intérêt pratique.

Nos objectifs spécifiques sont dans un premier temps la réduction, pour une précision pratique, de la taille du domaine de calcul et des temps de résolution en comparaison avec des méthodologies éléments finis utilisant les conditions généralisées de Bayliss-Gunzburger-Turkel du second ordre, ce qui permet de solutionner des problèmes de fréquences plus élevées pour des ressources de calcul données.

Dans un deuxième temps, notre objectif est une diminution significative de la taille des systèmes d'équations à résoudre par une réduction explicite du phénomène de pollution ceci dans le but d'utiliser des solveurs directs.

Plan de la thèse

La présente thèse s'articule autour de trois chapitres qui ont fait l'objet de publications parues (chapitres 1 et 2) et une soumise (chapitre 3). Trois problématiques sont abordées dans ces chapitres à savoir :

a. La résolution itérative du système discret de Helmholtz par une méthode de projection dans l'espace de Krylov préconditionnée par des préconditionneurs algébriques ;

b. Les conditions absorbantes locales généralisées d'ordre élevées ;

c. Les moyens implicite et explicite pour réduire la pollution ou dispersion numérique dans les schémas MEF.

Ainsi au chapitre 1, après une revue de littérature portant sur les conditions absorbantes, nous présentons la discrétisation par la méthode des éléments finis linéaires (schémas de Galerkin et Galerkin-moindres carrés, GLS) du problème de Helmholtz extérieur en 2D et 3D reformulé dans un domaine borné à l'aide des conditions absorbantes de Bayliss-Gunzburger-Turkel d'ordre deux.

Nous développons en particulier une méthode originale de calcul du paramètre τ associé à la méthode GLS. Nous étudions par la suite les performances d'une résolution itérative du système d'équations de Helmholtz par la méthode de projection GMRES avec initialisation munie de trois préconditionneurs ILUT, ILUTC et ILU0 afin d'en accélérer la convergence. Une comparaison de la précision des schémas de Galerkin et Galerkin moindres carrés est également effectuée.

Au chapitre 2, nous substituons la condition de Bayliss-Gunzburger-Turkel d'ordre 2 par une condition absorbante d'ordre élevé, mieux adaptée aux hautes fréquences, basée sur les approximants complexes de Padé. Le processus de construction de ces conditions à partir de l'opérateur DtN est développé. Nous associons ces conditions absorbantes aux schémas éléments finis linéaires de Galerkin et Galerkin-moindres carrés pour résoudre itérativement à l'aide du solveur ILUT-GMRES des problèmes 2D de diffraction acoustique hautes fréquences. Nous analysons les performances de cette technique de couplage par rapport à celle utilisant les conditions généralisées de Bayliss-Gunzburger-Turkel d'ordre deux pour différentes formes d'obstacle en particulier le cas où celui-ci est un sous-marin. La solution de ce type problème d'ondes courtes par la MEF nécessite habituellement la résolution d'un système d'équations de plusieurs millions d'inconnus. L'objectif est la réduction de la taille du domaine de calcul (et donc implicitement la pollution numérique) et les temps de calcul. Des comparaisons entre la précision des éléments finis linéaires et stabilisés par la technique GLS est menée.

Dans le chapitre 3, nous couplons les conditions absorbantes de Padé, développées dans le chapitre 2, avec des éléments finis quadratiques et des éléments finis quadratiques à base d'ondes planes afin de réduire explicitement le problème de pollution. L'objectif étant cette fois non-seulement la réduction de la taille du domaine de calcul mais également celle du système d'équations de façon à pouvoir le résoudre de manière directe. Ainsi, des problèmes mettant en jeu des fréquences plus élevées que ceux du chapitre deux sont traitées.

Une comparaison éléments finis quadratiques et ceux à base d'ondes planes permet de mettre en évidence outre la convergence hp, la convergence suivant le nombre d'ondes planes par nœud.

Nous terminons cette thèse par une conclusion générale et des recommandations futures.

Nous détaillons dans les annexes quelques aspects de mise en oeuvre des techniques proposées. Ainsi, dans l'annexe A, nous développons la méthodologie proposée dans le cas 3D. Les résultats relatifs à un obstacle sphérique y sont présentés. Dans l'annexe B, la procédure utilisée pour calculer les poids et les coordonnées des points utilisés lors de l'intégration numérique d'ordre supérieur est détaillée. Enfin, dans l'annexe B, nous présentons de façon succincte le principe de la construction d'un préconditionneur déflaté.

CHAPITRE 1

PRECONDITIONING TECHNIQUES FOR THE SOLUTION OF THE HELMHOLTZ EQUATION BY THE FINITE ELEMENT METHOD

Riyad Kechroud [a], Azzeddine Soulaïmani [a], Yousef Saad [b], Shivaraju Gowdab

[a] Département de Genie Mecanique,École de Technologie Superieure,

1100 Notre-Dame Ouest, Montréal,Québec,Canada H3C 1K3

[b] Department of Computer Science and Engineering, University of Minnesota,

4-192 EE/CS Building, 200 Union Street S.E., Minneapolis, MN 55455, USA

This chapter is published as an article in Mathematics and Computers in Simulation vol.65(2004) pp. 303–321.

In the harmonic regime most diffraction phenomena are governed by the Helmholtz equation. Propagation/scattering problems are often defined over open (non-bounded) domains and are, as a result, solved by the boundary element method. In this case only the external surface is discretized. This leads to systems of equations of relatively small dimensions which are, however, dense. For 3-D problems in which relatively high frequencies come into play, the required memory and computational resources can quickly exceed those afforded by available workstations. For these reasons and also because integral-based techniques are restricted to linear and isotropic problems, the finite element method is currently enjoying a regain of interest.

The use of the finite element method requires that we define the boundary of the discretized domain. From a practical point of view, the actual obstacle is surrounded by an artificial boundary, located at a finite distance from the external surface. The scattered field outside the computational domain is thus represented either by boundary conditions known as 'absorbing' (ABC), which are specified on this boundary, or by infinite elements. In both cases, the idea is to prevent the reflection of waves by the artificial boundary. Berenger (Bérenger,1994) proposed to replace the boundary by an absorbing layer, or PML

(Perfectly Matched Layer), of finite width, whose role is precisely to damp the waves diffracted by the obstacle. The size of the computational domain is thus increased by the width of the PML.

The technique referred to as DtN (Dirichlet to Neumann), and introduced by Givoli and Keller (Keller and Givoli,1989), can be viewed as a general procedure for specifying exact boundary conditions, known as 'transparent' (TBC), in the case of artificial boundaries of simple geometric shapes (circle, ellipse, sphere, ellipsoid). Since the TBC is non local, it leads to couplings between all degrees of freedom at the artificial boundary, which may entail excessive memory requirements. To overcome these difficulties, local absorbing boundary conditions, such as those of Robin, have been developed. This simple condition is easy to implement but gives poor results.

Enquist and Majda (Enquist and Majda,1977) proposed an approach which consists of approximating the DtN operator. Bayliss and al. (Bayliss et *al.*,1982) developed an asymptotic solution outside the domain to establish these conditions. However, the local ABC cannot entirely eliminate the parasitic reflections. On the numerical side, the solution of the Helmholtz equation is particularly difficult when the frequencies involved are high, because of the loss of the elliptic character, and because of the oscillatory behavior of its solution. The meshes must therefore be very fine in the case of a standard discretization scheme in order to minimize numerical noise. Special discretization schemes, whose implementations are rather involved, have been developed to circumvent these difficulties.

The system of equations obtained from the Galerkin discretization scheme is sparse, complex and symmetric (but non-Hermitian). It is also generally not diagonal dominant and its Hermitian part is not positive definite.

The iterative method GMRES (Saad and Schultz,1986),combined with an efficient preconditioner was found to be fairly robust for solving systems of this type, especially when the frequencies involved are high. Indeed, direct methods become exceedingly expensive

both in terms of memory and computations when solving very large size systems. Industrial applications often lead to the solution of systems of equations of several millions of unknowns. When attempting to convert this complex system into a real one the number of unknowns doubles, though each of the unknowns is now real and occupies half the space occupied by a complex number. What is more serious is the impact on the preconditioner. Converting the complex problem into a real one in the standard way amounts to reordering the complex data and the resulting system becomes more difficult to precondition. In this case the preconditioned GMRES algorithm converges in a reasonable time only when a full factorization of a Crout type (Zebic,1992) is performed. This factorization remains expensive. Numerical analysts are currently devoting enormous efforts to develop effective preconditioners. However, their methods have had limited success for highly indefinite problems (Mardochée,2001).

In this work we propose to investigate the usefulness of a complex version of ILUT (Incomplete LU factorization with Threshold), developed by Saad (Saad,1994) and ILUTC developed by Li et al. (Li et *al.*,2002). These preconditioners are derived from direct solution methods. The basic idea is to apply an incomplete factorization of the type LU, with reduced cost, to the original system of equations resulting from the discretization of the Helmholtz equation. Our tests show that these preconditioners results in better performances.

The paper is organized as follows. In the first section we establish the mathematical model which governs acoustic phenomena in d-dimension spaces (d=1,2,3). This model is reformulated in a variational form using weighted residuals. Two discretization schemes will be considered, namely the Galerkin and the Galerkin Least-Squares methods. The second section introduces the solution method while section 3 and 4 present numerical tests and discusses the performance of the solution techniques.

1.1 Mathematical model

We are interested in diffraction of an acoustic wave originating from infinity on a bounded obstacle with boundary Γ. The wave propagates in an open medium Ω_e. The objective is to develop a model using the finite element method to deal with problems of acoustic diffraction. First we present the boundary value problem which governs these phenomena in unbounded media. This problem is not adapted to a numerical solution by the finite element method. It is reformulated by invoking the DtN technique, into another problem which is better adapted to this type of solution. The radiation condition at infinity is thus replaced by a particular boundary condition on an artificial boundary.

1.1.1 General model

The d-dimensional (d=1,2,3) problem to solve on the open domain Ω_e is as follows (Colton and Kress,1992) :

$$\begin{cases} \Delta u + k^2 u = f \quad \text{in} \quad \Omega_e \\ u = -u_{inc} \quad \text{on} \quad \Gamma \\ or \ \dfrac{\partial u}{\partial n} = -\dfrac{\partial u_{inc}}{\partial n} \quad \text{on} \quad \Gamma \\ \lim\limits_{r\to\infty} r^{\frac{d-1}{2}} \left(\dfrac{\partial u}{\partial r} - iku\right) = 0 \end{cases} \tag{1.1}$$

where u and f denote, respectively, the wave diffracted by Γ and a source function such that $f = 0$ outside the artificial boundary, which typically assumes respectively a circular (spherical) shape in two (three) dimension problems. The fourth equation of the above problem is the Sommerfeld radiation condition. It guarantees the uniqueness of the solution of this boundary value problem. Only the outgoing waves are therefore allowed and the energy flux is positive.

1.1.2 DtN boundary conditions

It is possible to bound the computational domain by imposing a relation between the unknown function and its normal derivative, on an artificial boundary Γ_{art}. This condition denoted by DtN (Dirichlet to Neumann), replaces the radiation condition at infinity. It represents the characteristic impedance outside the computational domain Ω. The computational domain Ω is then limited internally by Γ and externally by Γ_{art}. Denoting by M the DtN operator, the boundary value problem (1.1) can be reformulated as follows :

$$\left\{\begin{array}{rcll} \Delta u + k^2 u & = & 0 & \text{in } \Omega \\ u & = & -u_{inc} & \text{on } \Gamma \\ or\ \dfrac{\partial u}{\partial n} & = & -\dfrac{\partial u_{inc}}{\partial n} & \text{on } \Gamma \\ \dfrac{\partial u}{\partial n} & = & -Mu & \text{on } \Gamma_{art} \end{array}\right. . \tag{1.2}$$

It is known that this boundary value problem admits a unique solution (Zebic,1992). The exact nonlocal condition introduced by (Keller and Givoli,1989), translates the fact that the artificial boundary Γ_{art} does not yield any artificial reflection. It is therefore a Transparent Boundary Condition (TBC) in which Mu can be expressed as an expansion into Hankel functions of the first kind. This Hankel series expansion is obtained from an analytic solution of the Helmholtz equation in the domain outside of Ω. It is limited to an order m such that $kR \leq m$, in order to guarantee uniqueness of the solution to the boundary value problem (1.2).

Other methods consist of taking only approximations to the TBC. These conditions are then termed 'absorbing' (ABC). Thus, we do not encounter difficulties inherent to the nonlocality of the TBC. However, artificial reflections on Γ_{art} are not avoided. The simplest idea is to impose the Robin condition, namely :

$$\frac{\partial u}{\partial n} = -M_0 u = iku \quad \text{on} \quad \Gamma_{art} \tag{1.3}$$

This condition, which resembles the Sommerfeld radiation condition, does not perform too well. To reduce reflections on the artificial boundary some authors have proposed boundary conditions of higher order. Using the framework of pseudo- differential operators, Enquist and Majda (Enquist and Majda,1977) developed a sequence of local ABCs of increasing order. Bayliss and Turkel (Bayliss et *al.*,1982) use an asymptotic development in $1/r$ of the solution u in order to form a sequence of local operators. In two dimensions, The second order Bayliss-Turkel conditions can be written as :

$$\frac{\partial u}{\partial n} = ik - \frac{u}{2R} + \frac{u}{8R^2(1/R - ik)} + \frac{1}{2(1/R - ik)R^2}\frac{\partial^2 u}{\partial \theta^2} \tag{1.4}$$

In 3D, this condition is written as :

$$\frac{\partial u}{\partial n} = +ik - \frac{u}{R} - \text{div}_{\Gamma_{ext}}\left(\frac{1}{2ik}\left(1 + \frac{i}{kR}\right)^{-1}\nabla_{\Gamma_{ext}} u\right) \tag{1.5}$$

More details on the finite elements implementations of (4) and (5) can be found in (Antoine and al.,1999 ; Djellouli et al.,2000 ; Tezaur et al.,2000)

1.1.3 Variational formulation

In order to apply the finite element method, the problem (2) is reformulated in a variational form : Find u in $H_1(\Omega)$ such that :

$$a(u, v) = b(v) \; \forall \; v \in \; H_1(\Omega) \tag{1.6}$$

where a is a symmetric bilinear form defined on $H_1(\Omega) \times H_1(\Omega)$ by :

$$a(u, v) = \int_\Omega \nabla u \nabla v d\Omega \; - \; k^2 \int_\Omega uv d\Omega \; + \int_{\Gamma_{ext}} \Lambda I uv d\Gamma \tag{1.7}$$

and b is a linear form defined on $L_2(\Omega)$ by :

$$b(v) = \int_\Omega f v d\Omega \tag{1.8}$$

It is obvious that when the variational problem (6) is approximated by a finite element method, the second order Bayliss-Turkel conditions (4) and (5) introduces only additional mass- and stiffness like matrices defined on Γ.

In the Galerkin-Least-Squares discretization scheme the variational formulation is adjusted in order to account for the residual of the partial differential equation. Under this constraint, the weak form of the equation is :

$$a_{GLS}(u,v) = b_{GLS}(v) \text{ with } \begin{cases} a_{GLS}(u,v) &= a(u,v) + \tau \displaystyle\int_{\Omega} \mathcal{H}u\mathcal{H}v d\Omega \\ b_{GLS}(u,v) &= b(u,v) + \tau \displaystyle\int_{\Omega} \mathcal{H}u\, f d\Omega \end{cases} \tag{1.9}$$

where $\mathcal{H}$ is the Helmholtz differential operator $\mathcal{H}(.) = \Delta(.) + k^2(.)$ and τ is a parameter whose choice depends on some design criterion.

1.1.4 Analytic and Numerical computation of the parameter τ

For a regular mesh in two dimensions , consisting of bilinear finite elements and with a constant mesh size h, the parameter τ determined by Harrari et al. (Harari et *al.*,1996) is expressed as :

$$\tau = \frac{1}{k^2}\left(1 - \frac{6(4 - f_x - f_y - 2f_xf_y)}{(kh)^2(2+f_x)(2+f_y)}\right) \quad \text{with} \quad \begin{cases} f_x &= \cos(kh\,\cos\theta), \\ f_y &= \cos(kh\,\sin\theta) \end{cases}$$

where θ is the direction of propagation of the plane waves. Two values of τ corresponding to $\theta = 0$ and to $\theta = 22.5$ deg. are often used in practice (Harari et *al.*,1996; Oberai and Pinsky,2000).

For non regular meshes, we propose as an alternative to compute the parameter τ numerically. This is done within each finite element. The basic idea starts from the system of

equations which arise from the discretized version of the variational formulation above :

$$[K]_e \{u\}_e - (1 - \tau k^2) k^2 [M]_e \{u\}_e = \{0\}$$

where $[K]_e$ and $[M]_e$ are the element stiffness and mass matrices respectively. Multiplying both sides of the above expression by the row vector $\{u\}_e^\star = \{\bar{u}\}_e^T$, the transpose and complex conjugate of u, yields the desired expression for the parameter τ :

$$\tau = (1 - \tau')/k^2$$

where τ' is given by :

$$\tau' = \frac{\{u\}_e^\star [K]_e \{u\}_e}{k^2 \{u\}_e^\star [M]_e \{u\}_e} \quad \text{with} \quad \{u\}_e = \{exp\,(i(k\cos(\theta)x_i + k\sin(\theta)y_i))\}$$

and x_i, y_i are the coordinates of the nodes of the element. It is straightforward to extend this approach to the three-dimensional case and to isoparametric finite elements.

1.2 Solution method

In what follows, we use quadrilateral finite elements in 2D and tetrahedral ones in 3D. The discretized version of (6) or (9) result in a linear system of equations of the form :

$$Au = b \tag{1.10}$$

The coefficient matrix A in the above system, is sparse, symmetric, and complex. Note that it is also non-Hermitian and not diagonally dominant.

As can be seen, the effect of the DtN condition in the discretization scheme by standard finite elements results only in the addition of the complex matrix C to form the global matrix A. In addition, the terms C_{ij} are zero whenever the nodes with index i or j do not belong to the artificial boundary Γ_{art}. If the DtN condition is non-local then clearly the

terms C_{ij} are nonzero for all nodes of index i, or j belonging to Γ_{art}, and this can destroy the band structure of the matrix if a particular numbering is not used.

We exclude the use of direct methods in this study because of their potential excessive cost – especially for 3D problems. Among iterative methods, preconditioned Krylov subspace techniques (Saad,1996) are the most general-purpose and appear to be a good alternative to direct solvers.

A preconditioned Krylov subspace method for solving the linear system (1.10) consists of an accelerator and a preconditioner (Saad,1996). In what follows we call M the preconditioning matrix, so that, for example, the right-preconditioned system :

$$AM^{-1}y = b \qquad \text{where} \quad x = M^{-1}y \tag{1.11}$$

is solved instead of the original system (1.10). The above system is solved via an "accelerator", a term used to include a number of methods of the Krylov subspace class. Thus, a right-preconditioned Krylov subspace method computes an approximate solution from the affine space :

$$x_0 + \text{Span}\{r_0, AM^{-1}r_0, \cdots, \left(AM^{-1}\right)^{m-1} r_0, \},$$

which verifies certain conditions. For example, the GMRES algorithm (Saad,1996) requires that the residual $r_m = b - Ax_m$ has a minimal 2-norm.

The most common way to define the preconditioning matrix M is through Incomplete LU factorizations. An ILU factorization is obtained from an approximate Gaussian elimination process. When Gaussian elimination is applied to a sparse matrix A, a large number of nonzero elements may appear in locations originally occupied by zero elements. These fill-ins are often small elements and may be dropped to obtain Incomplete LU factorizations.

Among these procedures, is ILU(0) which is obtained by performing the standard LU factorization of A and dropping all fill-in elements that are generated during the process.

Thus, the L and U factors have the same pattern as the lower and upper triangular parts of A (respectively). More accurate factorizations denoted by ILU(k) have been defined which drop fill-ins according to their 'levels' in the elimination process, where the levels attempt to reflect size and are defined recursively (Saad,1996). We will not consider levels other than level zero in this work.

Another class of preconditioners is based on dropping fill-ins according to their numerical values. One of these methods is ILUT (ILU with Threshold). This procedure uses basically a form of Gaussian elimination which generates the rows of L and U one by one. Small values are dropped during the elimination, using a parameter $droptol$. A second parameter, p, is then used to keep the largest p entries in each of the rows of L and U. This procedure is denoted by $ILUT(droptol, lfil)$ of A. Practical values of $lfil$ and $droptol$ are $lfil = \alpha NNZ/n$, with NNZ the number of non-zero entries of the original matrix, n the number of unknowns, α is a positive integer, and $10^{-9} \leq droptol \leq 10^{-3}$. The quotient NNZ/n refers to the average number of nonzero entries in A. - Among other preconditioners we tested, is a complex version of a Crout-based incomplete factorization. A detailed description of this technique is beyond the scope of this article and we refer the reader to (Li et *al.*,2002). The method is based on computing the i-th column of L and the i-th row of U at the i-th step, for $i = 1, \ldots, n-1$. There are two attractions of this algorithm. The first is that it presents important advantages in terms of cost, when compared with the standard ILUT. A second advantage is that it enables a more elaborate and rigorous dropping strategy which aims at making $I - L^{-1}AU^{-1}$ small rather than making $A - LU$ small as is traditionally done.

All the incomplete LU factorization techniques have been developed for cases when the original matrix A has some diagonal dominance properties. The procedures still work for cases when the matrix is not diagonally dominant and this is the main reason why ILU techniques have had an excellent success across a broad spectrum of applications. The matrices which arise from the Helmholtz equation can be highly indefinite. In this situation

the resulting incomplete LU factorization can be inaccurate and result in an ineffective preconditioner. We are therefore in a situation where many of the standard techniques can be expected to fail and some of the techniques which are not necessarily competitive might be useful. Among these we can mention, for example, an approach based on the normal equations :

$$A^H A x = A^H b \,.$$

The above system is Hermitian positive definite and can be solved with the conjugate gradient method, preconditioned by a diagonal matrix, or with an incomplete Cholesky factorization. Here there are two difficulties. The first is that $A^H A$ can sometimes be much denser than the original matrix. The second is that positive definiteness does not guarantee the existence of a good-quality incomplete Cholesky factorization. In general, this approach is not recommended as the condition number of $A^H A$ is the square of that of A - so convergence may be slow. Our experiments with this approach have not been conclusive so far and will not be reported here. In essence, the difficulty is now shifted to that of preconditioning the matrix $A^H A$ which may be as hard or harder than that of preconditioning the original matrix.

1.3 Numerical Experiments in 2D

Two problems are considered for the numerical experiments in 2D. The first problem is a square domain and is used to study the convergence of ILUT for different values of $lfil$ and drop-tolerance for a well-conditioned problem. For the second problem the domain considered is circular and it is used to study the impact of discretization schemes and to study the performance of GMRES for different frequency regimes and for different preconditioners. The condition number of the linear system arising from the discretization varies with the number of elements per wavelength. The analytical solution is available for both the problems and it is used to compute the error in the numerical solution. The computations are performed in double precision on Intel Pentium III based PCs (with 512KB

RAM and 600MHz clock speed processor).

Problem 1.

The problem domain Ω is a unit square (Fig.1.1) $\Omega = (0,1) \times (0,1)$. The governing differential equation is :

$$\begin{cases} \Delta u + k^2 u &= 0 \quad \text{in} \quad \Omega_c \\ \dfrac{\partial u}{\partial n} + iku &= g \quad \text{in} \quad \Gamma_{art} \end{cases} \tag{1.12}$$

The function g is selected such that the exact solution has the expression : $u(x,y) = \exp[ik\cos(\theta)x + k\sin(\theta)y]$. The incident angle is set at $\theta = 45$. The domain is discretized with a structured mesh with a mesh size of $h = 1/200$. The wavelength is $\lambda = 0.628$, so the ratio λ/h is 125.66. For the solution of the linear system obtained after applying the boundary conditions, the Krylov subspace size is set to 20. The initial guess is zero and the GMRES iteration is stopped when the residual norm is reduced by 10^{-8} or when the number of iterations exceeds 500.

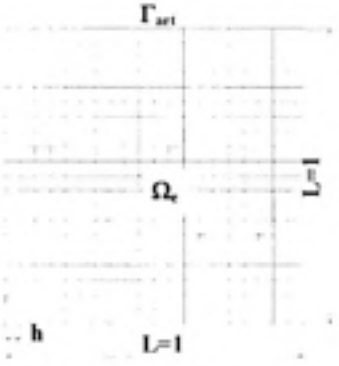

Figure 1.1 ***Square shaped computational domain with a structured mesh.***

Table 1.1 shows the number of iterations taken by ILUT-GMRES and the error in the computed solution for different values of $lfil$ and drop-tolerance. As expected, for this well conditioned systems, we get the smallest number of iterations for the highest value of $lfil$ and lowest value of drop-tolerance. Figure 1.3 illustrates the convergence behavior of ILUT-GMRES for different values of $lfil$. The results show that as the $lfil$ is increased the convergence rate increases. It also shows that ILU0 stagnates.

Table 1.1

Numerical results for problem 1 with ILUT-GMRES

$\alpha =$ $lfil * n/nnz$	Drop tolerance	# steps to converge	Final res. norm	Time (sec)	% L_2 error Re. part	error % Im. part
11.11	1.00E-05	20	1.60E-08	182	0.10	0.11
5.55	1.00E-05	176	2.50E-08	265	0.10	0.11
2.22	1.00E-05	500	7.80E-08	377	5.24	5.34
11.11	1.00E-04	380	2.60E-08	628	0.10	0.11
5.55	1.00E-04	350	2.76E-08	492	0.10	0.11
2.22	1.00E-04	500	5.06E-04	363	3.00	3.30
11.11	1.00E-03	500	5.10E-04	402	5.92	6.36
5.55	1.00E-03	500	5.70E-04	610	5.91	6.36
2.22	1.00E-03	500	1.33E-03	344	6.90	7.60

Problem 2.

In this problem a soft obstacle, which is a disk of radius $r_0 = 0.5m$ is considered. The incident wave is plane with a wavelength λ, and it propagates along the x-axis. The second order Bayliss-Turkel boundary conditions are used on the artificial boundary, located at a distance $2r_0$ from the obstacle. The discretization uses isoparametric quadrilateral elements with 4 nodes (Fig. 1.3). The analytic solution is known and can be found in (Zebic,1992; Bowman,1969).

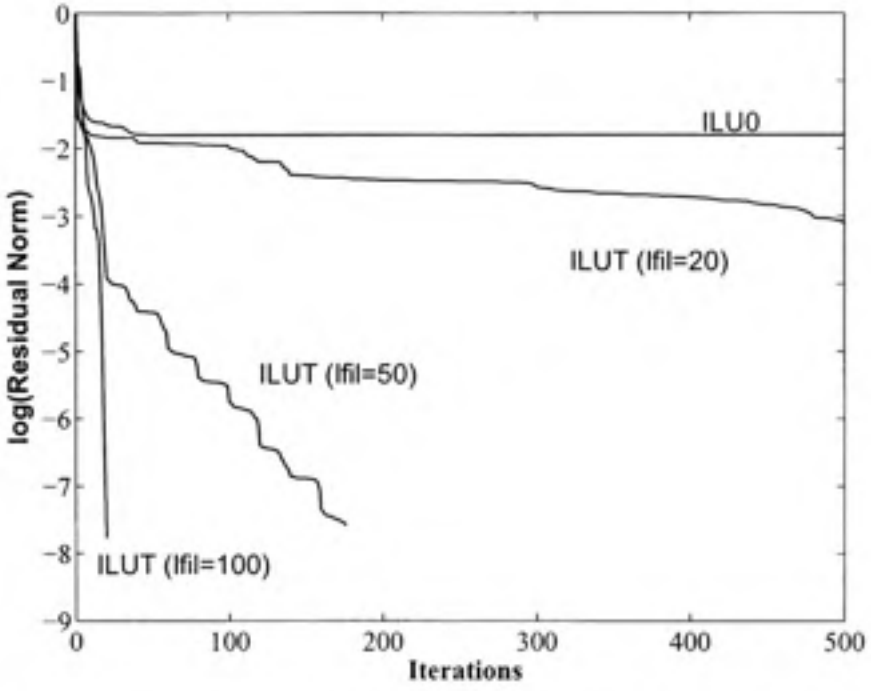

Figure 1.2 ***Convergence histories for problem*** 1 ***with ILUT-GMRES for different values of*** $lfil$ ***- residual norms vs iteration.***

1.3.1 Impact of discretization

Under the same conditions ($k = 2\pi$) and for different meshes, the accuracy of the results obtained with the GLS scheme are superior to those with the classical Galerkin scheme, see Table 1.2. The number of iterations and execution times are in both cases almost identical. The Galerkin least-squares scheme leads to a good accuracy even for a rough mesh resolution using 10 points per wavelength. The accuracy of the results is comparable with that obtained in (Zebic,1992), using a classical Galerkin scheme with an exact non-local Dirichlet to Neumann (DtN) boundary condition. As a comparison, the errors on the real part obtained by Zebic were $5.15, 1.33, 0.34$ for $\lambda/h = 10, 20, 40$ respectively. The preconditioner selected by Zebic (Zebic,1992) is based on an incomplete CROUT factorization. In this reference, the finite elements used are triangles with 3 nodes.

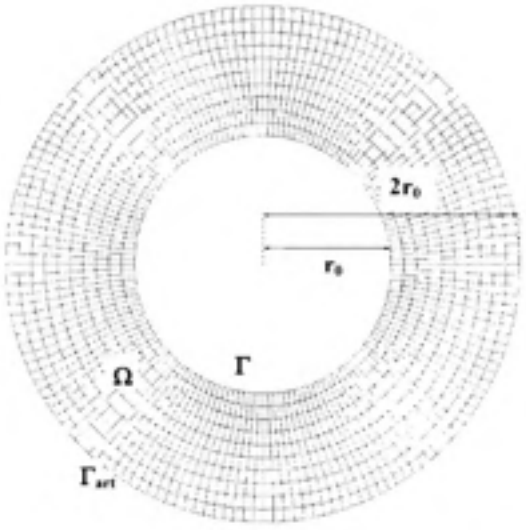

Figure 1.3 ***Crown shaped computational domain with a structured mesh.***

Table 1.2

Error in the finite element solution for Galerkin and Galerkin Least-squares(GLS) discretization schemes for different mesh-sizes. The values in the parenthesis correspond to GLS scheme. Order 2 Bayliss-Turkel boundary conditions used

λ/h	Relative L_2 error on the real part	Relative L_2 error on the imaginary part	Number of Iterations	Time (sec)
10	4.42 (2.00)	4.51(2.07)	76 (77)	1.37 (1.43)
20	1.14 (0.51)	1.16 (0.50)	138 (139)	4.42 (4.52)
40	0.30 (0.12)	0.31 (0.10)	220 (219)	12.93 (12.83)

These results show that the Bayliss-Turkel condition gives a good accuracy for an artificial boundary that is close to the obstacle (here at a distance λ) even with an inaccurate mesh resolution corresponding to $\lambda/h = 10$.

1.3.2 Impact of the dropping strategy in ILU type precondtioners

This experiment uses the same physical setting with the wave number $k = 2\pi$. The restart value for GMRES (Krylov subspace dimension) is fixed to $im = 10$ and the stopping criterion is to reduce the residual norm by 8 orders of magnitude. The mesh size corresponds to $\lambda/h = 40$.

Two parameters can be used to set the dropping strategies in ILUT and ILUTC. The first is defined by $lfil$, which sets the maximum number of nonzero elements kept in each row of L and U (or row of U and L^T for ILUTC). The second is a drop tolerance $droptol$ which is used to prune a row of its smallest elements. Two strategies have often been used. The first sets $droptol$ to a small value (e.g., $droptol = 1e-05$), and uses $lfil$ as the primary criterion for dropping. So, relatively small values are dropped according to $droptol$ and the procedure keeps the largest $lfil$ values in L and U. The advantage of this strategy is that it enables a good control of fill-in, since the number of nonzero entries in the factorization is bounded. The second strategy does the opposite. It sets $lfil$ to a large value (e.g., $8 \times nnz(A)/n$) and uses $droptol$ as the primary criterion for dropping. This second strategy is known to be more reliable. However, it may require a large amount of storage, since the parameter $lfil$ is set to be rather large.

The first experiment illustrates the first strategy. We set $droptol$ to 10^{-5} and vary $lfil$. As the results in Table 1.3 show, the number of iterations required by GMRES to reach convergence decreases when $lfil$ increases in the intervals $[5, 15]$ and $[19, 30]$. However, for $lfil$ in the interval $[15, 19]$, the number of iterations increases with increasing $lfil$, showing that the number of iterations is not necessarily a monotonically decreasing function of $lfil$. This is likely due to the fact that in the case of highly indefinite matrices, the factors L and U may become unstable (i.e., $||(LU)^{-1}||$ can become huge) – and so the gains in accuracy made in the factorization are outweighed by the instability. For the experiments performed here, the relative L_2 errors of the real parts and imaginary parts

are 0.30 % (0.12 % for GLS scheme) and 0.31 %(0.10 % for GLS scheme), respectively. It is also interesting to observe that the number of iterations to reach convergence can be reduced in the interval [15, 19] by changing the drop-tolerance to 10^{-3} (from 10^{-5}).

Table 1.3

Iteration count (Iter) and CPU time (Time) versus the $lfil$ parameter of ILUT. Tolerance is set to 1.e-05. GLS scheme results between parentheses

Lfil	5	10	15	18	19
Iter.	220 (219)	90 (90)	69 (69)	78 (78)	170 (143)
Time (sec)	12.93 (12.83)	8.16 (8.08)	8.21 (8.12)	10.06 (9.94)	19.29 (16.48)
Lfil	20	21	22	25	30
Iter.	132 (139)	75 (72)	52 (52)	26 (26)	14 (14)
Time (sec)	16.50 (17.06)	10.71 (10.40)	8.67 (8.73)	6.38 (6.34)	5.53 (5.99)

In summary, an increase of $lfil$ is not always beneficial with the strategy based on $lfil$. This known fact (Saad,1996; Mardochée,2001) is well illustrated in the example tested here.

The second set of experiments will test the second strategy which is based on keeping $lfil$ large and varying $droptol$. In this experiment $lfil$ is set to $8 \times nnz(A)/n$.The discretization corresponds to $\lambda/h = 40$. Here, we must add another measure of performance which reflects the amount of memory used by the preconditioner. This measure, sometimes referred as the "fill-factor", is the ratio of the number of nonzero elements in L, U over $nnz(A)$ the number of nonzero entries in the original matrix. For iterative methods a reasonable fill-factor is between 1 and 2. Harder problems can often be solved with a fill-factor of up to, say, 4 or 5.

Table 1.4 and 1.5 show the results with three values of $droptol$. It is interesting to observe that, in contrast with the $lfil$-based strategy, the number of iterations now decreases as a more accurate factorization is computed. However, ILUT may require much more memory to achieve this.

Table 1.4

Performance of ILUT using $lfil = 8 \times nnz/n$, im=50 when droptol is varied, for systems associated with different wavenumbers (Standard Galerkin scheme)

	$droptol = 0.05$			$droptol = 0.01$			$droptol = 0.001$		
$k =$	2π	10π	16π	2π	10π	16π	2π	10π	16π
Fill-fact	0.91	1.07	0.89	1.67	2.04	2.04	4.87	12.98	13.53
Iter.	194	582	1561	47	363	777	16	Stag.	Stag.
Time	12.24	243.40	1025.98	3.66	169.78	582.82	2.22	*	*
(%) Re	0.30	2.09	6.03	0.30	2.09	6.03	0.30	*	*
(%) Im	0.31	2.08	6.03	0.31	2.08	6.03	0.31	*	*

Table 1.5

Performance of ILUTP(ILUT with pivoting) using $lfil = 8 \times nnz/n$, im=50, and permtol=0.1, when droptol is varied, for systems associated with different wavenumbers (Standard Galerkin scheme)

	$droptol = 0.05$			$droptol = 0.01$			$droptol = 0.001$		
$k =$	2π	10π	16π	2π	10π	16π	2π	10π	16π
Fill-fact	1.65	2.15	2.13	2.67	3.48	3.83	5.86	13.71	14.011
Iter.	67	587	3492	32	466	5331	14	stag.	stag.
Time	4.65	275.66	3291.30	2.70	251.34	4584.12	2.29	*	*
(%) Re	0.30	2.09	6.03	0.30	2.09	6.03	0.30	*	*
(%) Im	0.31	2.08	6.03	0.31	2.08	6.03	0.31	*	*

1.3.3 Performance of GMRES-ILUT for different frequency regimes

We continue with the same physical setting, but in this experiment the wavelength λ is now varied. The parameter τ of the GLS method is evaluated numerically in each element. Different mesh sizes are considered depending on the wavenumber. The parameter $lfil$ is selected to be relatively small in order to reduce the cost of computing the ILUT factorization.

Table 1.6

Behavior of ILUT-preconditioned GMRES for different wavenumbers and different mesh sizes

Discr. Scheme	# nodes	λ/h	Wave # k	Iter. count	% error		Time (sec)
					Re part	Im part	
Galerkin	7421	40	2π	1545	0.30	0.31	64.77
GLS				1541	0.13	0.11	51.66
Galerkin	7421	10	8π	725	16.07	15.85	30.34
GLS				756	8.29	8.33	31.52
Galerkin	29141	40	8π	1490	1.41	1.42	297.33
GLS				1493	0.22	0.20	300.35
Galerkin	29141	20	16π	9770	10.91	10.88	1945.54
GLS				10207	1.54	1.55	2030.96
Galerkin	58101	40	16π	GMRES Stag.			
GLS							
Galerkin	65160	45	16π	GMRES Stag.			
GLS							

The results reported in Table 1.6 are obtained with $lfil = 2$. The following observations can be made.

- Consider the situation of small values of the wave number k. In this case the resolution of the mesh corresponding to $\lambda/h = 40$ (40 mesh points per per wavelength), yields an excellent agreement between the results of the finite element method and the analytical solution. The Galerkin and the GLS schemes give essentially the same accuracy and require almost the exact same number of GMRES steps to converge.

Table 1.7

Behavior of ILUT-preconditioned GMRES for a wave number k=16π and two different mesh resolutions. Case $lfil = 1$

Discr. Scheme	Number of nodes	λ/h	Wave # k	Iter. count	% error (Re part)	% error (Im part)	Time (sec)
Galerkin	58101	40	16π	8175	6.03	6.03	3101.81
GLS				8312	3.82	3.82	3208.43
Galerkin	65160	45	16π	13304	5.77	5.77	5609.76
GLS				13140	4.04	4.05	5228.25

Table 1.8

Iteration count (Iter) and CPU time (Time) versus the $lfil$ parameter of ILUT. GLS scheme results between parentheses

$k = 8\pi, \lambda/h = 40$, # nodes=29141, $im = 10$, $droptol = 1E-5$, $nnz/n = 9$					
Lfil	02	05	09	15	18
iter.	1490 (1493)	774 (755)	353 (352)	1127 (1119)	ILUT-GMRES stagnates
Time (sec)	297.33 (300.35)	195.30 (181.54)	114.4 (110.90)	450.14 (557.25)	
$k = 16\pi, \lambda/h = 40$, # nodes=58101, $im = 10$, droptol=1E-5, $nnz/n = 9$					
Lfil	01	02	07	09	18
iter.	8175 (8312)	ILUT-GMRES Stagnates	1013 (1006)	2087 (2107)	ILUT-GMRES stagnates
Time (sec)	3101.81 (3208.43)		587.56 (588.15)	1296.21 (1306.71)	

– Consider the case when the wavenumber is a little larger ($k = 8\pi$). In this case, when the mesh resolution is low ($\lambda/h = 10$), only the Galerkin-Least-squares approach leads to a good agreement between the resulting solution and the analytic solution. For a higher resolution ($\lambda/h = 40$), both discretization schemes yield an excellent agreement between the results of the finite element method and the analytical solu-

tion. The solution cost is almost identical in both schemes. Note also that a relatively small value of the Krylov subspace dimension suffices to yield convergence.

- We consider the situation of a relatively larger value of the wavenumber ($k = 16\pi$). When a mesh resolution of 20 points per wavelength, the accuracy of the result obtained with the GLS scheme is excellent in contrast with the one obtained with the classical Galerkin method. When the mesh resolution doubles ($\lambda/h = 40$), then ILUT-GMRES stagnates. As mentioned above, this is likely due to an unstable factorization. To check this we considered a less accurate ILUT factorization which uses a smaller value of $lfil$. The results are shown in Table 1.7.

Increasing the mesh resolution leads to more accurate numerical results for the Galerkin scheme in spite of the fact that the Babuška condition (Ihlenburg and Babuška,1995) ($k^3h^2 < 1$) is not satisfied in the case when $\lambda/h = 40$ ($k^3h^2 = 1.24$ in this situation). It should be recalled that the Babuška condition is only a sufficient condition but it is not necessary. Increasing the mesh resolution to 45 points per wavelength, which gives $k^3h^2 = 0.97$, yields also a slight improvement of the accuracy. In contrast with the Galerkin scheme, the GLS scheme does not lead in this case to a reduction of the accuracy despite the fact that the Babuška condition is satisfied. This is perhaps to be attributed to the choice of the parameter τ which is tightly linked to the scheme. This merits further investigation. In any case, the accuracy obtained by the GLS scheme are superior to those of the classical Galerkin scheme.

As was done in section 4.2 the fill-in parameter has been varied in order to obtain an optimal value (second half of Table 1.8). nnz/n We found that this corresponds to $lfil = 7$ and the number of iterations, in the case of Galerkin scheme, dropped to 1013 compared with 8175 for $lfil = 1$ (see table 1.8).

Finally, it is to be noted that the choice $im = 10$ for the Krylov subspace dimension is far from optimal. Other tests not reproduced here indicate the choice $im = 30$ is better for

most tests.

1.3.4 Performance of different preconditioners for GMRES

We focus now on the performance of GMRES preconditioned with ILU0, ILUT and ILUTC. We consider again the situation of a relatively larger value of the wavenumber ($k = 16\pi$) with a mesh resolution such that $\lambda/h = 40$. We report in table 1.9 the performances of GMRES preconditioned by ILUT, ILUCrout and ILU0. It can be shown that the performances of the solvers ILUT-GMRES and ILUTC-GMRES are closely dependent on the parameter lfil. For high value of the parameter $lfil$, specifically $lfil = 18$, both solvers ILUT-GMRES and ILUTC-GMRES stagnate due to an unstable factorization. For the optimal lfil, equal to 7, the solver ILUTC-GMRES converges in only 828 iterations whereas the solvers ILU0-GMRES and ILUT-GMRES converges respectively in 1145 and 1013 iterations. It is interesting to note that in the case of $lfil = 2$, both ILUT-GMRES and ILUTC-GMRES stagnate whereas, in the case of $lfil = 3$, only ILUT-GMRES stagnates.

1.3.5 Computing preconditioners from problems with lower wavenumbers

It was observed in Section 1.3.2 that increasing the accuracy of the preconditioner does not necessarily lead to faster convergence. We argued that a possible explanation for this is that the resulting incomplete factorization may start becoming instable. In the next experiment, we propose a way to exploit this observation. As the wavenumber increases, the coefficient matrix becomes more indefinite, resulting in a poor quality preconditioner. A possible remedy is to use a preconditioner obtained from a lower wavenumber.

Figure 1.4 shows the performance of this strategy for the case when we attempt solve the same problem as in Section 1.3.2 for $k = 10\pi$, (so $\lambda/h = 40$). Numbers in parenthesis show the fill-factors in each case. The preconditioners are obtained from ILUT using $droptol = 0.05$ and a large lfil ($lfil = 10 \times nnz(A)/n$). Interestingly enough, the pre-

Table 1.9

Iteration count (Iter) and CPU time (Time) versus the $lfil$ for different preconditioners

$k = 16\pi, \lambda/h = 40$, # nodes=58101, $im = 10$, droptol=1E-5, $nnz/n = 9$					
Solver : ILUT-GMRES					
Lfil	1	2	3	4	5
iter.	8175	Stagn.	Stagn.	1686	1219
Time	3101.81			806.24	663.83
Lfil	6	7	8	9	18
iter.	1037	1013	1103	2087	stagn.
Time	576.35	587.56	672.29	1296.21	
Solver : ILUCrout-GMRES					
Lfil	1	2	3	4	5
iter.	3681	Stagn.	1901	1171	951
Time	1652.18		961.84	643.22	553.14
Lfil	6	7	8	9	18
iter.	891	828	839	970	stagn.
Time	545.14	545.46	574.38	662.28	
Solver : ILU0-GMRES					
iterations : 1145					
Time : 555.94					

conditioner computed for $k = 10\pi$, i.e., for the actual matrix, requires to store about twice $nnz(A)$ entries, but it does not lead to convergence. In contrast, the preconditioner for $k = 2\pi$ requires much less memory ($\approx 0.9 \times nnz(A)$) and produces convergence. It is interesting to also note the trend. The higher k (i.e., the closer the preconditioner is to the actual matrix), the worse the result. This is not too unexpected for highly indefinite matrices.

1.4 Numerical Experiments in 3D

We consider the solution of three-dimensional scattering problems. For this purpose, we focus on a sphere shaped scatterer with radius a=0.5m. The spherical artificial boundary is placed at 0.5m from the obstacle (Fig.1.5).

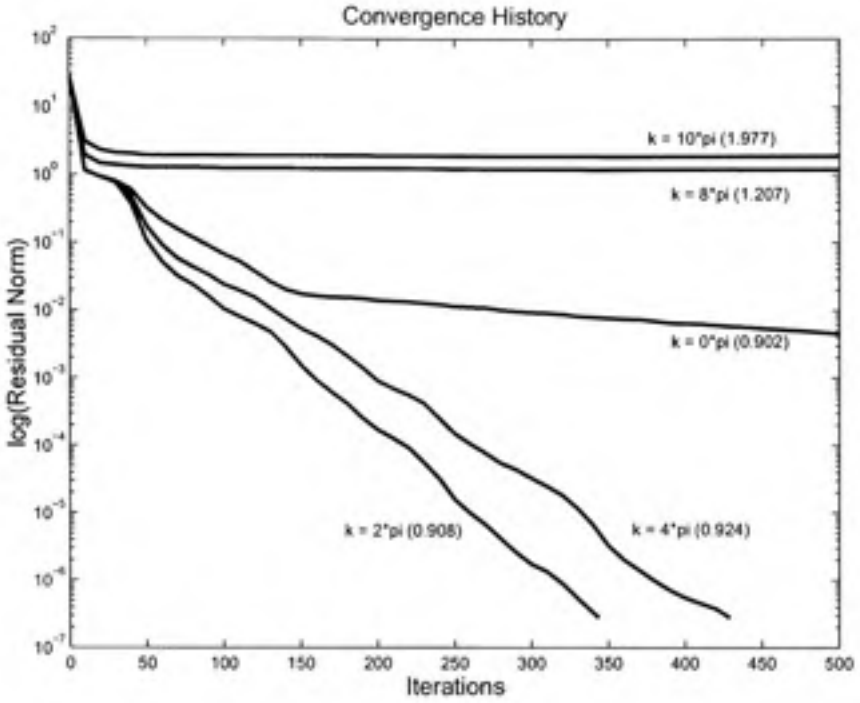

Figure 1.4 ***Convergence histories - residual norms vs iteration for preconditioners obtained from lower wavenumbers. Numbers in parenthesis show the fill-factors.***

The incident plane wave travels along the positive z axis. The analytical solution of Dirichlet's and Neumann's problems can be found in (Bowman,1969; Colton and Kress,1992). In all the following experiments, we discretize the computational domain by linear tetrahedral elements and solve the resulting system of equations on a Pentium IV computer with 2Go of RAM using double precision arithmetic (with 1GHz clock speed processor). The restart value for GMRES is fixed to im=50 and the stopping criterion is eps=10^{-8}. The drop tolerance for ILUT and ILUCrout is set to 10^{-5}. Three grids having 3995, 23662 and 113060 nodes are chosen. The mesh resolutions λ/h are therefore equal respectively to 9, 17 and 30 for $\lambda = 1$. The practitioners are interested in the computation of the radiated wave in the far-field zone. The behavior of the scattered field for an incident wave is gene-

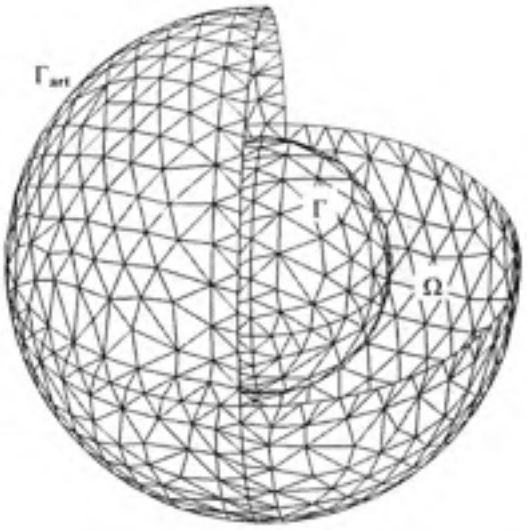

Figure 1.5 ***Spherical shaped computational domain.***

rally described by the radar cross section (RCS). More precisely, in the three-dimensional case, the RCS is defined by (Bowman,1969)

$$RCS(\varphi,\theta) = 10\lg(4\pi|u_o(\varphi,\theta)|^2) \tag{1.13}$$

In the above equation, we set $u_o(\varphi,\theta)$ as the scattering amplitude of the radiated field (Bowman,1969) following the $\overrightarrow{n} = (\cos(\phi)\sin(\theta), \sin(\phi)\sin(\theta), \cos(\theta))$ diffusion direction.

1.4.1 Problem 1 : Dirichlet Problem

Under the same conditions, the results obtained in Table 1.10 show that the ILUT-GMRES solver requires fewer step than ILU(0)-GMRES to converge. However, the CPU time is slightly greater for ILUT-GMRES. For a wave number equal to 2π, the accuracy of the obtained results is improved when the mesh resolution is increased. The error is less then 3% for the finest mesh adopted which corresponds to a mesh resolution of $\lambda/h = 30$.

As Table 1.10 shows, ILUT-GMRES conveges in 72 iterations whereas ILU0-GMRES converges in 144 iterations. Under the same conditions ILUC-GMRES converges after 90 iterations (CPU time=215.71s). On the other hand, Figure 1.6 shows a good agreement between the computed and the analytical RCS . For wave numbers equal respectively to π and $\pi/2$, the correlation between numerical results and the analytical solution is good despite the fact that the artificial boundary is too close to the scatterer in this case.

Table 1.10

Performances of the solvers ILUT-GMRES and ILU0-GMRES for different wavenumbers and different mesh sizes (Soft Scatterer)

Precond.	# nodes	lfil / $(\frac{nnz}{n})$	Wave # k	# iterations	% error (Re part)	% error (Im part)	Time (sec)
ILUT	3953	12	2π	23	11.17	9.56	1.81
ILU0	3953		2π	37	11.17	9.56	1.72
ILUT	23662	13	2π	42	04.57	3.86	19.09
ILU0	23662		2π	78	04.57	3.86	13.22
ILUT	113060	13	2π	72	02.02	2.12	204.90
ILU0	113060		2π	144	02.02	2.12	178.41
ILUT	3953	12	π	17	2.64	3.19	1.81
ILU0	3953		π	30	2.64	3.19	1.58
ILUT	23662	13	π	30	1.25	1.60	17.42
ILU0	23662		π	56	1.25	1.60	14.67
ILUT	113060	13	π	50	0.85	1.14	195.83
ILU0	113060		π	109	0.85	1.14	161.86
ILUT	3953	12	$\pi/2$	15	1.78	1.50	1.77
ILU0	3953		$\pi/2$	28	1.78	1.50	1.13
ILUT	23662	13	$\pi/2$	26	0.78	0.65	16.94
ILU0	23662		$\pi/2$	56	0.78	0.65	14.67
ILUT	113060	13	$\pi/2$	41	0.50	0.43	193.19
ILU0	113060		$\pi/2$	109	0.50	0.43	199.25

1.4.2 Problem 2 : Neumann Problem

Table 1.11 shows that the solver ILUT-GMRES is faster than the ILU0-GMRES in terms of iterations count and CPU time. For a wave number equal to 2π, the accuracy of the

obtained results is improved when the mesh resolution is increased. The error is less then 3% for the finest mesh adopted ($\lambda/h = 30$). According to table 1.11, ILUT-GMRES and ILU0-GMRES converges respectively after 128 and 282 steps.

Table 1.11

Performances of the solver ILUT-GMRES vs. ILU0-GMRES for different wavenumbers and different mesh sizes (Hard Scatterer)

Precond.	# of nodes	lfil / ($\frac{nnz}{n}$)	Wave # k	GMRES steps	% error (Re part)	% error (Im part)	Time (sec)
ILUT	3953	12	2π	35	12.28	12.35	2.06
ILU0	3953		2π	50	12.28	12.35	1.73
ILUT	23662	13	2π	67	4.89	5.35	15.83
ILU0	23662		2π	127	4.89	5.35	17.29
ILUT	113060	13	2π	128	2.34	2.62	102.88
ILU0	113060		2π	282	2.34	2.62	152.5
ILUT	3953	12	π	25	7.30	4.17	1.77
ILU0	3953		π	40	7.30	4.17	1.55
ILUT	23662	13	π	44	2.89	1.76	13.75
ILU0	23662		π	91	2.89	1.76	13.70
ILUT	113060	13	π	87	1.69	1.19	89.70
ILU0	113060		π	197	1.69	1.19	117.33
ILUT	3953	12	$\pi/2$	21	3.69	4.33	1.67
ILU0	3953		$\pi/2$	37	3.69	4.33	1.45
ILUT	23662	13	$\pi/2$	37	2.17	1.50	12.38
ILU0	23662		$\pi/2$	82	2.17	1.50	12.92
ILUT	113060	13	$\pi/2$	73	1.87	0.68	81.41
ILU0	113060		$\pi/2$	197	1.87	0.68	119.23

Under the same conditions ILUTC-GMRES converges in 130 iterations (CPU Time=101.91s). The predicted and the analytical RCS are also in good agreement (Figure 1.6). For wave numbers equal respectively to π and $\pi/2$, the adopted grid leads to a good accuracy.

1.4.3 Impact of the discretization scheme

In the previous numerical experiences, only the Galerkin scheme was used. We focus now on the Galerkin-Least squares scheme (GLS). The results obtained for a wave number

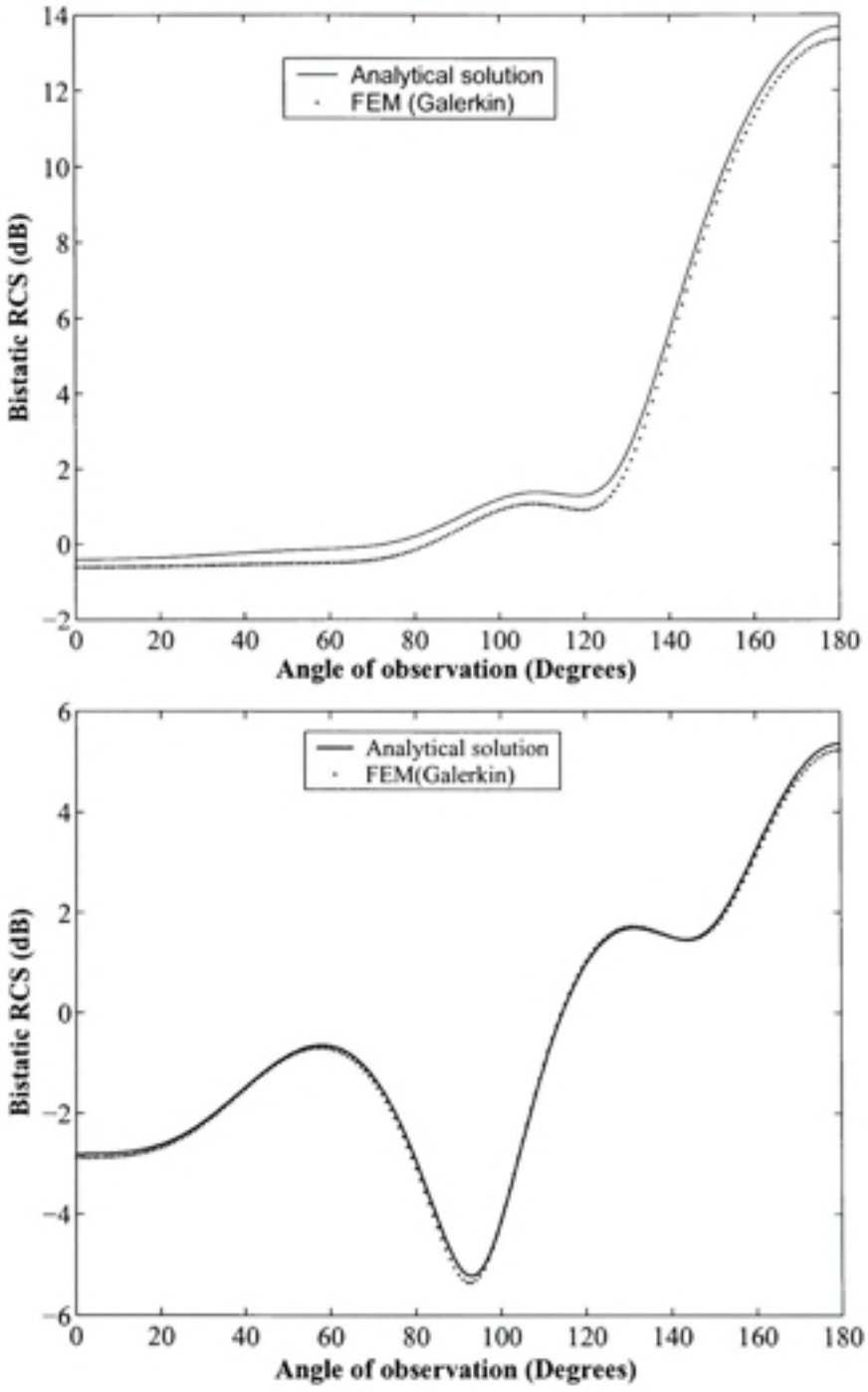

Figure 1.6 ***Bistatic Radar Cross Section for k=2π and $\phi = 0$. top : soft scatterer, bottom : hard scatterer.***

equal to 2π using ILUT-GMRES are summarized in Table 1.12. They show that the accu-

Table 1.12

Performances of the solver ILUT-GMRES for different different mesh sizes (Galerkin and GLS Scheme)

Problem	Scheme	# of nodes	# of iterations	% error (Re part)	% error (Im part)	Time (sec)
Diri	Gal.	3953	23	11.17	9.56	1.81
Diri	GLS	3953	23	6.37	6.37	1.81
Diri	Gal.	23662	42	4.57	3.86	19.09
Diri	GLS	23662	42	2.96	3.23	14.39
Diri	Gal.	113060	72	2.02	2.12	204.90
Diri	GLS	113060	73	1.61	2.00	186.86
Neum	Gal.	3953	35	12.28	12.35	2.06
Neum	GLS	3953	37	10.26	9.83	2.19
Neum	Gal.	23662	67	4.89	5.35	15.83
Neum	GLS	23662	68	4.54	4.68	19.55
Neum	Gal.	113060	128	2.34	2.62	102.62
Neum	GLS	113060	129	2.41	2.68	132.22

racy of the numerical solution is improved for Dirichlet's and Neumann's problems when we use the GLS scheme.

1.5 Conclusion

A numerical method based on the finite element method has been implemented for solving the Helmholtz equation for acoustic wave diffraction. Complex versions of the ILU factorization with Threshold (ILUT) and the Crout form of ILU (ILUCrout) were used as preconditioners and a complex version of GMRES was used as an accelerator.

In the first benchmark test, the classical ILU(0) preconditioner did not give rise to a reliable solution technique. The performance of ILUT was good for low, medium, and high frequencies, provided appropriate fill-in levels and drop parameters are used to compute the ILU factorization.

The second test problem is a more realistic acoustic benchmark test. The effects of the mesh resolution, the wave number value and the fill-in parameter on the accuracy and the computational performance were analyzed. The GLS scheme is more accurate than the classical Galerkin scheme for low mesh resolutions. A new formula for the GLS stabilization method was also proposed. It was observed that the second order Bayliss-Turkel boundary condition performs well compared with the exact DtN. Two strategies were adopted. In the first one, a small drop tolerance value was chosen and the lfil parameter was varied. The optimal value of the fill-in parameter depends on the wave number. It was observed that increasing the fill-in parameter is not always beneficial. A somewhat surprising finding of this study is that for high wave numbers the fill-in parameter must sometimes be reduced to obtain a useable incomplete factorization. Indeed, because the matrix becomes highly indefinite, an accurate ILUT or ILUCrout factorization seems to often yield unstable factors and this is often prevented by computing a less accurate ILUT or ILUCrout factorization. In the second strategy, we kept the lfil large and varied the droptol. In this case, the number of iterations generally decreases as more accurate factorizations are computed. However, ILUT may require far more memory in this situation. For 3D acoustic scattering problems, the solver ILUT-GMRES seems suitable for the

solution of Neumann's problem for the wave numbers investigated. However, the solver ILU0-GMRES seems suitable for Dirichlet's problem despite the fact that it requires more iterations than ILUT-GMRES and ILUC-GMRES solvers. The new methodology for the evaluation of the design parameter τ of the GLS scheme was extended to 3D problems. Similarly to the the 2D case, when the mesh resolution is low, the GLS scheme is more accurate than the classical Galerkin scheme.

In the next chapter, we develop a simple but reliable as well as cost effective computational procedure for representing the near and/or far field behavior of the scattered field.

BIBLIOGRAPHIE

Antoine, Xavier, Barucq Héléne, and Bendali Abderrahmane. 1999. ≪Bayliss-Turkel like radiation condition on surfaces of arbitrary shape≫. *Journal of Mathematical Analysis and Applications*, vol.229, n°3, p.184-211.

Bayliss, Alvin, Gunzburger Max and Turkel Eli. 1982.≪Boundary conditions for the numerical solution of elliptic equations in exterior regions ≫. *Society for Industrial and Applied Mathematics : Journal of Applied Mathematics*, vol.42, n°2, p.430-451.

Bérenger, Jean-Pierre. 1994. ≪A perfectly matched layer for the absorption of electromagneticwaves≫. *Journal of Computational Physics*, vol.114, n°2, (Octobre), p.185-200.

Bowman, John J., Senior Thomas B.A. and Uslenghi Piergiorgio L.E. 1969. *Electromagnetic and acoustic scattering by simple shape*, 1st ed. Amsterdam, The Netherlands : North-Holland Publishing Co. 728p.

Colton, David and Kress Rainer. 1992. *Inverse acoustic in electromagnetic scattering theory*. 2nd ed. ≪Applied Mathematics Sciences≫. vol.93, Berlin, Germany : Springer, 305 p.

Djellouli, Rabia, Farhat Charbel, Macedo Antonini and Tezaur Radek. 2000. ≪Finite element solution of two-dimensional acoustic scattering problems using arbitrarily shaped convex artificial boundaries≫. *Journal of Computational Acoustics*, vol.8, n°1, (Mars), p.81-99.

Enquist, Bjorn and Majda Andrew. 1977. ≪Absorbing boundary conditions for the numerical simulation of waves≫. *Mathematics of Computation*, vol.31, n°139, (Juillet), p.629-651.

Harrari, Isaac, Grosch Karl, Hughes Thomas J.R., Malhotra Manish, Pinsky Peter M., Stewart Jean R. and Thompson Lonny L. 1996. ≪Recent developpments in finite element methods for structural acoustics≫. *Archives of Computional Methods in Engineering*, vol.3, n°2-3, p.131-109.

Ihlenburg, Franck and Babuška Ivo. 1995. ≪Finite element solution of the helmholtz equation with high wavenumber Part I : the h-version of the fem.≫. *Computers and Mathematics with Applications*, vol.30, n°9, (Novembre), p.9-37.

Keller, Joseph B. and Givoli Dan. 1989. ≪Exact non reflecting boundary conditions≫. *Journal of Computational Physics*, vol.82, n°1, (Mai), p.172-192.

Li, Na, Saad Youcef and Chow Edmond. 2002. *Crout versions of ILU for general sparse matrices*. Coll. ≪Minnesota Supercomputer Institute Technical Report≫, UMSI-2002-021, Minneapolis (MN) : University of Minnesota, Minneapolis, 17p.

Mardochée, Magolu M.M. 2001. ≪Incomplete factorization based preconditionings for solving the helmholtz equation≫. *International Journal for Numerical Methods in Engineering* , vol.50, n°5, p.1077-1101.

Oberai, A. Assad and Pinsky M. Peter. 2000. ≪A numerical comparaison of finite element methods for the helmholtz equation≫. *Journal of Computational Acoustics*, vol.8, n°1, p.211-221.

Saad,Yousef. 1994. ≪ILUT : a dual threshold incomplete ILU factorization≫.*Numerical Linear Algebra with Applications*, vol.1, n°4 , p.387-402.

Saad, Yousef.1996 *Iterative Methods for Sparse Linear Systems*. 1st ed. Boston, USA : PWS Publishing Co., 447 p.

Saad, Yousef and Schultz Martin H. 1986. ≪GMRES : A Generalized minimal residual algorithm for solving nonsymmetric linear aystems ≫. *Society for Industrial and Applied Mathematics : Journal on Scientific and Statistical Computing*, vol.7, n°3, p.856-869.

Tezaur, Radek, Macedo Antonini, Farhat Charbel and Djellouli Rabia. 2000. ≪Three dimensional finite element calculations in acoustic scattering using arbitrarily shaped convex artificial boundaries≫. *International Journal for Numerical Methods in Engineering*, vol.53, n°3, p.1461-1476.

Zebic, Anabelle. 1992. *Equation de helmholtz : étude numérique de quelques preconditionneurs pour la méthode gmres*. Coll. ≪Rapport Technique de l'INRIA≫, RR-1802, Rocquencourt (France) : Institut National de Recherche en Informatique et en Automatique, 66p.

Résumé

Nous avons étudié dans ce chapitre de la résolution itérative de problémes 2D et 3D de diffraction acoustique régis par l'équation de Helmholtz. Deux schémas de discrétisation éléments finis ont été comparés. Le premier est associé à la méthode de Galerkin alors que le deuxième est associé à la méthode de Galerkin-moindres carrés. Une méthode originale de calcul du paramètre τ associé à ce dernier schéma a été proposée. Trois types de préconditionneurs algébriques : ILUT, ILUTC et ILU0 ont été testés afin d'accélérer la convergence du solveur GMRES.

Dans le prochain chapitre, nous développons une méthodologie simple et efficace permettant de calculer efficacement et à moindre coût la solution des problèmes de diffraction acoustique en 2D que ce soit en champ proche ou en champ lointain.

CHAPITRE 2

NUMERICAL ACCURACY OF A PADÉ-TYPE NON-REFLECTING BOUNDARY CONDITION FOR THE FINITE ELEMENT SOLUTION OF ACOUSTIC SCATTERING PROBLEMS AT HIGH-FREQUENCY

R. Kechroud[1],X. Antoine[2,3],and A. Soulaïmani[1],

[1] Département de Génie Mécanique, École de Technologie Supérieure,

1100 Notre-Dame Ouest, Montréal (Québec), Canada H3C 1K3

[2] Laboratoire de Mathématiques pour l'Industrie et la Physique, UMR 5640, UFR MIG, Université P. Sabatier,

118, route de Narbonne,31062 Toulouse Cedex, France

[3]Applied and Computational Mathematics, Division of Engineering and Applied Sciences, California Institute of Technology,

1200 E. California Blvd, 207-50, Pasadena, CA 91125, U.S.A.

This chapter is published as an article in International Journal For Numerical Methods In Engineering 2005 ; vol.64 :1275-1302.

The numerical solution of acoustic scattering problems in the high-frequency spectrum, and for large targets, remains one of the most challenging issues in scientific computing (Zienkiewicz,2000). Two major difficulties characterize these problems : the first difficulty is linked to *the unboundedness of the computational domain* and the second difficulty involves *a small asymptotic parameter*, the wavelength of the incident field compared to the characteristic size of the scatterer. Different numerical techniques, such as the boundary element methods (Colton and Kress,1983 ; Rokhlin,1990 ; Bruno and Kunyansky[1],2001 ; Bruno and Kunyansky [2],2001 ; Antoine and Darbas,2005 ; Nédélec,2001), the finite element methods (Harari,1996 ; Harari and Magoulès,2004 ; Djellouli et *al.*,2000 ; Tezaur et *al.*,2002 ; Bayliss et *al.*,1982 ; Bayliss and Turkel,1980 ; Bérenger,1994 ;Givoli,1999 ; Hagstrom,1999 ; Kechroud et *al.*,2004 ; Tsynkov,1998), the infinite element methods (Il-

henburg,1998), are available to solve these problems. However, the difficulties of simulation need to be further investigated to increase the accuracy of the computed solution and/or the frequency of the incident signal. Indeed, these two important practical issues generally require fine discretization grids associated to small spatial discretization steps. As a result, the solution of a large and highly indefinite linear system is generally required by means of an iterative solver (Antoine and Darbas,2005; Djellouli et *al.*,2000; Tezaur et *al.*,2002; Kechroud et *al.*,2004; Saad,1996).

Among all these improvements, the construction of accurate local approximate truncation boundary conditions defined on general-shaped and optimized fictitious boundaries is of utmost importance in computational acoustics. Since the pioneering work of Engquist and Majda (Engquist and Majda,1977) and Bayliss *et al.* (Bayliss et *al.*,1982 ; Bayliss and Turkel,1980), numerous developments and improvements have been achieved (Djellouli et *al.*,2000 ; Tezaur et *al.*,2002 ; Bérenger,1994 ; Givoli,1999 ; Hagstrom,1999 ; Kechroud et *al.*,2004 ; Tsynkov,1998 ; Antoine et *al.*,2006 ; Antoine et al.,1999) but the possibility of considering high-frequencies still remains challenging. In a series of recent papers (Djellouli et *al.*,2000; Tezaur et *al.*,2002; Farhat et *al.*,2002; Farhat and Hetmaniuk,2002; Hetmaniuk and Farhat,2003), it has been shown that the Bayliss-Gunzburger-Turkel-like (BGT-like) Absorbing Boundary Condition (ABC) developed in (Antoine et *al.*,1999) yields efficient and flexible iterative finite element solvers (Djellouli et *al.*,2000 ; Tezaur et *al.*,2002 ; Antoine,2001)which allow the handling of complex scattering configurations. This ABC has the interesting feature of being easy-to-implement in a finite element formulation for general arbitrarily-shaped two- and three-dimensional fictitious boundaries. The possibility of choosing a general fictitious boundary is an extremely important issue in the development of codes since it is the essential problem in the reduction of the computational domain. The general fictitious boundaries are important and are often met in practice if one considers an elongated scatterer, for example a three-dimensional submarine in computational acoustics (similar situations and questions occur for the full set

of Maxwell's equations in computational electromagnetism). However, even if the BGT-like ABC is flexible (Djellouli et *al.*,2000; Tezaur et *al.*,2002), the solution to a scattering problem in the high-frequency domain requires one to take into account higher harmonics in the scattered field (Antoine et *al.*,2006; Harari and Djellouli,2004). The BGT-like radiation boundary condition, which accurately models the first propagative modes, needs to be placed at a larger distance from the scatterer if one wishes to preserve an accurate computation. As a result, the involvement of a large size computational domain is required leading to stronger pollution effects in a Galerkin finite element method. Fine discretization meshes are therefore needed and lead to the resolution of very large scale indefinite linear systems.

Exact non-reflecting boundary operators can be used for scattering simulations. Unfortunately, to the best of the authors' knowledge, these exact operators are only available for specific simple shapes : half-plane, rectangles (by adding the suitable corner's conditions of Collino), circle, sphere (Givoli,2004) and ellipsoids (Thompson et *al.*,2000). This restriction to simple shapes is a serious bottleneck if we wish to solve scattering problems by general scatterers. Indeed, only having simple shapes at our disposal for the ABC directly contradicts our desire to choose a smooth arbitrarily-shaped fictitious boundary to reduce the computational domain. Another crucial point is also that we wish to have a local boundary condition admitting a sparse matrix representation in order to minimize the additional cost involved in the volumetric finite element solution. This characteristic is not associated to an exact condition which is non-local by nature.

A very promising research direction relies on the development of high-order Padé-type non-reflecting boundary conditions (Givoli,2004 ; Guddati and Tassoulas,2000 ; Thompson et *al.*,2001) as noticed in the recent review paper by Givoli (Givoli,2004). The author emphasizes the fact that high-order Padé-type non-reflecting boundary conditions are useful since they require the involvement of only a few additional (partial) differential equations on the fictitious surface for a nontrivial improvement of accuracy. Moreover, these

equations are second-order with respect to the tangential derivatives and hence do not need the consideration of high-order finite element methods (linear being sufficient). Furthermore, the equations being of differential type, they lead to sparse matrix representations in a finite element (or finite difference) context preserving the properties of the volumetric formulation associated with the Helmholtz equation. In our opinion, a compromise has to be reached. Indeed, it seems that we must choose between :

- an exact and *non-local* boundary condition given for a special simple shape but no optimized computational domain and an extra computational cost linked to the non-local character of the operator
- and the possibility of considering general shapes but with an approximate (and asymptotic in a certain way) *local* high-order boundary condition to optimize the computational domain for a general scatterer (and, incidentally, also to reduce the pollution in the finite element method) and to reduce the memory storage and time consuming.

We propose to investigate the second direction in view of the solution of high-frequency scattering problems for engineering calculations.

Our basic philosophy is to produce a high-order Padé-type BGT-like radiation condition for a general shape. The initial work of Bayliss *et al.* has been based on the development of a series of differential operators with the goal to annihilate the first terms of the high-frequency asymptotic expansion of the scattered field. Fundamentally, this approach makes the restrictive assumption that the scattered field admits an *a priori* Ansatz as a series in inverse integer powers of the wavenumber. This Ansatz is surely true if one considers that we are in the far-field zone but fails if we assume that we are in the near-field region. Indeed, as predicted by the general theory of diffraction, fractional terms (like $k^{-1/3}$) should be involved in the *a priori* near-field Ansatz of the diffracted field. If one expects to build an efficient extension of the BGT-like ABC, which can also be applied in the near-field zone in order to reduce the computational domain, then the annihilation operators should incorporate fractional powers of the wavenumber. In the initial

paper about the derivation of the BGT-like ABC (Antoine et *al.*,1999), the classical calculus of pseudodifferential operators has been used to extend the original BGT condition to the BGT-like ABC used in (Djellouli et *al.*,2000; Tezaur et *al.*,2002). Once again, this classical calculus assumes that we only consider integer powers of the wavenumber. This explains the singularity which appears in the principal symbol of the approximate non-reflecting boundary operator yielding the BGT conditions and which induces some errors in the approximation of the exact Dirichlet-to-Neumann map near the (local) cut-off frequencies. A detailed and formal study has been developed in (Antoine et *al.*,2006) which emphasizes these problems and proposes an alternative solution to increase the accuracy of the BGT-like ABC using a new smooth principal symbol for the approximation of the exact DtN map for an arbitrarily shaped scatterer. It is shown in (Antoine et *al.*,2006) that this new operator is quite efficient and accurate in the On-Surface Radiation Condition (OSRC) context (Antoine,2001; Kriegsmann et *al.*,1987) and most particularly in the high-frequency spectrum. This condition is also easy-to-use in a finite element code. Finally, the efficient extensions to both the three-dimensional acoustic and electromagnetism are given in (Darbas,2004). We propose here to numerically investigate its capability as an ABC to consider a small computational domain while remaining accurate (for far-field calculations for instance) in the high-frequency regime. We will also emphasize the fact that this new condition only requires a small changes to a basic finite element solver.

The plan of the paper is as follows. In Section 1, we recall some basic results concerning the sound-hard scattering problem and the BGT-like ABC. In Section 2, we introduce the Padé-type ABC and its formulation using some auxiliary surface functions. We explain the main features and properties of this condition and describe the main issues concerning its derivation. Section 3 concerns a possible (and non-unique) associated coupled variational formulation, its Galerkin Least-Squares finite element approximation (see (Harari,1996; Harari and Magoulès,2004) for instance) and its implementation in a preconditioned ILUT iterative GMRES solver (Kechroud et *al.*,2004; Saad,1996). (Note that

at this step, our goal is restricted to analyze the improvement induced by the new ABC in terms of mesh reduction and *not* to propose a high-performance iterative solver. Further developments still need to be realized essentially with respect to the preconditioning techniques. These implementation details are given to show that only small adaptations are required. We furthermore emphasize some difficult questions related to the new conditions, essentially, the solution to the associated linear system and the related choice of the variational formulations.) Section 4 deals with some first experiments concerning the behavior of the new ABC for different models of scatterers and general fictitious shapes. In Section 5, we analyze its performance to solve the scattering problem by a submarine-shaped scatterer. Section 6 deals with a few numerical results concerning the computational cost of our iterative scheme. In the last section, we discuss the conclusion and propose some possible directions and extensions.

2.1 Exact and approximate mathematical models

2.1.1 The two-dimensional exterior acoustic scattering problem

Let us define Ω^- as a two-dimensional bounded scatterer with boundary Γ. We denote by Ω^{ext} the associated exterior domain of propagation. Then, the scattering of an incident time-harmonic acoustic wave u^{inc} by an impenetrable scatterer Ω^- embedded in a homogeneous medium Ω^{ext} can be formulated as the following exterior boundary value problem (BVP) (Colton and Kress,1983; Nédélec,2001) find the scattered field u such that :

$$\begin{cases} \Delta u + k^2 u = 0, \ \text{ in } \Omega^{\text{ext}}, \\ u = g = -u^{\text{inc}} \ \text{ or } \ \partial_{\mathbf{n}_\Gamma} u = g = -\partial_{\mathbf{n}_\Gamma} u^{\text{inc}}, \ \text{ on } \Gamma, \\ \lim\limits_{|x|\to\infty} |x|^{1/2}(\nabla u \cdot \dfrac{x}{|x|} - iku) = 0. \end{cases} \tag{2.1}$$

The operator $\Delta = \sum_{j=1}^{2} \partial^2_{x_j}$ designates the usual Laplacian operator in Cartesian coordinates and $(\Delta + k^2)$ is the well-known Helmholtz operator. The real positive number k is the

wavenumber in the unbounded domain Ω^{ext}. This parameter is related to the wavelength λ of the incident signal by the relation $k = 2\pi/\lambda$. In the sequel, we consider an incident plane wave $u^{\text{inc}}(x) = e^{ik\mathbf{x}\cdot\mathbf{d}}$, where $\mathbf{d} = (\cos(\theta^{\text{inc}}), \sin(\theta^{\text{inc}}))^T$ is the normalized incidence vector in the polar coordinate system. The boundary conditions respectively model the classical sound-soft (Dirichlet) or sound-hard (Neumann) scattering problem for a datum g expressed in terms of incident field, denoting by $\mathbf{n}_\Gamma$ the outward unitary normal vector to Ω^- at the boundary Γ. Finally, the last relation is the well-known Sommerfeld radiation condition which yields the uniqueness of the solution to the BVP and the positiveness of the energy flux.

2.1.2 Formulation in a bounded domain with the BGT2-like NRBC

The solution to the above BVP can be obtained by truncating the exterior domain of propagation by a fictitious boundary Σ which surrounds the scatterer. For numerical purposes, one crucial choice consists of selecting a suitable *local* boundary condition on Σ to reduce the computational domain Ω of boundary $\Gamma \cup \Sigma$ without generating spurious reflections at the boundary. Such a condition is often called an *Artificial* or a *non-reflecting* Boundary Condition (ABC). We refer to (Givoli,1999; Hagstrom,1999; Tsynkov,1998; Givoli,2004) for a survey on the techniques of ABCs. Several methods for designing such conditions are available.

It has recently been shown by Farhat *et al.* (Djellouli et *al.*,2000 ; Tezaur et *al.*,2002 ; Farhat et *al.*,2002 ; Farhat and Hetmaniuk,2002 ; Hetmaniuk and Farhat,2003) that the second-order Bayliss-Gunzburger-Turkel-like (BGT) radiation condition derived in (Antoine et al.,1999) yields some efficient finite element calculations for two- and three-dimensional direct and inverse acoustic scattering problems for arbitrarily-shaped fictitious surfaces. For the sake of conciseness, we propose to only consider the sound-hard scattering problem, since the extension to the sound-soft scattering problem is straightforward. The approximate truncated BVP with the second-order BGT-like radiation condition

(Antoine et *al.*,1999) is set as :

$$\begin{cases} \Delta u + k^2 u = 0, \ \text{ in } \Omega, \\ \partial_{\mathbf{n}_\Gamma} u = g, \ \text{ on } \Gamma, \\ \partial_{\mathbf{n}_\Sigma} u = -M_2 u \ \text{ on } \Sigma, \end{cases} \tag{2.2}$$

where the unit normal vector $\mathbf{n}_\Sigma$ to Σ is outwardly directed to Ω. For brevity, we denote by u the approximate scattered field solution to the BVP (2.2). The last equation of system (2.2) defines an ABC on the general fictitious boundary Σ which is assumed to be convex. In (Antoine et *al.*,1999), this condition is built as a second-order Taylor expansion of the Dirichlet-to-Neumann (DtN) operator. We recall this process in the next subsection to compare the improvements of the new ABC with the usual BGT-like ABC. In two dimensions, the resulting symmetrical differential operator M_2 is defined by :

$$-M_2 u = iku - \frac{\kappa}{2}u + \frac{\kappa^2}{8(\kappa - ik)}u + \partial_s\left(\frac{1}{2(\kappa - ik)}\partial_s u\right) \tag{2.3}$$

where s is the counterclockwise directed arclength over Σ and $\kappa = \kappa(s)$ is the curvature at this point.

For the finite element approximation, the curvature is approximated by the following scheme : let $K = (ABC)$ be a triangle with vertices A, B and C on Σ_h (the discrete polygonal interpolated fictitious boundary), then the curvature can be accurately approximated at point B by :

$$\kappa(B) \simeq \frac{4\text{area}(K)}{abc}. \tag{2.4}$$

Real numbers a, b and c are the different side lengths of K satisfying $a \geq b \geq c$. The area of K is evaluated by the stable formula :

$$\text{area}(K) = \frac{\sqrt{(a+(b+c))(a+(b-c))(c+(a-b))(c-(a-b))}}{4}. \tag{2.5}$$

In the case of boundaries with curvature discontinuities, as for example for a rectangle, this numerical curvature has proven to be efficient (Antoine,2001; Antoine,2002).

Even if this condition is accurate in the medium frequency range (Djellouli et *al.*,2000; Tezaur et *al.*,2002), its precision decreases in the high-frequency regime if the fictitious boundary is too close to the scatterer. To obtain suitable calculations, a larger computational domain must be considered. As explained in details in the introduction, this leads to the solution of very large-size sparse linear systems which are computationally expensive both in memory and time, even with sophisticated solvers (see for instance the FETI-H method used in (Tezaur et *al.*,2002) for three-dimensional calculations). As a result, this is a significant limitation to the investigation of high-frequency direct scattering problems.

2.2 A high-order Padé-type ABC for high-frequency scattering

In a recent work (Antoine et *al.*,2006), a modification to the second-order BGT-like ABC has been proposed in the On-Surface Radiation Condition (OSRC) context (Antoine,2001; Antoine,2002; Kriegsmann et *al.*,1987). The new radiation condition takes the following form :

$$\partial_{n_\Sigma} u = ik\sqrt{1+\partial_s(\frac{1}{k_\epsilon^2}\partial_s)}\,u - \frac{\kappa}{2}u + \frac{\kappa^2}{8(\kappa-ik)}u - \partial_s(\frac{\kappa}{2k^2}\partial_s u), \qquad (2.6)$$

setting $k_\epsilon = k + i\epsilon$ as a new damped complex wavenumber. The ϵ damping parameter is optimized in (Antoine et *al.*,2006) as explained below and is related to both the frequency and curvature by : $\epsilon = 0.4k^{1/3}\kappa^{2/3}$. In the sequel, $\sqrt{z}$ designates the principal determination of the square-root of a complex number z with branch-cut along the negative real axis.

Let us emphasize the different original points concerning the derivation of this condition (see (Antoine et *al.*,2006) for more details). The first idea consists of locally mapping a neighborhood of a point on the surface to an open neighborhood of the half-plane using patches. The local portion of the exterior (respectively interior) space is mapped to the right (respectively left) half-plane, the part of the fictitious boundary coincides locally with the half-plane $\{x = 0\}$. Using the techniques of classical pseudodifferential calculus, the

principal (classical and homogeneous) symbol λ_1 (Taylor,1981) to the exterior Dirichlet-to-Neumann (DtN) map can be computed. Essentially, this term is :

$$\lambda_1 = ik\sqrt{1 - \frac{|\xi|^2}{k^2}}, \tag{2.7}$$

where ξ is the covariable by Fourier transform of s by mapping. For example, if one considers the symbol $\sigma(P) = -|\xi|^2$, the corresponding operator P is the Laplace-Beltrami operator $P = \Delta_\Sigma = \partial_s^2$ over the surface Σ. This means that, in terms of operator, we have a first approximation of the DtN map by a truncation of its *a priori* infinite (and unfortunately non-uniform) symbolical asymptotic expansion in homogeneous symbols. A higher-order approximation is :

$$\text{DtN} \approx \Lambda_{2-j} = \text{Op}(\sum_{l=j}^{1} \lambda_j) \tag{2.8}$$

taking into account the first $(2-j)$ terms. The notation $\text{Op}(\sigma)$ designates the operator given by inverse Fourier transform through the symbol σ. Let us now refer back to the equation (2.7). This operator is accurate if it is set on a straight boundary but becomes inaccurate for a curved boundary (a circle for example (Antoine et *al.*,2006)). More precisely, its singularity for frequencies $|\xi| \approx k$ implies that it does not model correctly the harmonics near the cut-off frequencies. These harmonics correspond to tangential modes which must be well-modelled as shown in (Antoine et *al.*,2006; Harari and Djellouli,2004) if one expects to have a fictitious boundary Σ closer to the physical boundary Γ, more particularly for high-frequencies. To realize this goal, the solution proposed in (Antoine et *al.*,2006) consists of locally regularizing the symbol λ_1 as :

$$\lambda_{1,\epsilon} = ik\sqrt{1 - \frac{|\xi|^2}{k_\epsilon^2}}, \tag{2.9}$$

with $k_\epsilon = k + i\epsilon$. The parameter ϵ is chosen so that it minimizes the reflection coefficient associated to the tangential modes for the circular cylinder of radius R. The estimate of this coefficient yields an nearly optimal parameter ϵ as : $\epsilon = 0.4k^{1/3}R^{-2/3}$. The associated

formal operator :

$$ik\sqrt{1+\frac{1}{k_\epsilon^2 R^2}\partial_\theta^2} \tag{2.10}$$

is then extended as :

$$ik\sqrt{1+\partial_s(\frac{1}{k_\epsilon^2}\partial_s)} \tag{2.11}$$

for a general smooth arbitrarily-shaped boundary Σ setting : $\epsilon = 0.4k^{1/3}\kappa^{2/3}$. The other corrective terms are kept from the usual classical approach (Antoine et *al.*,1999) and results in the condition (2.6). The new regularized and smooth symbol yields a uniform approximation of the DtN operator for any frequency ξ. This is not the case of the usual BGT-like ABC which only models the first propagative modes. Indeed, this condition is a local version of (2.8) using some second-order Taylor approximants for $k \gg |\xi|$; this remark is completely in accordance with the analytical study developed by Harari and Djellouli in (Harari and Djellouli,2004). We must emphasize the fact that the new ABC is not and cannot be an exact condition. Indeed, the estimate of the almost optimal parameter ϵ is formally developed for a circular cylinder to remove the singularity from the principal symbol. No estimates are available to control the error in the truncation of the approximate pseudodifferential operators and no strong mathematical foundations are yet given for the derivation of this condition. In our opinion, a deeper study would require the development of new pseudodifferential tools to study the behaviour of the DtN map in the transition region. However, these aspects remain a difficult task and further studies are required.

The main drawback of the new boundary condition is that it involves a non-local operator -the square-root operator- which is expensive to compute directly (Antoine et *al.*,2006). A possible approach to avoid this drawback consists of using a suitable rational approximation of this operator. This results in the solution to a set of a local differential equations defined on Σ and gives a local representation of this non-local operator which can thus be

quickly evaluated. In (Antoine et *al.*,2006), the approach of Milinazzo *et al.* (Milinazzo et *al.*,1997) has been used to propose an efficient approximation of the square-root operator using some complex Padé-type approximations of order N. More precisely, the following approximation (called the rotating branch-cut approximation) is used :

$$\sqrt{1+z} \approx C_0 + \sum_{j=1}^{N} \frac{A_j z}{1 + B_j z}, \tag{2.12}$$

where

$$C_0 = \exp(i\frac{\theta}{2}) R_N(\exp(-i\theta) - 1) \tag{2.13}$$

and

$$A_j = \frac{\exp(-i\frac{\theta}{2}) a_j}{(1 + b_j(\exp(-i\theta) - 1))^2} \quad B_j = \frac{\exp(-i\theta) b_j}{(1 + b_j(\exp(-i\theta) - 1))^2}. \tag{2.14}$$

Here, θ stands for the chosen angle of rotation and $(a_j, b_j)_{j=1,...,N}$ are the standard real Padé coefficients given by :

$$a_j = \frac{2}{2N+1} \sin^2(\frac{j\pi}{2N+1}) \quad b_j = \cos^2(\frac{j\pi}{2N+1}). \tag{2.15}$$

We define $R_N(z)$ as the real Padé approximation of the square-root :

$$R_N(z) = 1 + \sum_{j=1}^{N} \frac{a_j z}{1 + b_j z}. \tag{2.16}$$

Finally, an approximation of order N of the ABC (2.6) is given by :

$$\partial_{\mathbf{n}_\Sigma} u = ik(C_0 u + \sum_{j=1}^{N} A_j \varphi_j) - \frac{\kappa}{2} u + \frac{\kappa^2}{8(\kappa - ik)} u - \partial_s(\frac{\kappa}{2k^2} \partial_s u), \text{ on } \Sigma, \tag{2.17}$$

where $\{\varphi_j\}_{j=1,..N}$ are the auxiliary surface functions defined on Σ which fulfill the following differential equations :

$$(1 + \partial_s(\frac{B_j}{k_\epsilon^2} \partial_s))\varphi_j = \partial_s(\frac{1}{k_\epsilon^2} \partial_s) u, \text{ on } \Sigma, \ j = 1, ..., N. \tag{2.18}$$

Parameters $N = 8$ and $\theta = \pi/4$ have proven to yield the best accuracy in the OSRC techniques. We will again discuss this crucial choice in the sequel in the framework of ABCs.

2.3 Iterative Krylov finite element solution

2.3.1 Variational formulation

To apply the finite element method, the sound-hard scattering problem with the ABC (2.6)-(2.12) is written in a variational form find $(u, \varphi_1, ..., \varphi_N)$ in $H^1(\Omega) \times H^1(\Sigma)^N$ such that :

$$\mathcal{A}(u, v) + \sum_{j=1}^{N} \mathcal{B}_j(\varphi_j, v) = b(v), \quad \forall\, v \in H^1(\Omega) \tag{2.19}$$

where $\mathcal{A}$ is the symmetrical bilinear form defined on $H^1(\Omega) \times H^1(\Omega)$ by :

$$\begin{aligned} \mathcal{A}(u, v) = &\int_\Omega \nabla u \nabla v d\Omega \; - \; k^2 \int_\Omega uv d\Omega \; - ikC_0 \int_\Sigma uv d\Sigma + \frac{1}{2}\int_\Sigma \kappa uv d\Sigma \\ &-\frac{1}{8}\int_\Sigma \frac{\kappa^2}{\kappa - ik} uv d\Sigma + \frac{1}{2k^2}\int_\Sigma \kappa \partial_s u \partial_s v d\Sigma. \end{aligned} \tag{2.20}$$

The spaces $H^1(\Omega)$ and $H^1(\Sigma)$ are the usual Sobolev spaces, respectively on Ω and Σ. For $j = 1, ..., N$, we have that $\mathcal{B}_j$ is also a symmetrical bilinear form defined on $H^1(\Sigma) \times H^1(\Sigma)$ and given by the following expression :

$$\mathcal{B}_j(\varphi_j, v) = -ikA_j \int_\Sigma \varphi_j v d\Sigma. \tag{2.21}$$

The right-hand side b is a linear form related to the initial incident field by the weak representation :

$$b(v) = \int_\Gamma g v d\Gamma. \tag{2.22}$$

Obviously, variational equation (2.19) is not sufficient. It is necessary to add to the system the decoupled differential constraints (2.18) between the auxiliary functions and the unknown approximate scattered field :

$$\mathcal{C}(u, \psi_j) + \mathcal{D}_j(\varphi_j, \psi_j) = 0, \; \forall \psi_j \in H^1(\Sigma), \quad j = 1, ..., N, \tag{2.23}$$

where $\mathcal{C}$ and $\mathcal{D}_j$ are two symmetrical bilinear forms defined on $H^1(\Sigma) \times H^1(\Sigma)$ respectively by :

$$\mathcal{C}(u, \psi_j) = \int_\Sigma \frac{1}{k_\epsilon^2} \partial_s u \partial_s \psi_j d\Sigma \tag{2.24}$$

and

$$\mathcal{D}_j(\varphi_j, \psi_j) = \int_\Sigma \varphi_j \psi_j d\Sigma - \int_\Sigma \frac{B_j}{k_\epsilon^2} \partial_s \varphi_j \partial_s \psi_j d\Sigma. \tag{2.25}$$

This formulation introduces only some additional mass and stiffness-like matrices linked to the finite element discretization of equations (2.19) and (2.23). This particularly interesting aspect of (2.19) and (2.23) is related to the fact that the Padé approximation yields a localization of the square-root operator. Moreover, each bilinear form $\mathcal{A}$, $\mathcal{B}$, $\mathcal{C}$ and $\mathcal{D}$ is symmetrical. This is an interesting advantage from a memory storage point of view.

At this point of the method, we must emphasize the fact that other alternative variational formulations could be investigated. This point is important from the practical point of view if one wishes to solve the resulting system by means of an iterative solver. Indeed, the condition number of the system is deeply linked to the variational formulations. Other global symmetrical formulations (and this is not the case here since $\mathcal{B}$ is not the transposed bilinear form of $\mathcal{C}$) could be investigated. However, it seems that this is at the price of the development of a mixed variational formulation and the use of adapted finite element methods. This aspect can be more specifically observed in the three-dimensional case (because of the presence of the surface divergence and surface gradient operators). But these extensions are beyond the scope of the present paper.

2.3.2 The Galerkin-Least-Squares finite element method

We will compare two finite element methods in the sequel of the paper. The first one is the classical Galerkin Finite Element Method (FEM). To partially avoid the dispersion effects generally associated to this first technique, we also consider the Galerkin-Least-Squares (GLS) discretization scheme. In the GLS approach, the variational formulation is adjusted

to take into account the residual of the partial differential equation. Under this constraint, the stabilized weak form of the equation is :

$$\mathcal{A}_{\text{GLS}}(u,v) + \sum_{j=1}^{N} \mathcal{B}_j(\varphi_j, v) = b(v), \tag{2.26}$$

setting

$$\mathcal{A}_{\text{GLS}}(u,v) = \mathcal{A}(u,v) + \int_{\widetilde{\Omega}} \eta \mathcal{L}u \mathcal{L}v d\Omega,$$

where $\mathcal{L} = (\Delta + k^2)$ is the Helmholtz operator and $\widetilde{\Omega}$ designates the union of interior elements. This last choice is generally made according to the regularity requirements of typical, piecewise smooth finite-element functions. One crucial question is the choice of the stabilization parameter η which is generally based on a design criterion. Harari *et al.* (Harari,1996) evaluate η analytically assuming that the scattered wave is planar. As a result, the accuracy of the obtained results depends on the direction of propagation. Two values of η corresponding to a direction equal to 0 and to 22.5 degrees are often used in practice (Harari,1996) for a mesh based on bilinear finite elements. In our numerical experiments, we use the numerical definition of the parameter η proposed by (Kechroud et *al.*,2004). From numerical investigations, it appears that the η corresponding to 22.5 degrees yields the best results for a mesh based on triangular elements. In the sequel, we only report the numerical results associated to this value. Moreover, this approximation will be compared to the classical linear Galerkin finite element discretization. Numerical results will be reported for comparison.

2.3.3 Preconditioned iterative Krylov scheme

The linear finite element discretization results in a linear coupled system of equations of the form :

$$\begin{pmatrix} \mathbf{A}_h & \mathbf{B}_h \\ \mathbf{C}_h & \mathbf{D}_h \end{pmatrix} \begin{pmatrix} \mathbf{u}_h \\ \boldsymbol{\varphi}_h \end{pmatrix} = \begin{pmatrix} \mathbf{b}_h \\ \mathbf{0}_h \end{pmatrix}, \tag{2.27}$$

where $\mathbf{u}_h \in \mathbb{C}^{N_h}$ is the unknown complex-valued approximation of the scattered field u and $\boldsymbol{\varphi}_h$ is the complex vector field of discretized auxiliary functions $(\varphi_{1h}, \ldots, \varphi_{Nh})$. Hence, this vector is in $\mathbb{C}^{N_{\Sigma_h} N}$, where N_h and N_{Σ_h} are respectively the number of degrees of freedom of the linear finite element method on the interpolated domains Ω_h and Σ_h. Vector $\mathbf{b}_h \in \mathbb{C}^{N_h}$ is given by the linear form b.

The complex linear system (2.27) is sparse and globally non-symmetric. Furthermore, this is also a non-Hermitian and non-diagonally dominant system of equations. A direct solution can be reached by using a Gauss elimination solver. However, due to the excessive cost of these latter methods, especially at high frequencies for three-dimensional problems where the solution to a large size linear system is required, iterative schemes are generally preferred. This is the reason why we adapt this point of view even if a direct solver could also be used in the two-dimensional case.

The proposed solution is based on the Schur complement which consists of eliminating the unknown $\boldsymbol{\varphi}_h$ in system (2.27) so that the new system to solve is :

$$\mathbf{G}_h \mathbf{u}_h = \mathbf{b}_h \quad \text{setting} \quad \mathbf{G}_h = \mathbf{A}_h - \mathbf{B}_h \mathbf{D}_h^{-1} \mathbf{C}_h. \tag{2.28}$$

Among the possible iterative methods, a restarted GMRES (Saad,1996) solver accelerated by an ILUT preconditioner (based on $\mathbf{A}_h$) is then used (Kechroud et *al.*,2004). To check that no additional error is introduced in our algorithm, we have fixed the residual of the GMRES to 10^{-6} which (after verifications) is sufficient to have a negligeable error compared to the one arising in both the ABC and finite element approximations.

Our goal here is mainly to analyze the accuracy of the new Padé-type ABC. However, for the sake of completeness, we will report in Section 6 some numerical results concerning the behavior of the iterative scheme in terms of speed up and convergence rate which are closely linked to the structure of the linear system to be solved (as already mentioned above). From these computations, we must first notice that the added cost linked to the

solution to each auxiliary equation is efficiently realized using a restarted GMRES preconditioned by the ILUT technique at a small additional overall cost. Indeed, the convergence is obtained in 2 or 3 iterations with an excellent accuracy. A second point is that the convergence breakdown of the iterative scheme observed in (Kechroud et *al.*,2004) can be overcame by adding a damping parameter to the Helmholtz operator with which the preconditioner is built (called in the sequel deflated ILUT). Finally, to obtain a more efficient preconditioner for the iterative solution, we should rather consider the matrix $\mathbf{G}_h$ for building a suitable preconditioner, as in the case of generalized saddle point problems (Little et *al.*,2003). This very difficult aspect for highly indefinite linear systems is beyond the scope of this paper and further investigations are still required. Concerning the memory storage, the additional cost compared to the one associated to the BGT-like ABC is only linked to the surface linear systems resulting from the auxiliary equations. We will later see that $N = 2$ equations is sufficient for a very important reduction of the volumetric mesh. So globally, for one given problem using a close fictitious boundary Σ, the memory will be sligthly increased but with a gain of accuracy.

2.4 Performances and comparisons for some model test problems

We consider in this section two model sound-hard scatterers to test the proposed algorithm : a unit circular cylinder $\mathcal{D}$ and an elliptical cylinder $\mathcal{E}$ with a major semi-axis equal to $a = 1$ and a minor semi-axis equal to $b = 0.2$, both centered at the origin. The reference solution is computed by using the CHIEF integral equation method developed in (Kirkup,1998). The mesh resolution for this technique has been fixed to 80 elements per wavelength.

2.4.1 The sound-hard circular cylinder

In all the computations, we assume that $\mathcal{D}$ is illuminated by a plane wave with a zero-degree incidence. The wave number is set to $k = 50$. The circular fictitious boundary is placed at a distance $m\lambda$ from the scatterer (Fig.2.1)

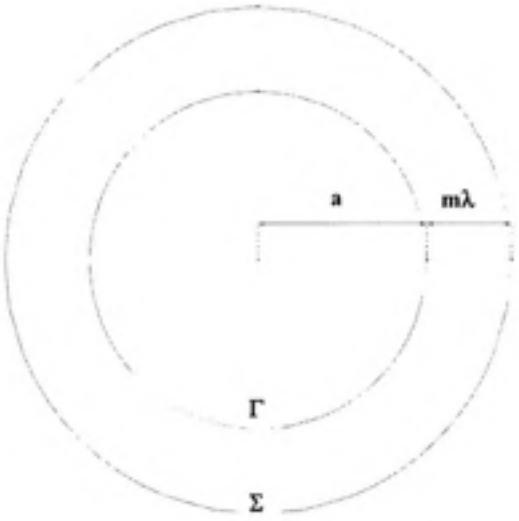

Figure 2.1 ***The circular shaped scatterer surrounded with a circular artificial boundary.***

. The average mesh resolution -the average number of elements per wavelength- is given by $n_\lambda = \lambda/h_{\max}$, where $h_{\max}$ is the largest element size of the finite element method. The relative Root-Mean Square (RMS) error (in percents) on the computational domain Ω_h (respectively Γ_h) is computed in the $L_2(\Omega_h)$-norm (respectively $L_2(\Gamma_h)$-norm) with respect to the reference analytical solution expressed as a Mie series. We also compute the far-field pattern given by the scattering amplitude :

$$a_\infty(\vartheta) = \frac{e^{-i\frac{\pi}{4}}}{\sqrt{8\pi k}} \int_\Gamma (\partial_{\mathbf{n}_\Gamma(y)} u(y) - ik\vartheta \cdot \mathbf{n}_\Gamma(y) u(y)) e^{-ik\vartheta \cdot y} d\Gamma(y) \qquad (2.29)$$

through the bistatic Radar Cross Section (RCS) (also called the target strength)

$$\mathrm{RCS}(\vartheta) = 10\log_{10}(2\pi|a_\infty(\vartheta)|^2) \ \text{(dB)}, \tag{2.30}$$

setting $\boldsymbol{\vartheta} = (\cos(\vartheta), \sin(\vartheta))^T$.

Let us begin by setting the two parameters N and θ defining the Padé-type ABC. We present in Tables 2.1 (for $m = 1/4$) and 2.2 (for $m = 1$) the error in the computational domain and on the trace by increasing the number of auxiliary Padé functions and modifying the rotation angle θ between 0 and $\pi/2$. The resolution of the Galerkin FEM is $n_\lambda = 40$ to obtain a satisfactory accuracy. A judicious choice of angle is $\theta = \pi/6$ or $\theta = \pi/3$ and $N = 2$. In the sequel, we report the results for these two angles. Generally speaking, $\pi/6$ yields a better accuracy than $\pi/3$ for a closer boundary. This will be essential in the case of the submarine-shaped scatterer. However, to notice the sensitivity of the results according to θ and for the sake of completeness, we choose to also report the results concerning $\pi/3$. We do not give here the results for $N = 1$ which yield a similar accuracy as for the BGT-like ABC.

Table 2.1

RMS relative error on the interior solution (on the trace) of the computed scattered field for different values of the parameters defining the Padé-type ABC and the BGT-like ABC. The mesh resolution is fixed to $n_\lambda = 40$ and $m = 1/4$ for the Galerkin scheme

	$N = 2$	$N = 4$	$N = 8$	BGT
$\theta = 0$	3.30 (3.08)	5.57 (5.26)	4.63 (4.41)	17.40 (17.18)
$\theta = \pi/6$	1.94 (1.91)	4.35 (4.12)	4.68 (4.45)	17.40 (17.18)
$\theta = \pi/3$	4.07 (3.95)	4.64 (4.12)	4.67 (4.44)	17.40 (17.18)
$\theta = \pi/2$	6.02 (6.18)	4.81 (4.58)	4.67 (4.44)	17.40 (17.18)

Let us now investigate in details the accuracy issue linked to the new ABC. To that end, we report on Tables 2.3 (Galerkin) and 2.4 (GLS) the error on both the computational domain and the trace accordingly to the size of the computational domain at different mesh

Table 2.2

RMS relative error on the interior solution (on the trace) of the computed scattered field for different values of the parameters defining the Padé-type ABC and the BGT-like ABC. The mesh resolution is fixed to $n_\lambda = 40$ and $m = 1$ for the Galerkin scheme

	$N = 2$	$N = 4$	$N = 8$	BGT
$\theta = 0$	1.16 (0.73)	1.08 (0.76)	1.08 (0.76)	8.04 (8.80)
$\theta = \pi/6$	1.22 (0.87)	1.08 (0.76)	1.08 (0.76)	8.04 (8.80)
$\theta = \pi/3$	1.26 (1.07)	1.08 (0.76)	1.08 (0.76)	8.04 (8.80)
$\theta = \pi/2$	3.35 (4.21)	1.06 (0.71)	1.08 (0.76)	8.04 (8.80)

Table 2.3

Circular cylinder : RMS error for different mesh resolutions of the Galerkin FEM and ABC positions. The values in parenthesis correspond to the error on the trace

m	n_λ	N_h	N_{Σ_h}	BGT	Padé $(\pi/6, 2)$	Padé $(\pi/3, 2)$
1/8	10	998	499	21.31(21.31)	8.03(7.32)	10.70(10.23)
	20	2997	999	21.66(21.45)	2.64(2.40)	5.79(5.66)
	40	9995	1999	21.76(21.48)	1.97(1.90)	4.71(4.64)
1/4	10	1497	499	18.15(17.81)	8.99(7.78)	11.24(10.28)
	20	5994	999	17.45(17.25)	3.00(2.75)	5.40(5.17)
	40	21989	1999	17.40(17.18)	1.94(1.91)	4.07(3.95)
1/2	10	2994	499	16.38(15.15)	10.70(7.76)	11.74(8.78)
	20	10989	999	13.03(13.37)	3.48(2.81)	4.47(3.69)
	40	41979	1999	12.39(12.97)	1.81(1.76)	2.90(2.70)
1	10	4990	499	19.17(11.50)	16.11(7.64)	15.91(7.53)
	20	19980	999	9.51(8.61)	4.14(1.86)	4.00(2.01)
	40	79960	1999	8.04(8.80)	1.22(0.87)	1.26(1.07)
2	10	9980	499	26.99(8.84)	26.37(7.55)	26.35(7.61)
	20	39960	999	7.97(4.16)	6.99(2.02)	7.03(2.16)
	40	159920	1999	3.75(4.06)	1.76(0.64)	1.78(0.64)

resolutions. For each case, the mesh is described by N_h and N_{Σ_h}. We clearly see that for an *a priori* fixed error, we can move the fictitious boundary closer to the scatterer for the Padé-type ABC without a significant deterioration in accuracy. This is not the case of the usual BGT-like ABC which can yield a poor precision. This remark shows that we can significantly reduce the size of the computational domain using the new ABC. Moreover,

Table 2.4

Circular cylinder : RMS error for different mesh resolutions of the $GLS_{22.5}$ FEM and ABC positions. The values in parentheses correspond to the error on the trace

m	n_λ	N_h	N_{Σ_h}	BGT	Padé $(\pi/6, 2)$	Padé $(\pi/3, 2)$
1/8	10	998	499	21.73(21.81)	7.23(7.26)	9.65(9.75)
	20	2997	999	21.71(21.49)	2.08(1.98)	5.31(5.25)
	40	9995	1999	21.76(21.48)	1.81(1.76)	4.57(4.50)
1/4	10	1497	499	17.94(17.98)	8.39(9.19)	10.18(10.88)
	20	5994	999	17.27(17.02)	2.32(2.37)	4.82(4.75)
	40	21989	1999	17.34(17.11)	1.70(1.70)	3.88(3.78)
1/2	10	2994	499	13.29(12.14)	8.48(7.75)	9.62(8.80)
	20	10989	999	12.10(12.27)	2.90(2.37)	3.75(3.47)
	40	41979	1999	12.16(12.68)	1.49(1.56)	2.73(2.62)
1	10	4990	499	12.59(7.35)	12.10(8.38)	12.33(8.85)
	20	19980	999	7.67(7.59)	3.15(2.27)	3.39(2.74)
	40	79960	1999	7.66(8.59)	1.14(1.09)	1.41(1.40)
2	10	9980	499	19.52(6.20)	19.68(8.08)	19.70(8.17)
	20	39960	999	5.65(3.10)	5.14(2.22)	5.17(2.23)
	40	159920	1999	3.30(3.87)	1.34(0.80)	1.37(0.67)

for a distance $m\lambda$ and a given mesh resolution n_λ, the Padé-type ABC leads to a much smaller error than the BGT-like ABC. Once again, we do not report here the error associated to the case $N = 1$ which is similar to the one obtained with the BGT-like condition. According to the previous results, we can then get a smaller domain of computation or an improvement in accuracy during the simulation if we use the Padé-type ABC. This conclusion can be related to the property that, unlike the BGT-like ABC, the new ABC is built to include both the propagative and the evanescent harmonics involved in the scattered field. Moreover, the latter condition incorporates in an approximate way the high order harmonics present in the field computation and which can propagate near a tangential direction to the fictitious boundary ; the harmonics are more important when Σ is close to Γ. We also notice that a mesh resolution $n_\lambda = 20$ mostly leads to an acceptable accuracy, in particular in the calculation of the trace. This can be further slightly reduced with the help of the GLS scheme. The reduction in the size of the computational domain partially limits the pollution effects which are generally involved in a FEM at high-frequencies (see

Table 2.5

Circular cylinder : RMS error for different mesh resolutions of the GLS FEM and BGT-like ABC positions. The values in parentheses correspond to the error on the trace

m	n_λ	GLS_0	$GLS_{22.5}$	GLS_{30}	GLS_{45}	GLS_{60}	GLS_{90}
1/8	10	22.40(22.48)	21.73(21.81)	21.91(21.99)	23.33(23.31)	23.33(23.31)	22.45(22.53)
	20	21.79(21.55)	21.71(21.49)	21.74(21.51)	21.85(21.60)	21.98(21.72)	21.80(21.56)
	40	21.78(21.49)	21.76(21.48)	21.77(21.49)	21.79(21.50)	21.82(21.53)	21.78(21.49)
1/4	10	19.13(19.21)	17.94(17.98)	18.21(18.22)	19.52(19.48)	19.97(19.76)	19.21(19.28)
	20	17.21(16.87)	17.27(17.02)	17.26(16.99)	17.21(16.87)	17.22(16.84)	17.21(16.87)
	40	17.31(17.05)	17.34(17.11)	17.33(17.10)	17.31(17.06)	17.31(17.04)	17.31(17.05)
1/2	10	13.35(12.24)	13.28(12.14)	13.25(12.02)	13.57(12.21)	12.97(11.40)	13.35(12.24)
	20	11.44(11.38)	12.10(12.28)	12.00(12.15)	11.50(11.44)	10.99(10.78)	11.41(11.34)
	40	11.94(12.40)	12.16(12.68)	12.13(12.64)	11.96(12.42)	11.82(12.24)	11.93(12.39)
1	10	13.28(9.98)	12.59(7.35)	13.16(7.80)	14.70(10.16)	14.39(11.29)	13.38(10.10)
	20	7.02(7.45)	7.67(7.59)	7.63(7.57)	7.25(7.52)	6.80(7.60)	7.00(7.46)
	40	7.43(8.50)	7.66(8.59)	7.63(8.58)	7.46(8.52)	7.36(8.54)	7.42(8.50)
2	10	19.00(9.40)	19.52(6.10)	20.51(6.55)	21.48(9.22)	19.66(10.77)	19.05(9.53)
	20	5.29(3.36)	5.65(3.10)	5.87(3.11)	6.03(3.37)	5.42(3.62)	5.30(3.39)
	40	3.15(3.81)	3.30(3.87)	3.31(3.86)	3.25(3.83)	3.13(3.82)	3.15(3.81)

Table 2.6

Circular cylinder : RMS error for different mesh resolutions of the GLS FEM and Padé$(\pi/6, 2)$ ABC positions. The values in parentheses correspond to the error on the trace

m	n_λ	GLS_0	$GLS_{22.5}$	GLS_{30}	GLS_{45}	GLS_{60}	GLS_{90}
1/8	10	8.12(8.58)	7.23(7.27)	7.37(7.50)	8.24(8.72)	7.80(8.34)	8.17(8.64)
	20	1.96(1.96)	2.08(1.98)	2.02(1.95)	1.87(1.89)	1.54(1.57)	1.96(1.97)
	40	1.72(1.67)	1.81(1.76)	1.79(1.73)	1.68(1.63)	1.62(1.57)	1.71(1.67)
1/4	10	12.00(13.47)	8.39(9.19)	9.29(10.20)	12.97(14.28)	13.80(15.32)	12.19(13.65)
	20	2.31(2.60)	2.32(2.37)	2.31(2.38)	2.36(2.60)	2.05(2.37)	2.31(2.60)
	40	1.53(1.55)	1.71(1.70)	1.68(1.67)	1.54(1.55)	1.41(1.43)	1.52(1.54)
1/2	10	12.46(13.50)	8.48(7.75)	9.15(8.56)	12.80(13.17)	14.83(15.94)	12.65(13.71)
	20	3.16(3.57)	2.50(2.37)	2.59(2.51)	3.27(3.51)	3.51(3.96)	3.20(3.61)
	40	1.39(1.57)	1.49(1.56)	1.48(1.55)	1.42(1.57)	1.35(1.56)	1.39(1.57)
1	10	14.58(11.87)	12.10(8.38)	13.01(8.97)	13.01(8.97)	15.92(11.91)	14.75(12.01)
	20	3.84(3.31)	3.15(2.27)	3.38(2.43)	4.18(3.27)	4.26(3.63)	3.88(3.35)
	40	1.26(1.30)	1.14(1.09)	1.18(1.12)	1.33(1.29)	1.33(1.39)	1.27(1.31)
2	10	19.54(11.15)	19.68(8.08)	20.70(8.41)	21.86(10.97)	20.17(12.17)	19.60(11.27)
	20	5.14(3.13)	5.14(2.23)	5.42(2.32)	5.84(3.05)	5.38(3.47)	5.16(3.17)
	40	1.36(1.01)	1.34(0.80)	1.41(0.82)	1.53(0.99)	1.42(1.09)	1.36(1.02)

Table 2.7

Circular cylinder : RMS error for different mesh resolutions of the GLS FEM and Padé$(\pi/3, 2)$ ABC positions. The values in parentheses correspond to the error on the trace

m	n_λ	GLS_0	$GLS_{22.5}$	GLS_{30}	GLS_{45}	GLS_{60}	GLS_{90}
1/8	10	9.62(10.08)	9.65(9.75)	9.56(9.74)	9.40(9.90)	8.38(8.98)	9.62(10.08)
	20	5.01(4.99)	5.31(5.25)	5.21(5.16)	4.84(4.83)	4.84(4.83)	4.99(4.98)
	40	4.46(4.40)	4.57(4.50)	4.54(4.47)	4.41(4.35)	4.32(4.26)	4.46(4.40)
1/4	10	12.38(13.83)	10.18(10.88)	11.64(11.48)	12.94(14.32)	13.09(14.76)	12.50(13.96)
	20	4.50(4.60)	4.82(4.75)	4.77(4.73)	4.54(4.62)	4.12(4.27)	4.48(4.59)
	40	3.72(3.64)	3.88(3.78)	3.86(3.77)	3.73(3.65)	3.61(3.54)	3.71(3.64)
1/2	10	12.83(13.87)	9.62(8.80)	10.15(9.47)	13.19(13.58)	14.94(16.19)	12.99(14.07)
	20	4.09(4.37)	3.75(3.47)	3.80(3.57)	4.19(4.32)	4.30(4.72)	4.12(4.41)
	40	2.64(2.64)	2.73(2.62)	2.72(2.62)	2.66(2.64)	2.60(2.05)	2.64(2.64)
1	10	14.95(12.42)	12.33(8.85)	13.27(9.46)	13.26(9.46)	17.01(13.99)	15.12(12.57)
	20	4.21(3.80)	3.39(2.74)	3.63(2.90)	4.52(3.75)	4.67(4.15)	4.25(3.84)
	40	1.62(1.60)	1.41(1.40)	1.46(1.44)	1.67(1.64)	1.72(1.75)	1.63(1.66)
2	10	19.58(11.14)	19.70(8.17)	20.73(8.48)	21.86(11.00)	20.17(12.09)	19.62(11.25)
	20	5.15(3.08)	5.17(2.23)	5.44(2.31)	5.84(2.99)	5.38(3.40)	5.16(3.11)
	40	1.33(0.87)	1.34(0.67)	1.40(0.69)	1.50(0.85)	1.39(0.95)	1.36(0.88)

(Djellouli et *al.*,2000) for a similar remark in the case of the BGT-like ABC). These two aspects are crucial since they allow an accurate computation of the scattered field based on the Helmholtz integral representation (2.29).

To analyze how the effect of the angle is involved in the GLS scheme, we report on Tables 2.5, 2.6 and 2.7, the errors of the GLS scheme for different angles and ABCs. A first observation is that, in the case of the BGT-like ABC, the error is not always decaying according to the mesh size. This can be explained by the fact that we compute the error between the exact Mie series solution and the BGT solution. Since there is always an important analytical error if the fictitious boundary is placed close enough to the scatterer, the convergence of the finite element method is polluted by this anaytical error. However, this latter error tends to disappear as m grows and the convergence of the finite element solution is again observed more clearly. We do not observe this problem with the Padé-type ABC which exhibits a much higher accuracy. Let us now consider Table 2.6. We remark

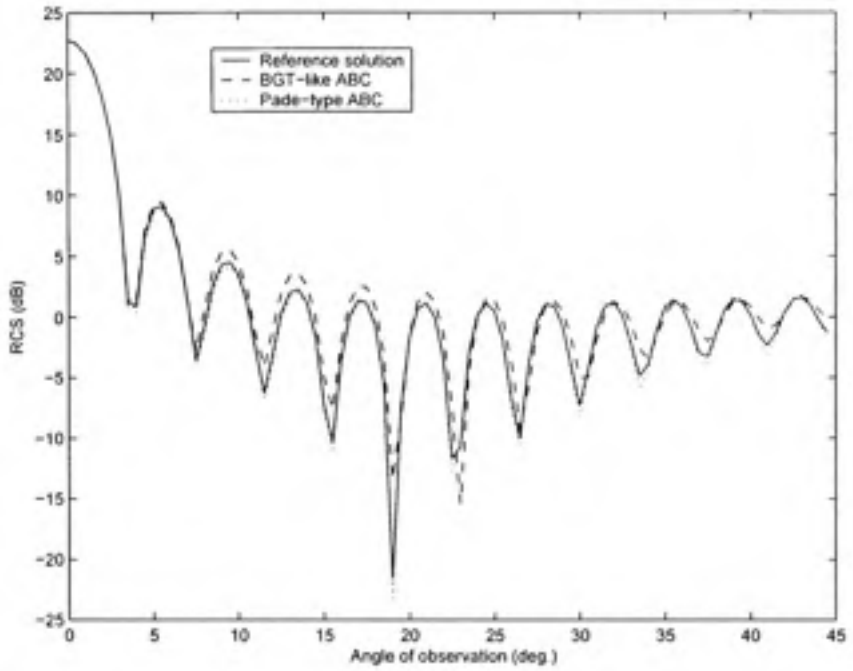

Figure 2.2 ***Far-field pattern (between 0 and 45 degrees) of the unit circular cylinder using the BGT-like ABC.***

that, from a general point of view, the direction 22.5 degrees is not far from being optimal to design a reliable GLS scheme for some densities $n_\lambda = 10$ and $n_\lambda = 20$. This is in accordance with the results derived by Harari and Nogueira in (Harari and Nogueira,2002). As a consequence, from now on, we will consider this almost optimal direction in the GLS scheme.

To end this section, we display in Figure 2.2 a part of the RCS associated to the BGT-like and Padé-type ABCs (setting $\theta = \pi/6$). The parameters are set to $k = 50$, $m = 1/8$ and the mesh resolution is $n_\lambda = 20$ elements per wavelength for the GLS method. We immediately observe that the computed RCS for the Padé-type condition is much more accurate than using the BGT-like condition. A similar accuracy for this latter condition would have required the placement of the boundary at $m = 2$ wavelengths. Thus, this would have dramatically increased the size of the finite element mesh and the associated linear system

to solve. Finally, all the results presented here extend to higher wavenumbers. Moreover, a better accuracy is still observed when solving the sound-soft scattering problem.

2.4.2 The sound-hard elliptical cylinder

We now consider the sound-hard elliptical scatterer $\mathcal{E}$ illuminated by a plane wave at a frequency $k = 50$ for an incidence angle equal to $\theta^{inc} = 20$ degrees. We report in Table 2.8 the RMS error on the trace of the computed solution for various ABCs for both the Galerkin (in parentheses) and GLS schemes.

Table 2.8

Elliptical cylinder : RMS error on the trace for different mesh resolutions of the $GLS_{22.5}$ FEM and ABC positions (on a circular (C) or elliptical shaped fictitious boundary. The values between parentheses correspond to the Galerkin FEM

m	n_Λ	N_Λ	N_{Σ_Λ}	BGT	Padé $(\pi/6, 2)$	Padé $(\pi/3, 2)$
1/8(C)	10	19325	508	6.85(11.32)	6.75(11.31)	6.75(11.33)
	20	76480	1016	1.85(2.98)	1.45(2.88)	1.45(2.89)
	40	304378	2031	1.31(1.31)	0.35(0.76)	0.35(0.77)
1/8	10	678	342	37.93(37.90)	6.65(10.58)	12.85(18.18)
	20	2183	684	38.46(38.38)	8.45(9.29)	10.92(12.24)
	40	7778	1366	38.70(38.72)	9.98(10.12)	11.05(11.34)
1/4	10	1104	348	33.21(35.68)	9.22(12.68)	14.44(19.09)
	20	3923	698	35.17(35.92)	6.49(8.32)	9.37(11.41)
	40	15021	1396	35.88(35.04)	7.95(8.37)	9.56(10.04)
1/2	10	2023	362	24.20(36.74)	14.83(12.90)	17.79(16.35)
	20	7724	724	32.09(35.17)	4.60(7.34)	9.32(9.32)
	40	29735	1448	33.14(34.71)	5.45(6.25)	7.15(7.68)
1	10	4078	391	19.04(30.07)	10.61(10.22)	12.82(9.75)
	20	15591	782	23.14(25.63)	3.64(3.70)	5.30(3.81)
	40	61599	1564	24.45(25.03)	3.16(3.13)	4.06(3.59)
1.5	10	6239	420	13.75(13.43)	9.55(12.23)	10.47(12.96)
	20	24335	840	15.60(14.99)	2.27(3.42)	3.14(4.07)
	40	96223	1680	16.38(16.22)	1.88(2.09)	2.26(2.44)
2	10	8566	449	9.17(17.29)	7.88(11.59)	8.34(11.47)
	20	33645	899	10.16(11.91)	2.30(2.95)	2.69(2.88)
	40	146847	1883	10.92(11.31)	1.34(1.41)	1.45(1.32)

Table 2.9

Elliptical cylinder : RMS error on the trace for different mesh resolutions of the $GLS_{22.5}$ FEM and ABC positions on a rectangular-shaped fictitious boundary.The values between parentheses correspond to the Galerkin FEM

m	n_λ	N_h	N_{Σ_h}	BGT	Padé $(\pi/6, 2)$	Padé $(\pi/3, 2)$
1/8	10	2054	390	37.44(39.80)	11.58(9.03)	11.56(14.65)
	20	7744	780	39.13(39.86)	8.83(9.38)	7.99(9.57)
	40	30120	1560	39.81(39.99)	10.42(10.56)	9.05(9.38)
1/4	10	2622	396	33.33(38.99)	10.64(10.70)	12.54(14.78)
	20	9858	791	36.75(38.14)	6.76(8.04)	6.97(8.62)
	40	38401	1584	37.72(38.06)	7.82(8.14)	6.96(7.42)
1/2	10	3838	417	25.37(38.36)	10.79(10.90)	12.90(12.25)
	20	14726	837	31.26(34.74)	4.77(6.38)	6.56(7.17)
	40	57631	1674	33.13(33.96)	5.02(5.59)	5.38(5.71)
1	10	6303	454	16.25(22.27)	8.63(12.06)	9.92(11.69)
	20	24786	906	17.74(18.56)	3.69(4.30)	5.20(4.98)
	40	98160	1820	18.69(18.49)	3.74(3.83)	4.83(4.72)
2	10	8566	449	7.15(14.94)	8.58(11.34)	9.10(11.41)
	20	33645	899	6.71(8.54)	4.51(5.19)	5.47(5.94)
	40	146847	1883	7.23(7.64)	4.45(4.37)	5.26(5.30)

We first choose a circular (C) fictitious boundary placed at a distance $R = a + m\lambda$ from the scatterer taking $m = 1/8$ (Fig.2.3). As we can observe, we get a good agreement between the solutions. However, due to the mismatch between the shape of a circular fictitious boundary and an elliptical scatterer, the number of degrees of freedom required in the solution procedure remains large. The mesh size cannot be further reduced. To circumvent this problem, we rather choose an elliptical-shaped fictitious boundary Σ taken conformal to the scatterer by setting its two semi-axes a' and b' to $a' = a + m\lambda$ and $b' = b + m\lambda$ (Fig.2.3). We give the results in Table 2.8. We can first notice that an important error arises if the BGT-like ABC is used. We also observe some fluctuations in the convergence of the solution even if we refine the mesh. Once again, and like the circular cylinder case, this can be associated to the convergence process between the integral equation and ABC solutions. If we now consider the Padé-type condition, we obtain a noticeable reduction in the error on the trace compared to the one obtained using the BGT-like ABC. Moreover,

the GLS solution yields an interesting improvement over the usual Galerkin procedure. If we consider for example $m = 1$ for the elliptical shape, then we get an error of 3.64% on the trace for $n_\lambda = 20$ (GLS procedure) and obtain a correct bistatic RCS computation for the Padé-type ABC (for $\theta = \pi/6$) as shown on Figures 2.5 and 2.4. An error of a few decibels is observable when the BGT-like ABC is used showing its limited accuracy in this configuration.

We now consider the possibility of reducing the size of the computational domain utilizing a rectangular-shaped fictitious boundary (Fig.2.3). To that end, we consider the rectangle Σ defined by the half-lengths along the x and y directions : $L = a + m\lambda$ and $\ell = b + m\lambda$. We report on Table 2.9 the results obtained for different mesh sizes. We can observe the better behavior of the Padé-type ABC over the BGT-like ABC even if the artificial boundary has some corners. This choice of shape shows that significant savings can be obtained with respect to the mesh size. For instance, we get an error of 4.77% on the trace for $m = 1/2$ and a density $n_\lambda = 20$ for the Padé condition. This results in a nontrivial reduction of the computational domain. A similar accuracy can be obtained with the BGT radiation condition but for a much larger computational domain. In the same situation, we get an error of about 31%.

From these first experiments, we conclude that the new Padé-type ABC can lead to a gain both in accuracy and memory savings by reducing the size of the computational domain compared to the usual BGT-like ABC. Moreover, the shape of the fictitious boundary can be optimized without loss of accuracy and efficiency. This adaptive capacity of this ABC to flexible general (convex) shapes allows us to solve more realistic scattering problems such as the one proposed in the section below : the scattering problem by a submarine-shaped scatterer.

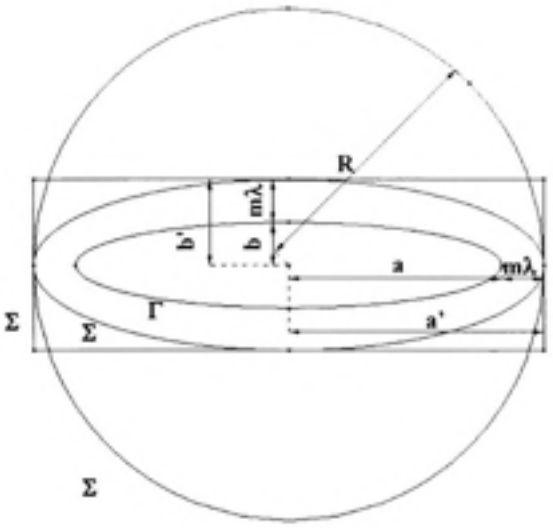

Figure 2.3 ***The elliptical shaped scatterer surrounded with an elliptical, a circular and a rectangular artificial boundary.***

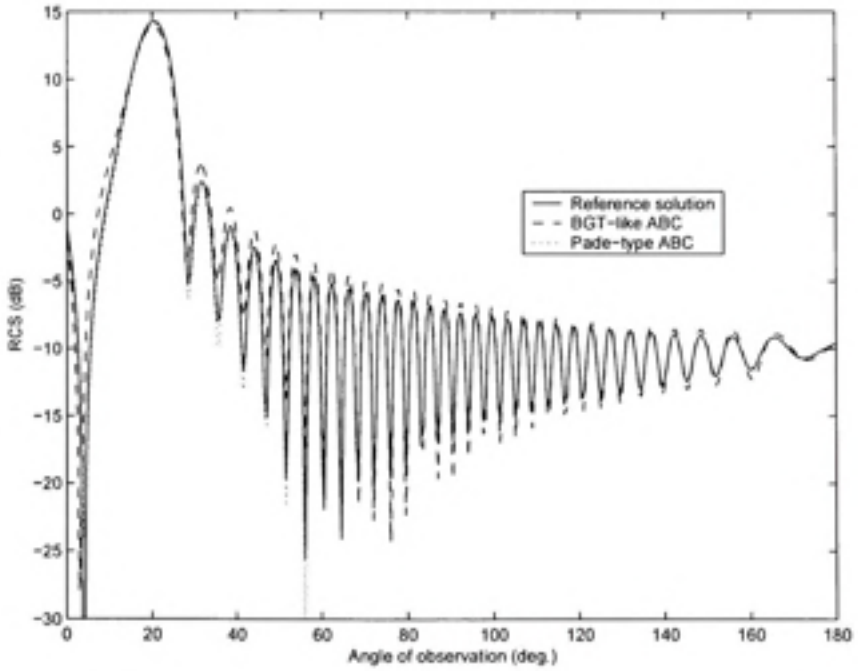

Figure 2.4 ***Far-field pattern (between 0 and 180 degrees) of the elliptical cylinder using the BGT-like and Padé-type ABCs.***

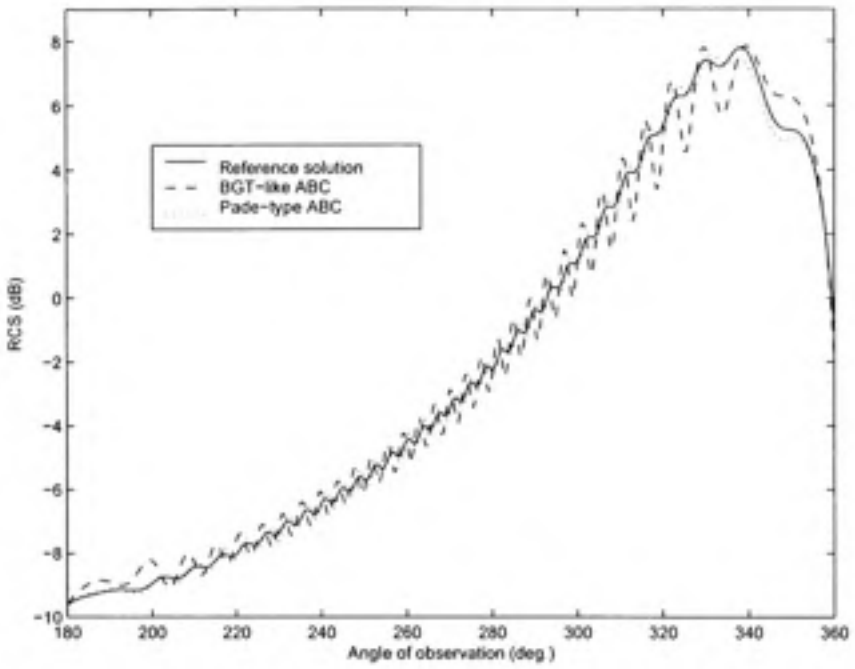

Figure 2.5 ***Far-field pattern (between*** 180 ***and*** 360 ***degrees) of the elliptical cylinder using the BGT-like and Padé-type ABCs.***

2.5 Sound-hard submarine-shaped scatterer

Let us now consider a more complex target : the submarine-shaped scatterer plotted in Figure 2.6. For the computations, we set the parameters to $L = 11$, $D = 1$ and $l = 0.5$.

To show that the above efficiency and accuracy are also realized in the far-field zone, we plot the RCS of the submarine-shaped scatterer for the reference solution in Figures 2.7 and 2.8. We compare the computations for the BGT-like and Padé-type ABCs set at $m = 1/2$ for a density of $n_\lambda = 20$ points per wavelength. We observe that the complicated structure of the far-field pattern is well-reproduced using the Padé-type condition while errors are visible for the BGT-like ABC.

The direction of the incident wave is set to $\theta^{\text{inc}} = 225$ degrees and the wavenumber k is chosen as $kD = 15$. This incident wave is known for producing the higher error in

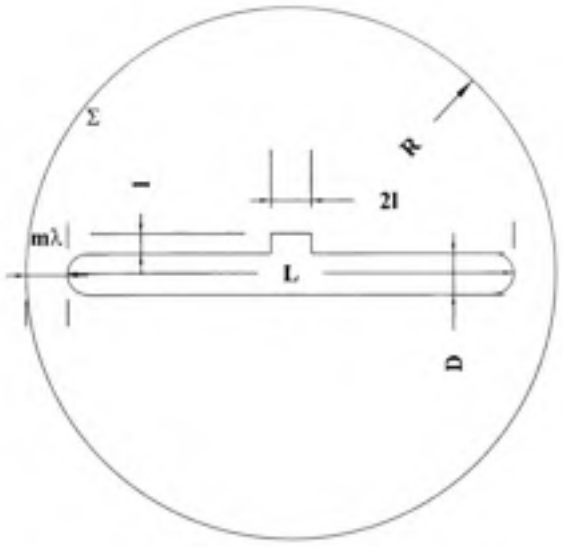

Figure 2.6 ***The submarine-shaped scatterer.***

the field computation (Djellouli et *al.*,2000). A first calculation is reported for a circular (C) fictitious boundary, different ABCs and two positions m. Even if a good agreement is reached, this does not significantly reduce the size of the linear system to be solved, and there is finally no significant gain in terms of mesh size. Once again, the main drawback of the circular boundary is that it is not suitable for an elongated body such as that of the submarine-shaped scatterer.

We now specify the two ABCs on an elliptical boundary Σ (Fig.2.9) having the following parameters $(a', b') = (L/2 + m\lambda, D/2 + l + m\lambda)$.

We report the results for the two angles $\theta = \pi/6$ and $\theta = \pi/3$. We see that the BGT-like ABC yields a correct accuracy but requires an important computational domain. Concerning the Padé-type ABC, a very impressive gain arises for the angle $\theta = \pi/6$ which allows the consideration of much smaller domains for a good accuracy. A good precision is also obtained for the angle $\theta = \pi/3$. This shows again that $\theta = \pi/6$ seems to be a kind of "optimal angle" for the new ABC if small domains are to be considered. This impres-

Table 2.10

Submarine shaped scatterer : RMS error on the trace for different mesh resolutions of the $GLS_{22.5}$ FEM and ABC positions on a circular (C) or elliptical shaped fictitious boundary. The values in parentheses correspond to the Galerkin FEM

m	n_λ	N_h	N_{Σ_h}	BGT	Padé $(\pi/6, 2)$	Padé $(\pi/3, 2)$
1/8(C)	10	56429	833	6.15(14.08)	5.69(14.02)	5.68(14.02)
	20	224151	1666	2.54(4.22)	1.33(3.67)	1.31(3.66)
	40	896663	3331	2.25(2.40)	0.54(1.01)	0.51(1.00)
1(C)	10	65153	888	5.42(14.23)	5.46(14.23)	5.46(14.22)
	20	224151	1776	1.48(3.74)	1.40(3.66)	1.40(3.67)
	40	1034390	3551	0.74(1.18)	0.48(0.98)	0.47(0.99)
1/2	10	7225	572	15.77(24.58)	8.74(15.01)	10.89(16.42)
	20	27990	1152	18.83(21.27)	3.87(6.37)	5.33(7.26)
	40	110182	2302	19.73(20.34)	3.83(4.50)	4.74(5.26)
1	10	10254	606	12.87(23.75)	7.48(15.40)	8.89(15.53)
	20	40293	1204	14.34(16.42)	2.81(4.87)	3.93(4.95)
	40	159432	2414	15.04(15.46)	2.64(2.99)	3.40(3.42)
2	10	16937	660	9.30(15.65)	7.53(13.67)	8.24(13.74)
	20	66900	1321	10.67(11.24)	2.30(3.84)	2.92(4.16)
	40	265586	2642	11.33(11.39)	1.65(1.80)	2.03(2.15)
4	10	32422	778	7.37(15.34)	7.29(13.78)	7.58(13.83)
	20	128900	1556	5.82(7.53)	1.67(3.64)	1.94(3.68)
	40	514549	3111	6.29(6.55)	0.84(1.15)	0.92(1.15)

sive decrease in the size of Ω_h leads to a powerful tool for prospecting high frequency scattering problems for complicated scatterers.

For completeness, we give in Table 2.11 the error on the trace if the submarine-shaped scatterer is surrounded by the rectangular fictitious boundary (Fig.2.10) centered at the origin and defined by the two lengths $a = L + 2m\lambda$ and $b = D + l + 2m\lambda$ along the x and y-axes respectively (the boundary is placed at a distance $m\lambda$ from the extremities of the submarine-shaped scatterer). Once again, we observe a better accuracy of the Padé-type ABC over the BGT-like ABC and the possibility of reducing the size of the computational domain. Unlike the elliptical-shaped fictitious surface, we do not observe a noticeable difference in the accuracy of the computed solutions according to the angle θ. Moreover, the use of the smoother elliptical fictitious boundary leads to a better approximation of the

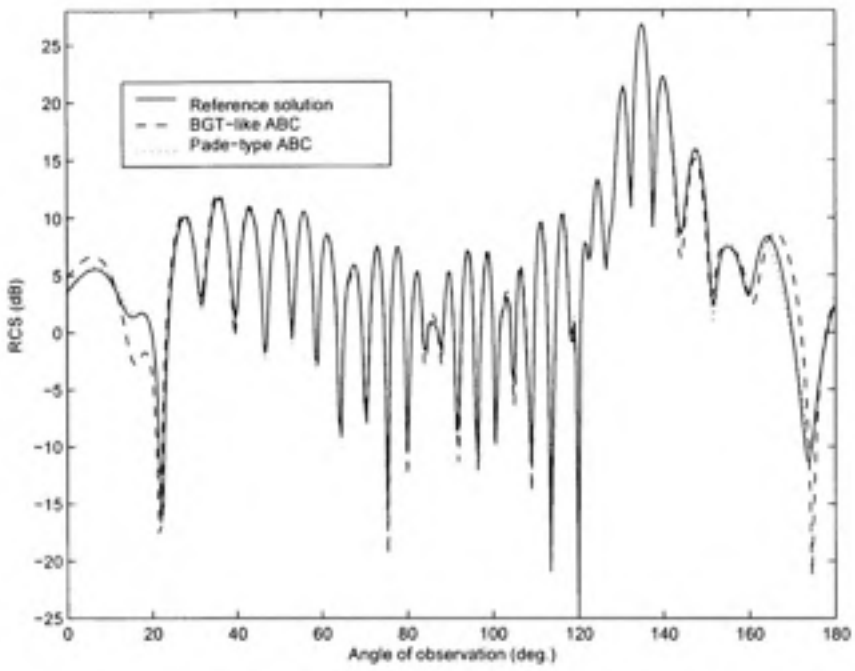

Figure 2.7 ***Far-field pattern (between 0 and 180 degrees) of the submarine-shaped scatterer using the BGT-like and Padé-type ABCs.***

scattered field for a given number of discretization points. This should be related to the fact that the rectangular boundary has some corners which can partially reflect back the wave striking Σ. Corner compatibility conditions are therefore required (cf. for instance (Vacus,2005) for the wave equation).

2.6 A few words on the computational aspects

To complete this study, we report a few results concerning the performance of the proposed preconditioned iterative Krylov algorithm (see Section 2.3.3). We consider again the scattering problem from the unit circular cylinder $\mathcal{D}$. The incident angle of the plane wave is zero degree and the wave number is set to $k = 50$.

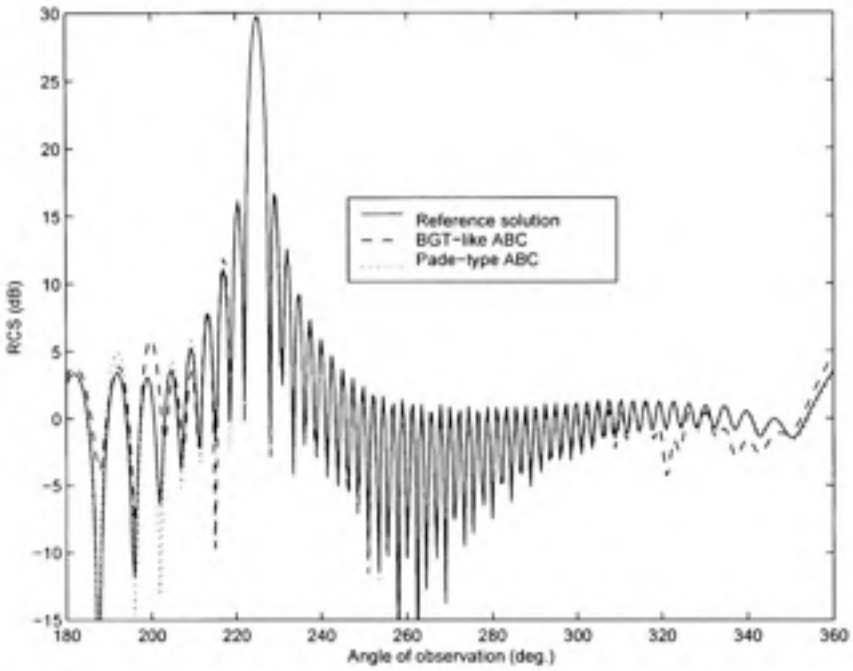

Figure 2.8 ***Far-field pattern (between 180 and 360 degrees) of the submarine-shaped scatterer using the BGT-like and Padé-type ABCs.***

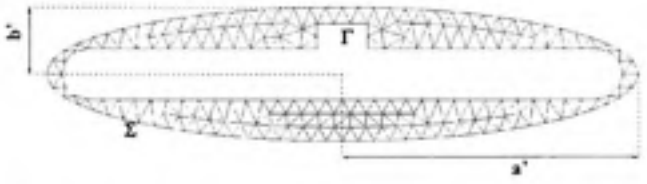

Figure 2.9 ***Mesh of the computational domain bounded by the submarine-shaped scatterer and the elliptical artificial boundary.***

For the following numerical experiments, the dimension of the Krylov space is set to `im`=50. The GMRES solver stops when the residual norm is less than 10^{-6}. Two parameters `lfil` and τ characterize the ILUT preconditionner. The fill-in parameter `lfil` is taken as the ratio between the number of non-zero entries (`nnz`) of the original matrix and the total number of unknowns. Therefore, we introduce $\texttt{lfil}_1 = \texttt{nnz}_1/N_h$ for the resolution of the main linear system based on $\mathbf{A}_h$ and $\texttt{lfil}_2 = \texttt{nnz}_2/N_{\Sigma h}$ for the resolution of

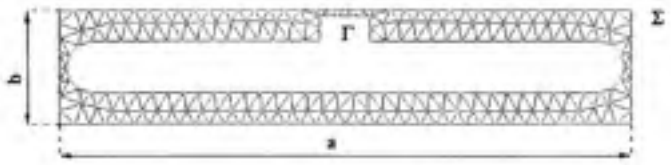

Figure 2.10 ***Mesh of the computational domain bounded by the submarine-shaped scatterer and the rectangular artificial boundary.***

Table 2.11

Submarine shaped scatterer : RMS error on the trace for different mesh resolutions of the $GLS_{22.5}$ FEM and ABC positions on the rectangular fictitious boundary. The values in parentheses correspond to Galerkin FEM

m	n_λ	N_h	N_{Σ_h}	BGT	Padé $(\pi/6, 2)$	Padé $(\pi/3, 2)$
1(C)	10	65153	888	5.42(14.23)	5.46(14.23)	5.46(14.22)
	20	224151	1776	1.48(3.74)	1.40(3.66)	1.40(3.67)
	40	1034390	3551	0.74(1.18)	0.48(0.98)	0.47(0.99)
1/8	10	4644	604	16.19(18.45)	9.75(13.87)	10.08(15.04)
	20	18051	1206	16.47(16.51)	8.21(8.32)	7.81(8.29)
	40	69959	2416	16.54(16.54)	8.83(8.80)	8.32(8.32)
1/4	10	5605	614	14.77(17.41)	7.91(12.52)	8.98(14.07)
	20	21190	1230	14.20(14.67)	6.87(7.03)	6.48(7.14)
	40	83679	2456	14.67(14.55)	7.48(7.43)	6.95(7.00)
1/2	10	7222	634	12.03(18.50)	9.01(13.78)	9.24(14.83)
	20	28557	1268	12.70(14.15)	5.68(6.68)	5.79(7.14)
	40	112690	2536	13.25(13.58)	6.32(6.48)	6.30(6.54)
1	10	11054	672	10.20(19.07)	7.88(14.65)	8.74(14.91)
	20	43857	1346	11.50(13.58)	4.45(6.04)	3.95(5.89)
	40	173154	2694	12.05(12.54)	4.45(4.81)	4.68(4.94)

the smaller subsystems associated with the surface Helmholtz-type equations defining the Padé-type ABC (essentially for solving the system given by $\mathbf{D}_h$). The second parameter τ for the dropoff strategy in ILUT factorization is taken equal to 10^{-5}. All the computations run on a Pentium IV PC with 2GB of RAM and a clock speed of 3.06 GHz.

We first report on Tables 2.12 and 2.13 the storage requirements (number of non-zero entries in words for both the linear system and preconditioner), number of GMRES iterations

and CPU time (in seconds) for the BGT-like and Padé-type ABCs for different sizes of the computational domain and discretizations.

Table 2.12

Storage requirements ($\texttt{nnz}_1$ for the system and the associated preconditioner, iterations count (`its`) and CPU time when the $GLS_{22.5}$ scheme and BGT-like ABC are used

m	n_λ	$\texttt{nnz}_1$ for the Syst. (Prec.)	`its`	CPU (s)
1/8	10	4490 (9982)	12	0.03
	20	16983 (29972)	12	0.03
	40	61969 (119942)	12	0.14
1/4	10	8483 (14972)	17	0.05
	20	37962 (71930)	14	0.09
	40	145927 (263870)	66	2.73
1/2	10	18962 (35930)	25	0.11
	20	72927(131870)	109	2.28
	40	285857(503750)	192	16.56
1	10	32934 (59882)	31	0.23
	20	135864 (239762)	328	13.29
	40	551724 (959522)	496	86.55
2	10	67864 (119762)	55	1.03
	20	275724 (497522)	430	35.47
	40	1111444 (1919042)	521	178.59

First, we see that for a fixed given fictitious boundary and discretization, the memory requirement for all ABCs is almost the same. The additional subsystems does not significantly increase the memory storage. Moreover, for one iteration, the additional time cost for solving these surface equations is low. The convergence rate of the preconditioned ILUT Krylov solver for these systems is fast (2 to 3 iterations). In terms of iterations, the linear system with the BGT-like condition is better preconditioned by our proposed preconditioner than with the Padé-type condition. This is due to the fact that this incomplete preconditioner is only built on $\mathbf{A}_h$ while it should be rather built on $\mathbf{G}_h$. This explains the increase of the overall computational cost of our procedure. This aspect remains one of the important point to investigate in the future developments related to our approach. Fortunately, the Padé-type ABC requires much smaller computational domains (and as a result a smaller linear system to solve) than the BGT-like ABC for a given accuracy. To focus

Table 2.13

Storage requirements ($\mathtt{nnz}_1$ for the system and the associated preconditioner, iterations count (`its`) and CPU time when the $GLS_{22.5}$ scheme and Padé$(\pi/3, 2)$-type ABC are used. The number of iterations and CPU times and reported in parenthesis in the corresponding columns for the Padé$(\pi/6, 2)$-type ABC

m	n_λ	$\mathtt{nnz}_1$ for the Syst. (Prec.)	$\mathtt{nnz}_2$ for the Sub-Syst. (Prec.)	its	CPU (s)
1/8	10	4490 (9982)	$2 \times 1497(2 \times 2994)$	49 (68)	0.56 (0.83)
	20	16983 (29972)	$2 \times 2997(2 \times 5994)$	50 (74)	1.39 (2.07)
	40	61969 (119942)	$2 \times 5997(2 \times 11994)$	51 (78)	4.25 (6.50)
1/4	10	8483 (14972)	$2 \times 1497(2 \times 2994)$	62(80)	0.75(0.97)
	20	7962 (71930)	$2 \times 2997(2 \times 5994)$	51(70)	1.73(2.37)
	40	145927 (263870)	$2 \times 5997(2 \times 11994)$	166(233)	17.83(25.03)
1/2	10	18962(35930)	$2 \times 1497(2 \times 2994)$	76(93)	1.00(1.22)
	20	72927(131870)	$2 \times 2997(2 \times 5994)$	277(346)	11.66(14.56)
	40	285857(503750)	$2 \times 5997(2 \times 11994)$	502(691)	76.41(105.18)
1	10	32934(59882)	$2 \times 1497(2 \times 2994)$	72(85)	1.38(1.63)
	20	135864(239762)	$2 \times 2997(2 \times 5994)$	660(872)	42.36(55.97)
	40	551724(959522)	$2 \times 5997(2 \times 11994)$	951(1327)	223.77(312.24)
2	10	67864(119762)	$2 \times 1497(2 \times 2994)$	110(132)	3.39(4.07)
	20	275724(497522)	$2 \times 2997(2 \times 5994)$	791(1114)	85.23(120.03)
	40	1111444(1919042)	$2 \times 5997(2 \times 11994)$	944(1350)	381.78(545.98)

on this aspect, we report on Table 2.14 the computational time required for the solution by each method to reach a given accuracy. For an acceptable level of accuracy less than to 2%, Padé-type ABC reduces the CPU time associated with the BGT-like ABC by a factor of 30 due to a reduction of the computational domain size. This factor is respectively equal to 90 (resp. 16) if the desired accuracy is less than 5% (resp.10%). Finally, the Padé-type ABC with the parameter $\pi/6$ yields the most accurate results at smaller costs.

Table 2.14

Accuracy vs. time solution for the BGT-like and Padé-type ABCs for the $GLS_{22.5}$ scheme

	BGT			Padé$(\pi/6,2)$			Padé$(\pi/3, 2)$		
Accuracy (%)	m	n_λ	CPU (s)	m	n_λ	CPU (s)	m	n_λ	CPU (s)
≤ 2	$> 2 \geq$	40	> 178.59	1/8	40	6.50	1	40	223.77
≤ 5	2	40	178.59	1/8	20	2.07	1/8	40	4.25
≤ 10	1	20	13.29	1/8	10	0.83	1/8	10	0.56

2.7 Conclusion

In this paper, we have proposed a numerical study of a new non-reflecting boundary condition for solving two-dimensional acoustic scattering problems in the high-frequency regime. This Padé-type ABC can be applied on any convex fictitious boundary, and allows us to deal with scattering problems involving elongated scatterers (such as a submarine-shaped scatterer, for instance) on some optimized fictitious shapes. Moreover, for high-frequencies, this ABC exhibits a higher accuracy over the usual BGT-like ABC for relatively small computational domains. Also, Padé-type ABC is more computationally efficient than BGT-like ABC for a prescribed level of accuracy. Finally, this condition can be easily implemented in a GLS finite element iterative solver to improve the global accuracy of the solution. The natural extension of the ABC to three-dimensional acoustic scattering follows the ideas presented here, and will be the subject of further works. A similar ABC has been derived in (Darbas,2004) for the three-dimensional Maxwell's equations and should lead to a similar behavior. Its numerical approximation is under progress. Finally, the improvement of the efficient iterative solution to the resulting linear system using the new ABC is still being studied. Its particular form requires the use of adapted preconditioners to accelerate the convergence rate of the GMRES solver. However, other kinds of efficient solver could also be proposed, and adapted to the results presented here.

In the next chapter, we address more specifically the numerical pollution in the finite element.

BIBLIOGRAPHIE

Antoine, Xavier, Barucq Hélène, and Bendali Abderrahmane. 1999. ≪Bayliss-Turkel like radiation condition on surfaces of arbitrary shape≫. *Journal of Mathematical Analysis and Applications*, vol.229, n°3, p.184-211.

Antoine, Xavier. 2001. ≪Fast Approximate computation of a time-harmonic scattered field using the on-surface radiation condition method≫. *Institute of Mathematics and its Applications (IMA) : Journal of Applied Mathematics*, vol.66, n°1, p.83-110.

Antoine, Xavier. 2002. ≪An Algorithm Coupling the OSRC and FEM for the Computation of an Approximate Scattered Acoustic Field by a Non-convex Body≫.*International Journal for Numerical Methods in Engineering*,vol.54, n°7, p.1021-1041.

Antoine, Xavier, Darbas Marion and Lu Ya Yan. 2006. ≪An Improved Surface Radiation Condition for High-Frequency Acoustic Scattering Problems≫, *Computer Methods in Applied Mechanics and Engineering*, vol.195, n°33-36, (Juillet), p.4060-4074(also available as Chapter 4 of the Ph.D. Thesis (Darbas,2004)).

Antoine, Xavier and Darbas Marion. 2005. ≪Alternative Integral Equations for the Iterative Solution of Acoustic Scattering Problems≫.*Quaterly Journal of Mechanics and Applied Mathematics*, vol.58, n°1, p.107-128.

Bayliss, Alvin and Turkel Eli. 1980. ≪Radiation boundary conditions for wave-like equations≫. *Communications on Pure and Applied Mathematics*, vol.33, n°6, p.707-725.

Bayliss, Alvin, Gunzburger Max and Turkel Eli. 1982. ≪Boundary conditions for the numerical solution of elliptic equations in exterior regions≫. *Society for Industrial and Applied Mathematics : Journal of Applied Mathematics*, vol.42, n°2, p.430-451.

Bérenger, Jean-Pierre. 1994. ≪A perfectly matched layer for the absorption of electromagneticwaves≫. *Journal of Computational Physics*, vol.114, n°2, (Octobre), p.185-200.

Bruno, Oscar P. and Kunyansky Leonid A. 2001.≪Surface scattering in three dimensions : an accelerated high-order solver≫.*Royal Society of London Proceedings Series A. Proceedings : Mathematical, Physical and Engineering Sciences*, vol.457, Vol.457, n°2016, (Decembre), p.2921-2934.

Bruno, Oscar P. and Kunyansky Leonid A. 2001. ≪A fast, high-order algorithm for the solution of surface scattering problems : basic implementation, tests, and applications≫. *Journal of Computational Physics*. vol.169, n°1, p.80-110.

Colton, David and Kress Rainer. 1983. *Integral Equation Methods in Scattering Theory*. 1st ed. ≪Pure and Applied Mathematics≫. New York, USA : John Wiley and Sons Inc., 286p.

Darbas, Marion. 2004.≪Préconditionneurs analytiques de type Caldéron pour les formulations intégrales des problèmes de diffraction d'ondes≫. Thèse de doctorat en mathématiques appliquées, Toulouse (France), Instiut national des sciences appliquées, Université Paul Sabatier, 253 p.

Djellouli, Rabia, Farhat Charbel, Macedo Antonini and Tezaur Radek. 2000. ≪Finite element solution of two-dimensional acoustic scattering problems using arbitrarily shaped convex artificial boundaries≫. *Journal of Computational Acoustics*, vol.8, n°1, (Mars), p.81-99.

Enquist, Bjorn and Majda Andrew. 1977. ≪Absorbing boundary conditions for the numerical simulation of waves≫. *Mathematics of Computation*, vol.31, n°139, (Juillet), p.629-651.

Farhat, Charbel, Radek Tezaur and Rabia Djellouli. 20002. ≪On the solution of three-dimensional inverse obstacle acoustic scattering problems by a regularized Newton method≫. *Inverse Problems*, vol.18, n°5, p.1229-1246.

Farhat, Charbel and Hetmaniuk Ulrich. 2002.≪A fictitious domain decomposition method for the solution of partially axisymmetric acoustic scattering problems. Part I : Dirichlet boundary conditions acoustic scattering problems≫. *International Journal for Numerical Methods in Engineering*, vol.54 (2002), n°9, p.1309-1332.

Givoli, Dan. 1999. ≪Exact representation on artificial interfaces and applications in mechanics≫.*Applied Mechanics Reviews*, vol.52, n°9, p.333-349.

Givoli, Dan. 2004.≪High-order local non-reflecting boundary conditions : a review≫.*Wave Motion*, vol.39, p.319-326.

Guddati, Murty N. and Tassoulas John L. 2000.≪Continued-fraction absorbing boundary conditions for the wave equation≫. *Journal of Computational Acoustics*, vol.8, n°1, p.139-156.

Hagstrom, Thomas. 1999. ≪Radiation boundary conditions for the numerical simulation of waves≫. *Acta Numerica*, p.47-106.

Harrari, Isaac, Grosch Karl, Hughes Thomas J.R., Malhotra Manish, Pinsky Peter M., Stewart Jean R., and Thompson Lonny L. 1996. ≪Recent developpments in finite element methods for structural acoustics≫. *Archives of Computional Methods in Engineering*, vol.3, n°2-3, p.131-109.

Harari, Isaac and Nogueira Carnot L. 2002. ≪Reducing dispersion of linear triangular elements for the Helmholtz equation≫. *Journal of Engineering Mechanics*, vol.128, n°3, (Mars), p. 351-358.

Harari, Isaac and Magoulès Frédéric. 2004. ≪Numerical investigations of stabilized finite element computations for acoustics≫. *Wave Motion*, vol.39, n°4, p. 339-349. (2004).

Harari, Isaac and Djellouli Rabia. 2004. ≪Analytical study of the effect of wave number on the performance of local absorbing boundary conditions for acoustic scattering≫. *Applied Numerical Mathematics*, vol.50, n°4, (Juillet), p.15-47.

Hetmaniuk, Ulrich and Farhat Charbel. 2003. ≪A fictitious domain decomposition method for the solution of partially axisymmetric acoustic scattering problems. Part 2 : Neumann boundary conditions≫. *International Journal for Numerical Methods in Engineering*, vol.58, n°1, p.63-81.

Ihlenburg, Franck, 1998. *Finite Element Analysis of Acoustic Scattering*. 1st ed. Coll. ≪Applied Mathematical Sciences≫, vol.132. New York : Springer-Verlag New York, Inc., 224 p.

Kechroud, Riyad, Soulaïmani Azzeddine, Saad Yousef and Gowda Shivaraju. 2004. ≪Preconditioning techniques for the solution of the Helmholtz equation by the finite element method≫. *Mathematics and Computer in Simulation*, vol.65, n°4-5, p.303-321.

Kirkup, Stephen. 1998. The Boundary Element Method in Acoustics : A Development in Fortran. Coll. ≪Integral Equation Methods in Engineering≪. nouvelle ed. Hebden Bridge : Integrated Sound Software, 158 p. The code is available at : http ://www.boundary-element-method.com/.

Kriegsmann, Gregory A., Taflove Allen and Umashankar Korada R. 1987. ≪A new formulation of electromagnetic wave scattering using the on-surface radiation condition method≫. *Institute of Electrical and Electronics Engineers : Transactions on Antennas and Propagation*, vol.35, n°2, p.153-161.

Leigh, Little, Yousef Saad and Laurent Smoch. 2003. ≪Block LU preconditioners for symmetric and nonsymmetric saddle point problems≪. *Society for Industrial and Applied Mathematics : Journal of Scientifique Computing*, vol.25, n°2, p.729-748.

Milinazzo, Fausto A., Zala Cedric A. and Brooke Gary H. 1997. ≪Rational square-root approximations for parabolic equation algorithms≫. *The Journal of the Acoustical Society of America*, vol.101, n°2, p.760-766.

Nédélec, Jean-Claude. 2001. *Acoustic and Electromagnetic Equations, Integral Representations for Harmonic Problems*. Coll. ≪Applied Mathematical Sciences≫, vol.144, New York : Springer-Verlag, Inc., 318 p.

Rokhlin, V. 1990. ≪Rapid solution of integral equations of scattering theory in two-dimensions≫. *Journal of Computational Physics*, vol.86, n°12, (Février), p.414-439.

Tezaur, Radek, Macedo Antonini, Farhat Charbel and Djellouli Rabia. 2000. ≪Three dimensional finite element calculations in acoustic scattering using arbitrarily shaped convex artificial boundaries≫. *International Journal for Numerical Methods in Engineering*, vol.53, n°3, p.1461-1476.

Thompson, Lonny L., Ianculescu Cristian and Huan R. 2000. ≪Exact radiation conditions on spheroidal boundaries with sparse iterative methods for efficient computation of exterior acoustics≫. In *Seventh International Congress on Sound and Vibration*. (Garmisch-Partenkirchen, Germany 4-7 July 2000), p.2101-2108, Berlin : Springer.

Thompson, Lonny L., Huan R. and He D. 2001. ≪Accurate radiation boundary conditions for the two-dimensional wave equation on unbounded domains≫. *Computer Methods in Applied Mechanics and Engineering*, vol. 191, n°3, (Novembre), p.311-351.

Saad, Yousef. 1996. *Iterative Methods for Sparse Linear Systems*. 1st ed. Boston, USA : PWS Publishing Co., 447 p.

Taylor, Michael E. 1981. *Pseudodifferential Operators*. 1st ed. Princeton, NJ : Princeton University Press. 451 p.

Tsynkov, Simon V. 1998. ≪Numerical solution of problems on unbounded domains. A review≪. *Applied Numerical Mathematics*, vol.27, n°4, (Août) p.465-532.

Vacus, Olivier. 2005. ≪Mathematical analysis of absorbing boundary conditions for the wave equation : the corner problem≫. *Mathematics of Computation*, vol.74, n°249, p.177-200.

Zienkiewicz, Olgierd C. 2000. ≪Achievements and some unsolved problems of the finite element method≫. *International Journal for Numerical Methods in Engineering*, vol.47, n°1-3, p.9-28.

Résumé

Nous avons présenté dans ce chapitre une méthodologie de résolution, basée sur un couplage éléments finis (linéaires et linéaires stabilisés) avec des conditions absorbantes d'ordre élevé de type Padé, des problèmes bidimensionnels de diffraction acoustique mettant en jeu des fréquences relativement élevées.

Outre le fait que cette condition absorbante peut être imposée sur n'importe quelle forme convexe de la frontière artificielle, son implémentation dans les codes éléments finis est facile.

La précision de la méthodologie proposée a été analysée et comparée aux conditions généralisées du second ordre de Bayliss-Gunzburger-Turkel pour différentes formes d'obstacles et en particulier pour un obstacle de forme allongée du type sous-marin. Des domaines de calcul relativement réduits et optimisés selon la forme de l'obstacle ont pu être adoptés sans perte de précision pratique.

Dans le prochain chapitre, nous portons une attention particulière au phénomène de pollution numérique inhérent à la méthode des éléments finis.

CHAPITRE 3

PERFORMANCE STUDY OF PLANE WAVE FINITE ELEMENT METHODS WITH A PADÉ-TYPE ARTIFICIAL BOUNDARY CONDITION IN ACOUSTIC SCATTERING

R. Kechroud[1], A. Soulaïmani[1], and X. Antoine[2,3],

[1] Département de Génie Mécanique, École de Technologie Supérieure,

1100 Notre-Dame Ouest, Montréal (Québec), Canada H3C 1K3

E-mail : riyad.kechroud.1@ens.etsmtl.ca, azzeddine.soulaimani@etsmtl.ca

[2] Institut National Polytechnique de Lorraine,

Ecole Nationale Supérieure des Mines de Nancy,

Département de Génie Industriel,

Parc de Saurupt, CS 14 234, 54042 Nancy cedex, France

Email : Xavier.Antoine@mines.inpl-nancy.fr

[3] Institut Elie Cartan Nancy (IECN), Université Henri Poincaré Nancy 1,

Nancy-Université, INRIA-CORIDA Team

B.P. 239, F-54506 Vandoeuvre-lès-Nancy Cedex,France

Email :Xavier.Antoine@iecn.u-nancy.fr

This chapter was submitted in the mid of September 2007 to the International Journal For Numerical Methods In Engineering as an article.

Solving exterior scattering problems at high-frequencies is an important engineering problem and a challenging computational task (Zienkiewicz,2000). Significative efforts have been devoted to this subject and improvements have been achieved over the last two decades but still difficulties remain unsolved. Various numerical approaches have been developed until now. For example, let us cite the integral equation method (Burton and Miller,1971 ; Colton and Kress,1983 ; Nédélec,2001 ; Bendali and Fares,2007) coupled to an iterative Fast Multipole Method (FMM) or other accelerated solvers (Chew et al.,2001 ;

Darve,2000 ; Rokhlin,1990 ; Bruno,2004), the volume Finite Element Method (FEM) (Thompson,2006 ; Ihenburg,1998) with truncated boundary (artificial or transparent boundary condition, DtN map, Perfectly Matched Layer,...) (Thompson,2006 ; Ihenburg,1998 ; Engquist and Majda,1977 ; Bayliss et al.,1982 ; Bayliss and Turkel,1980 ; Givoli,1999 ; Hagstrom,1999 ; Tsynkov,1998 ; Bérenger,1994 ; Turkel,2007), the infinite element method (Astley,2000; Gerdes,2000) or also the asymptotic techniques (Molinet et *al.*,2005). Despite their respective efficiencies, important difficulties still need to be solved. In this paper, we particularly focus on the approach based on FEM.

The Finite Element Method has received much attention because of its flexibility in modeling complex geometries, the availability of efficient basic finite element solvers which can be parallelized using for example domain decomposition methods (Thompson,2006; Djellouli et *al.*,2000; Tezaur et *al.*,2002; Farhat et *al.*,2002) and its ability to handle complex targets and media (Thompson,2006). However, when the frequency increases, some difficulties are met. Indeed, it is well-known that pollution effects (Thompson,2006 ; Ihenburg,1998 ; Babuška and Sauter,1997) arise in standard FEM limiting its ability for solving large scale scattering problems. For this reason, new finite element methods have been explored such as the Galerkin Least Squares methods, the element-free methods, the partition of unity method, the discontinuous enrichment method. Rather than citing the numerous contributions, we refer to the complete recent review paper by Thompson (Thompson,2006) describing most of the available finite element methods with exhaustive references. Another problem is related to truncating the exterior propagation medium into a suitable finite domain but at the same time also trying to minimize the spurious reflection at the fictitious boundary. This problem is well-known as building a transparent, an artificial or an absorbing boundary condition. Indeed, this topic has received great attention since the pioneering works of Engquist and Majda (Engquist and Majda,1977) and Bayliss, Gunzburger and Turkel (Bayliss et *al.*,1982; Bayliss and Turkel,1980) at the end of the seventies. Since then, many major improvements have been realized by (Givoli,1999;

Hagstrom,1999; Tsynkov,1998) or with the Perfectly Matched Layer method (Bérenger, 1994 ; Turkel,1998 ; Turkel,2007). Another related approach, which has received much attention these last years, is artificial boundary conditions based on rational approximants (Givoli,2004; Guddati and Lim,2005). It is shown for example in (Guddati and Lim,2005) that similar accuracy can be expected for these methods and the PML technique. In the case of elongated scatterers, which is our interest in this paper, a general high-order accurate Padé-type On-Surface Radiation Condition (OSRC) (Kriegsmann et al.,1987 ; Antoine,2007) been derived in (Antoine et *al.*,2005; Antoine et *al.*,2006) and its performance as an Artificial Boundary Condition (ABC) has been provided in (Kechroud et al.,2005 ; Kechroud et al.,2006) using standard finite element methods(Lagrange polynomial approximations). The conclusion is that the method leads to a drastic diminution of the size of the computational domain leading hence to the possibility of prospecting high-frequency problems. However, despite this noticeable improvement, the pollution problem still remains present into the finite element method. The aim of this paper is to show that this problem can be significantly relaxed by using more adapted finite element techniques. To this aim, we propose here to analyze the performance of the Plane Wave FEM (Laghrouche and Bettess,2000; Laghrouche et *al.*,2002; Ortiz,2001) coupled to the Padé-type ABC for two-dimensional scattering problems in order to strongly decrease the number of degrees of freedom of the final linear system. We shall point out here that in (Laghrouche and Bettess,2000; Laghrouche et *al.*,2002), PWFEM is coupled to the first order local ABC and in (Ortiz,2001) with higher order Higdon ABC. These ABCs lead to a relatively large computational domain. As a consequence, the number of plane waves used per node is important even for medium wavenumbers.

The structure of the paper is the following. In Section 1, we introduce the scattering problem and describe the Padé-type ABC and the associated variational formulation. In Section 2, the standard and plane wave-based FEM are described and discussed. Section 3 provides a complete numerical study of the performance of the Padé-type ABC coupled to

the Plane Wave FEM. In particular, Section 3.3 reports some results obtained in the case of a submarine-like shaped scatterer. Finally, a conclusion is given in Section 4.

3.1 A Padé-type artificial boundary condition

3.1.1 The two-dimensional scattering problem

Define $\Omega^- \subset \mathbb{R}^2$ as a two-dimensional impenetrable bounded domain with boundary $\Gamma := \partial\Omega^-$. The associated homogeneous exterior domain of propagation, which is the complemetary set of the scatterer Ω^- in $\mathbb{R}^2$, is denoted by Ω^e. Then, the scattering of an incident time-harmonic acoustic wavefield u^{inc} by Ω^- can be formulated as the following exterior Boundary Value Problem (BVP) find the scattered field u solution to :

$$\begin{cases} \Delta u + k^2 u = 0, \text{ in } \Omega^e, \\ \partial_{\mathbf{n}_\Gamma} u = -\partial_{\mathbf{n}_\Gamma} u^{inc} \text{ or } u = -u^{inc}, \text{on } \Gamma, \\ \lim\limits_{r\to\infty} \sqrt{r}(\partial_r u - iku) = 0. \end{cases} \tag{3.1}$$

If $\mathbf{a}$ and $\mathbf{b}$ are two complex-valued vector fields (and $\overline{z}$ denotes the complex conjugate of a complex number $z \in \mathbb{C}$), their inner product is defined by $\mathbf{a} \cdot \mathbf{b} = \sum_{j=1}^{2} a_j \overline{b_j}$, and the associated norm $\|\cdot\|$ is $\|\mathbf{a}\|^2 = \mathbf{a} \cdot \mathbf{a}$. Let $\mathbf{x} = (x_1, x_2) \in \mathbb{R}^2$, then the gradient ∇ of a complex-valued scalar field f and the divergence div of $\mathbf{a}$ are defined respectively by $\nabla f = (\partial_{x_1} f, \partial_{x_2} f)^T$ and $\text{div}\, \mathbf{a} = \sum_{j=1}^{2} \partial_{x_j} a_j$, designating by $\mathbf{a}^T$ the transposed of $\mathbf{a}$. Under these notations, the Laplace operator Δ is classically defined by $\Delta = \text{div}\, \nabla$. We consider that the incident wave u^{inc} is plane $u^{inc}(\mathbf{x}) = e^{ik\mathbf{d}\cdot\mathbf{x}}$. The wave number k is related to the wavelength λ by the relation $k = 2\pi/\lambda$. The direction of incidence $\mathbf{d}$ is given through the relation $\mathbf{d} = (\cos(\theta^{inc}), \sin(\theta^{inc}))^T$, where θ^{inc} is the scattering angle. If we define by $\mathbf{n}_\Gamma$ the outwardly directed unit normal to Ω^e at the boundary Γ, then, the sound-hard or Neumann (respectively sound-soft or Dirichlet) boundary condition on Γ corresponds to the second (respectively third) equation of (3.1). Finally, the last equation

is the Sommerfeld radiation condition which allows only outgoing waves at infinity, setting $r = \|\mathbf{x}\|$. This thereby guarantees the uniqueness of the solution to the BVP (3.1).

3.1.2 Bounding the domain by using a Padé-type ABC

It is well-known that the BVP (3.1) cannot be solved by usual domain based methods like the Finite Element Method (FEM) or the Finite Difference Method (FDM) if the infinite domain Ω^e is not truncated *via* a fictitious boundary Σ enclosing Ω^-. This implies that the considered domain of computation is now the one, denoted by Ω, delimited by Γ and Σ. To avoid in the best case or at least to minimize the reflection at the nonphysical boundary Σ, one must impose a suitable boundary condition at Σ. This condition takes different denominations like non-reflecting, artificial or absorbing boundary condition, according to its properties and aims (Givoli,1999), but its goal is always to try to give a good compromise between flexibility in terms of implementation into an existing code and minimization of the reflection or/and of the size of the computational domain. Generally, this condition is given through the Dirichlet-to-Neumann (DtN) operator or an approximation of this operator. More precisely, if M is an approximation of the DtN operator, we get the following new approximate BVP with an Artificial Boundary Condition (ABC) :

$$\begin{cases} \Delta u + k^2 u = 0, \text{in } \Omega, \\ \partial_{\mathbf{n}_\Gamma} u = -\partial_{\mathbf{n}_\Gamma} u^{inc} \text{ or } u = -u^{inc}, \text{ on } \Gamma \\ \partial_{\mathbf{n}_\Sigma} u = -Mu, \text{ on } \Sigma. \end{cases} \tag{3.2}$$

In a series of recent papers (Djellouli et *al.*,2000; Tezaur et *al.*,2002; Farhat et *al.*,2002), Farhat *et al.* show that the generalized second-order Bayliss-Gunzburger-Turkel (BGT2) like ABC derived in (Antoine et *al.*,1999) yields accurate finite element solutions in the mid-frequency regime for two- and three-dimensional direct and inverse acoustic scattering problems using arbitrarily-shaped convex fictitious boundaries Σ. Even if this condition is accurate in the medium frequency range, its accuracy decreases in the high-frequ-

ency regime if the fictitious boundary is too close to the scatterer. To obtain a much better accuracy, a larger computational domain must be considered resulting in the need to solve a larger size sparse linear system of equations. This is then computationally expensive both in memory and computing time even with sophisticated solvers like for instance the FETI-H method (Djellouli et *al.*,2000; Tezaur et *al.*,2002; Farhat et *al.*,2002).

An alternative to the BGT2-like ABC is to rather consider the Padé-type ABC derived in and validated in (Kechroud et *al.*,2005; Kechroud et *al.*,2006) for high-frequency acoustic scattering. This condition is expressed through a square-root operator which can be efficiently computed by paraxial approximation techniques. More specifically, this operator is given by the relation :

$$-Mu = ik\sqrt{1+\partial_s(\frac{1}{k^2}\partial_s)}u - \frac{\kappa}{2}u + \frac{\kappa^2}{8(\kappa-ik)}u - \partial_s(\frac{\kappa}{2k^2}\partial_s)u. \qquad (3.3)$$

In this expression, s is the counterclockwise directed arclength along Σ, ∂_s is the curvilinear derivative along Σ and κ is the curvature at a point of the surface. The notation $\sqrt{z}$ designates the principal determination of the square-root of a complex number z with branch-cut along the negative real axis. This operator which is in fact defined by a non-local pseudo-differential square-root operator must be efficiently represented through differential operators to have a sparse matricial representation. Following (Antoine et *al.*,2005; Antoine et *al.*,2006), this can be accurately done by a rotating branch-cut approximation of the square-root and Padé approximants (Milinazzo et *al.*,1997). Moreover, to get an accurate representation of the tangential rays into the ABC (3.3), a local regularization procedure must be applied to the square-root operator. This is done by the introduction of a complex wave number k_ϵ with small dissipation ϵ (much more details are given in (Antoine et *al.*,2006)). Finally, the modified regularized square-root operator used in (3.3) is replaced and approximated by :

$$\sqrt{1+\partial_s(\frac{1}{k_\epsilon^2}\partial_s)}u \approx C_0 u + \sum_{j=1}^{N} A_j\partial_s(k_\epsilon^{-2}\partial_s)(1+B_j\partial_s(k_\epsilon^{-2}\partial_s))^{-1}u \qquad (3.4)$$

where $k_\epsilon = k + i\epsilon$. An optimized choice of the damping parameter ϵ stated in (Antoine et al.,2006) is : $\epsilon = 0.4k^{1/3}\kappa^{2/3}$. In (3.4), the complex coefficients C_0, A_j and B_j are given by :

$$\begin{aligned} C_0 &= e^{i\frac{\alpha}{2}} R_N(e^{-i\alpha} - 1), \\ A_j &= \frac{e^{-\frac{i\alpha}{2}} a_j}{(1 + b_j(e^{-i\alpha} - 1))^2}, \\ B_j &= \frac{e^{-i\alpha} b_j}{(1 + b_j(e^{-i\alpha} - 1))^2}. \end{aligned} \tag{3.5}$$

The angle of rotation is α and (a_j, b_j), for $j = 1, ..., N$, are the standard real Padé coefficients given by :

$$a_j = \frac{2}{2N+1} \sin^2(\frac{j\pi}{2N+1}) \, , b_j = \cos^2(\frac{j\pi}{2N+1}), \tag{3.6}$$

denoting by R_N the Padé approximant of order N :

$$\sqrt{1+z} \approx R_N(z) = 1 + \sum_{j=1}^{N} \frac{a_j z}{1 + b_j z}. \tag{3.7}$$

In view of an efficient numerical treatment, the approximation of the Padé-type ABC (3.3)-(3.7) is represented by using Lindman's (Lindman,1985) auxiliary coupled functions trick :

$$-Mu = ik(u + \sum_{j=1}^{N} A_j \varphi_j) - \frac{\kappa}{2} u + \frac{\kappa^2}{8(\kappa - ik)} u - \partial_s(\frac{\kappa}{2k^2} \partial_s) u, \text{ on } \Sigma, \tag{3.8}$$

where the functions φ_j, $j = 1, .., N$, defined on Σ, are solutions of the following differential equations :

$$(1 + B_j \partial_s(\frac{1}{k_\epsilon^2} \partial_s))\varphi_j = \partial_s(\frac{1}{k_\epsilon^2} \partial_s) u. \tag{3.9}$$

3.1.3 Variational formulation with Padé-type ABC

Let us introduce V as the Sobolev space $H^1(\Omega)$ for a Neumann boundary condition or $H_0^1(\Omega)$ for a Dirichlet boundary condition. Let us define the product spaces $W_N := H^1(\Sigma) \times ... \times H^1(\Sigma)$, N times, and $X_N := V \times W_N$. Under these notations, a varia-

tional formulation of (3.2) with the Padé-type ABC (3.3)-(3.7) is find $(u, \varphi_1, ..., \varphi_N)$ in X_N such that :

$$\begin{cases} \mathcal{A}(u,v) + \sum_{j=1}^{N} \mathcal{B}_j(\varphi_j, v) = b(v), \\ \mathcal{C}(u,\psi_j) + \mathcal{D}_j(\varphi_j,\psi_j) = 0, \end{cases} \tag{3.10}$$

with $j = 1, ..., N$, and for test-functions $(v, \psi_1, ..., \psi_N) \in X_N$. The symmetrical bilinear form $\mathcal{A}$ acts from $V \times V$ into $\mathbb{C}$ and is defined by :

$$\begin{aligned} \mathcal{A}(u,v) = &\int_\Omega \left\{\nabla u \cdot \nabla v - k^2 uv\right\} d\Omega - ik \int_\Sigma uv d\Sigma + \frac{1}{2}\int_\Sigma \kappa uv d\Sigma \\ &-\frac{1}{8}\int_\Sigma \frac{\kappa^2}{\kappa - ik} uv d\Sigma + \frac{1}{2k^2}\int_\Sigma \kappa \partial_s u \partial_s v d\Sigma. \end{aligned} \tag{3.11}$$

Moreover, the bilinear forms $\{\mathcal{B}\}_{j=1,...,N}$, $\mathcal{C}$ and $\{\mathcal{D}\}_{j=1,...,N}$ are defined from $H^1(\Sigma) \times H^1(\Sigma)$ into $\mathbb{C}$ by :

$$\begin{aligned} \mathcal{B}_j(\varphi_j, v) &= -ikA_j \int_\Sigma \varphi_j v d\Sigma, \\ \mathcal{C}(u,\psi_j) &= \int_\Sigma \frac{1}{k_\epsilon^2} \partial_s u \partial_s \psi_j d\Sigma, \\ \mathcal{D}_j(\varphi_j,\psi_j) &= \int_\Sigma \varphi_j \psi_j d\Sigma - \int_\Sigma \frac{B_j}{k_\epsilon^2} \partial_s \varphi_j \partial_s \psi_j d\Sigma. \end{aligned} \tag{3.12}$$

We do not precise the definition of the linear form b which follows from the nature of the boundary condition on Γ.

The variational formulation (3.10) is an unconjugated formulation with bilinear operators. The following alternative conjugated formulation with sesquilinear operators can be obtained if the weighting functions v and ψ_j are substituted respectively by $\overline{v}$ and $\overline{\psi_j}$:

$$\begin{cases} \mathcal{A}(u,\overline{v}) + \sum_{j=1}^{N} \mathcal{B}_j(\varphi_j, \overline{v}) = b(\overline{v}), \\ \mathcal{C}(u,\overline{\psi_j}) + \mathcal{D}_j(\varphi_j,\overline{\psi_j}) = 0, \end{cases} \tag{3.13}$$

for $j = 1, ..., N$, and $\forall (v, \psi_1, ..., \psi_N) \in X_N$.

3.2 Finite element approximation

To discretize the variational formulations, the computational domain Ω is partitioned into quadratic triangular finite elements resulting in a covering Ω_h. The unknown scattered field u within each finite element can be approximated by using standard polynomial shape functions N_j, $j = 1, .., 6$, as follows :

$$u = \sum_{j=1}^{6} N_j u_j, \tag{3.14}$$

denoting by u_j, $j = 1, .., 6$, the nodal values of u at the interpolation points. This finite element is designated in the sequel as the T6 finite element (triangular finite element with six nodes)

Another way of building interpolating finite element functions, called (Laghrouche and Bettess,2000 ; Laghrouche et al.,2002) *plane wave finite element functions* , is to approximate the unknown field u within each triangular finite element by using the standard polynomial shape functions N_j, $j = 1, .., 6$, each function being enriched by n_q radiating plane waves $e^{ik\mathbf{d}_q \cdot (\mathbf{x} - \mathbf{x}_j)}$ centered at the j-th nodes and for n_q equally spaced directions of propagation :

$$\mathbf{d}_q = (\cos(\frac{2\pi(q-1)}{n_q}), \sin(\frac{2\pi(q-1)}{n_q}))^T, \; q = 1, .., n_q. \tag{3.15}$$

The resulting approximation of the wavefield, solution to (3.10), is seek through the following expansion on each triangle :

$$u = \sum_{j=1}^{6} \sum_{q=1}^{n_q} N_j e^{ik\mathbf{d}_q \cdot (\mathbf{x} - \mathbf{x}_j)} u_{jq} \tag{3.16}$$

with u_{jq} as the nodal values. This approximation is designated in the sequel of the paper as PWT6 finite element (Plane Wave with T6). One can also choose to discretize the alternative variational formulation (3.13). In this case, the finite element method is referred to as CPWT6 (Conjugate PWT6). The aim of these new basis functions is to partially reproduce the oscillations of the scattered field in Ω. The approximation (3.16) describes in a certain way the restriction of u on each triangle as a superposition of elementary plane waves of amplitude given by the shape functions N_j and with known phase through the idea of enrichment. The corresponding elementary matrices can be computed over each element analytically (Ortiz,2001) or numerically by using adapted integration procedures (Betess et *al.*,2003) or high-order Gauss-Legendre quadratures. Depending on the frequency, we have used up to 27 integration points during the numerical experiments presented in the next section. The finite element discretization of the variational problems (3.10) and (3.13) and using basis functions (3.14) or (3.16) leads to a linear system of coupled equations of the generic form :

$$\begin{pmatrix} \mathbf{A}_h & \mathbf{B}_h \\ \mathbf{C}_h & \mathbf{D}_h \end{pmatrix} \begin{pmatrix} \mathbf{u}_h \\ \boldsymbol{\varphi}_h \end{pmatrix} = \begin{pmatrix} \mathbf{b}_h \\ \mathbf{0} \end{pmatrix}. \tag{3.17}$$

The solution $(\mathbf{u}_h, \boldsymbol{\varphi}_h)$ is composed from the approximate wavefield $\mathbf{u}_h$ in $\mathbb{C}^{n_h}$, where n_h is the number of degrees of freedom of the finite element method (T6, PWT6 or CPWT6) for the covered domain Ω_h, h being the largest finite element size, and $\boldsymbol{\varphi}_h$ is in $\mathbb{C}^{Nn_{\Sigma_h}}$, designating by n_{Σ_h} the number of discretization points of the interpolated boundary $\Sigma_h := \partial\Omega_h$. We classically introduce $n_\lambda := h/\lambda$ as the density of discretization points per wavelength which is often used in scattering problems to measure the thickness of the mesh. The complex linear system (3.17) is sparse, globally non-symmetric, non-Hermitian and non-diagonally dominant. Its size is equal to #dof, where #dof designates the total number of degrees of freedom involved in the numerical solution. In the case of the unconjugated formulation, all sub-matrices $\mathbf{A}_h$, $\mathbf{B}_h$, $\mathbf{C}_h$ and $\mathbf{D}_h$ are however symmetric.

In this paper, we are mainly interested in studying the accuracy of the plane wave finite element method in conjunction with the Padé-type ABC. For this reason, we solve the linear system with a direct solver. It is known that plane wave finite element methods lead to ill-conditioned systems of equations (Laghrouche and Bettess,2000; Laghrouche et *al.*,2002; Ortiz,2001). This issue is not addressed here since only two-dimensional problems are studied and linear systems can be handled by a direct solver.

3.3 Numerical study

Based on the numerical experiments presented by Kechroud *et al.* in (Kechroud et *al.*,2005), we set the parameters of the Padé-type ABC to $N = 2$ and $\theta = \pi/6$ which yield a minimal spurious reflection at the boundary when solving exterior problems. The ABC plocation is measured by a parameter m which is the distance in terms of wavelengths between the boundary Γ_h of the scatterer Ω_h and the fictitious boundary Σ_h.

To measure the accuracy of the different finite element methods and formulations, we compute the relative Root-Mean Square (RMS) error (in percents %) between the reference solution and the approximate solution onto the computational domain Ω_h (respectively, Γ_h) in the $L^2(\Omega_h)$-norm (respectively, $L^2(\Gamma_h)$-norm). The reference solution is computed analytically if available or numerically with the CHIEF integral equation method (Kirkup,1998) for a high density n_λ. We also represent the far-field pattern given by the scattering amplitude :

$$u_\infty(\theta) = \frac{e^{i\frac{\pi}{4}}}{\sqrt{8\pi ik}} \int_\Gamma (\partial_{\mathbf{n}_\Gamma} u + ik\mathbf{n}_\Gamma \cdot \mathbf{d}' u) e^{-ik\mathbf{x}\cdot\mathbf{d}'} d\Gamma \tag{3.18}$$

through the bistatic Radar Cross Section (RCS) (also called the target strength) :

$$\mathrm{RCS}(\theta) = 10 \log_{10}(2\pi |u_\infty(\theta)|^2) \quad \text{(dB)} \tag{3.19}$$

setting $\mathbf{d}^r = (\cos(\theta), \sin(\theta))^T$ as the vector of observation in the polar coordinates system (r, θ).

3.3.1 The circular cylinder

The first test-case is the scattering problem of a plane wave of incidence $\mathbf{d} = (1, 0)^T$ by a circular cylinder of radius $a = 1$. The Padé-type condition is placed at a distance $b = 2$ (Fig.). It is known that the exact analytic solution to the exterior scattering problem (3.1) expands in Mie series (see Equation 3.23). However, comparing this solution to the one numerically computed with an artificial boundary condition would include some errors coming from the truncation by the fictitious boundary Σ. To avoid this problem and only observe the pollution involved into the finite element method, we begin by considering the solution to (3.2) with the Padé-type artificial boundary condition. Since this reference wavefield is solution to a bounded problem set in the crown Ω, then we can expand it as :

$$u^{ex}(r, \theta) = \sum_{m \in \mathbb{N}} \epsilon_m (-i)^m (A_m H_m^{(1)}(kr) + B_m H_m^{(2)}(kr)) \cos(m\theta), \tag{3.20}$$

where ϵ_m is the Neumann function which is equal to 1 for $m = 0$ and 2 otherwise. Functions $H_m^{(1)}$ and $H_m^{(2)}$ are respectively the first- and second-kind Hankel functions of order m. In the sequel, the prime $'$ denotes the derivative of a function with respect to the radial variable r and J_m is the Bessel function of order m. The complex-valued coefficients A_m and B_m are computed by imposing the Neumann boundary condition at Γ and the Padé-type condition at Σ. This leads to find (A_m, B_m) as the solution to the following linear system :

$$\begin{pmatrix} H_m^{(1)'}(ka) & H_m^{(2)'}(ka) \\ H_m^{(1)'}(kb) - ik_m H_m^{(1)}(kb) & H_m^{(2)'}(kb) - ik_m H_m^{(2)}(kb) \end{pmatrix} \begin{pmatrix} A_m \\ B_m \end{pmatrix} = \begin{pmatrix} -J_m'(ka) \\ 0 \end{pmatrix}, \tag{3.21}$$

setting

$$ik_m = ikC_0 - ik\sum_{j=1}^{N}\frac{A_j m^2/(b^2k_c^2)}{1-B_j m^2/(b^2k_c^2)} - \frac{1}{2b} + \frac{1}{8b^2(1/b-ik)} + \frac{m^2}{2k^2b^3}.$$

The solution to (3.21) is given by :

$$A_m = \frac{-J_m'(ka)}{\Delta_m}(H_m^{(2)'}(kb) - ik_m H_m^{(2)}(kb)),\ B_m = \frac{J_m'(ka)}{\Delta_m}(H_m^{(1)'}(kb) - ik_m H_m^{(1)}(kb)). \tag{3.22}$$

where $\Delta_m = H_m^{(1)'}(ka)(H_m^{(2)'}(kb) - ik_m H_m^2(kb)) - H_m^{(2)'}(ka)(H_m^{(1)'}(kb) - ik_m H_m^{(1)}(kb))$.

The analytical solution (3.20) is computed by using a finite number of Mie coefficients equal to $2kr + 5$ to ensure the convergence.

We consider a structured mesh built using using n_r elements in the radial direction and n_θ elements in the angular direction θ (Fig.3.1). We report on Table 3.1 the RMS error of the solution in the computational domain Ω_h and on the scatterer boundary Γ_h using the T6 FEM. We remark that the mesh refinement leads to a convergence of the numerical solution. Moreover, the error increases classically with ka. Most specifically, for $ka = 20$, a mesh resolution less than $n_r = 12$ and $n_\theta = 60$ does not give a satisfactory error. The situation is clearly much better if one considers now the PWT6 and CPWT6 FEM as seen on Table 3.2. Indeed, we can clearly observe an accuracy improvement of the error for the two coarse meshes $n_\theta \times n_r = 3 \times 15$ and $n_\theta \times n_r = 6 \times 30$ when the number of directions n_q increases. The CPWT6 always yields better results while it is necessary to consider an even number of directions n_q for the PWT6 FEM. For example, an error on the domain solution equal to 0.56% is obtained by the CPWT6 using 9360 dof while an error of 0.4% with 47040 dof is achieved for the T6 FEM. If we now fix an error of 5% at $ka = 20$, then we see that it can obtained using 12000 dof for the T6 FEM while only 3360 dof are required for the CPWT6 FEM using a mesh with 3×15 elements and $n_q = 4$ directions.

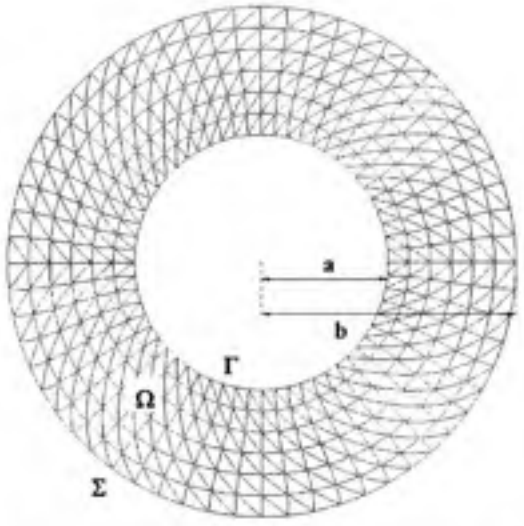

Figure 3.1 ***The circular shaped scatterer surrounded with a circular artificial boundary. The computational domain is meshed with structured quadratic finite elements .***

From the previous numerical experiments, it appears that the error control due to the pollution with high wave numbers could be achieved by increasing the mesh resolution while maintaining the number of directions constant in the CPWT6 and PWT6 schemes, or on the contrary, increasing the number of directions while keeping the mesh resolution constant. Furthermore, the CPWT6 and PWT6 schemes deliver globally the same accuracy for an even number of directions n_q. This is expected since for every wave going in one direction there is another one in the opposite direction. In this case, the complex representation of plane waves can be replaced by real-valued trigonometric basis functions. A consequence of this alternative representation is that the unconjugated variational formulation with sesquilinear operators (3.13) and the conjugated variational formulation with bilinear operators (3.10) become equivalent.

We now consider again the same scatterer for a wave number $ka = 60$. The direction of incidence of the plane wave is imposed such that $\mathbf{d} = (1,0)^T$. The exterior circular boundary Σ has a radius b equal to $a+m\lambda$((Fig.2.1)). To take into account now the effect of

Table 3.1

Sound-hard circular cylinder : relative RMS error (in %) in the computational domain Ω_h (respectively on Γ_h) of the T6 finite element for different meshes

$n_\theta \times n_r$	#dof	$ka = 1$	$ka = 5$	$ka = 10$	$ka = 20$
15×3	840	0.04 (0.02)	1.45 (0.87)	43.48 (40.68)	138.58 (48.55)
30×6	3120	0.01 (0.01)	0.10 (0.06)	2.39 (0.39)	67.87 (64.86)
60×12	12000	0.01 (0.01)	0.04 (0.03)	0.19 (0.06)	5.34 (1.47)
120×24	47040	0.01 (0.01)	0.03 (0.02)	0.03 (0.02)	0.40 (0.13)

Table 3.2

Sound-hard circular cylinder : relative RMS error (in %) in the computational domain Ω_h (respectively on Γ_h) of the CPWT6 and PWT6 finite elements for two coarse mesh $n_\theta \times n_r$ corresponding respectively to 3×15 and 6×30.

FEM	#dof	n_q	$ka = 1$	$ka = 5$	$ka = 10$	$ka = 20$
CPWT6	1×840	1	0.05 (0.04)	20.87 (1.15)	74.89 (5.94)	84.13 (16.30)
	2×840	2	0.05 (0.04)	0.23 (0.23)	6.81 (4.60)	54.02 (14.53)
	3×840	3	0.05 (0.04)	0.02 (0.03)	0.29 (0.28)	19.74 (5.76)
	4×840	4	0.05 (0.04)	0.02 (0.03)	0.05 (0.05)	2.70 (1.48)
PWT6	1×840	1	0.05 (0.04)	23.97 (26.42)	135.36 (94.35)	226.23 (179.65)
	2×840	2	0.05 (0.04)	0.23 (0.23)	6.81 (4.60)	54.02 (14.53)
	3×840	3	0.05 (0.04)	0.12 (0.10)	2.74 (2.62)	259.63 (225.30)
	4×840	4	0.05 (0.04)	0.02 (0.03)	0.05 (0.05)	2.70 (1.48)
CPWT6	1×3120	1	0.01 (0.01)	1.67 (0.12)	37.91 (0.78)	80.40 (4.03)
	2×3120	2	0.01 (0.01)	0.18 (0.18)	0.37 (0.19)	12.85 (7.03)
	3×3120	3	0.01 (0.01)	0.02 (0.03)	0.10 (0.08)	0.56 (0.42)
	4×3120	4	0.01 (0.01)	0.02 (0.03)	0.04 (0.02)	0.06 (0.06)
PWT6	1×3120	1	0.01 (0.01)	2.27 (1.22)	19.45 (12.59)	175.94 (120.43)
	2×3120	2	0.01 (0.01)	0.18 (0.18)	0.37 (0.19)	12.85 (7.03)
	3×3120	3	0.01 (0.01)	0.10 (0.10)	0.21 (0.11)	8.25 (4.29)
	4×3120	4	0.01 (0.01)	0.02 (0.03)	0.04 (0.02)	0.06 (0.06)

truncating the exterior domain, the reference solution solves the boundary value problem (3.1) in the polar coordinates system (r, θ) :

$$u^{ex}(r,\theta) = \sum_{m\in\mathbb{N}} \epsilon_m (-i)^m \frac{J_m'(ka)(kr)H_m^{(1)}(kr)}{H_m^{(1)'}(ka)} \cos(m\theta), \tag{3.23}$$

for the sound-hard scatterer and

$$u^{ex}(r,\theta) = \sum_{m\in\mathbb{N}} \epsilon_m (-i)^m \frac{J_m(ka)(kr)H_m^{(1)}(kr)}{H_m^{(1)}(ka)} \cos(m\theta), \tag{3.24}$$

for sound-soft problem. We report in Tables 3.3 and 3.4 the relative errors with respect to the analytical solution of the scattered field in Ω_h and on Γ_h for the sound-hard disk and only in Ω_h for the sound-soft case. We can note different important remarks :

- Using the PWT6 or CPWT6 FEM lead to a significant gain of accuracy in the solution for a low density of discretization points n_λ.
- Increasing n_q yields an interesting accuracy improvement. Again, an even value of n_q is required for stability reasons linked to the PWT6 FEM.
- An excellent accuracy is given even for a close fictitious boundary Σ leading to a drastic diminution of the total number of degrees of freedom.
- The accuracy is generally better for the sound-soft problem.

Another quantity of interest for practitioners is the RCS. To this end, we report on Figures 3.2 and 3.3 the RCS for a position of the boundary $m = 0.15$ and $n_\lambda = 1$, for $n_q = 2$ directions in the CPWT6 FEM for respectively the sound-hard and sound-soft problems. We observe an excellent agreement between the reference and the numerical solutions.

Table 3.3

Sound-hard and sound-soft circular cylinder : RMS error in the computational domain Ω_h (and on Γ_h for the sound-hard case) at $ka = 60$ and $\theta^{inc} = 0$ degree for the T6 FEM

m	n_λ	# dof	hard err. in %	soft err. in %
0.15	1	600	76.56(79.17)	47.07
	2	752	21.65(21.72)	5.71
	4	1452	4.48(4.79)	2.67
	8	2904	2.59(2.59)	0.63
	16	11548	2.59(2.59)	0.57
1.2	2	1344	38.60(38.20)	27.36
	4	5896	3.74(1.85)	3.74
	8	22676	0.89(1.11)	0.88
	16	89376	0.89(1.11)	0.88

Table 3.4

Sound-hard and sound-soft circular cylinder : RMS error in the computational domain Ω_h (and on Γ_h for the sound-hard case) at $ka = 60$ and $\theta^{inc} = 0$ degree for the PWT6 and CPWT6 FEM

m	n_λ	n_q	#dof	hard, CPWT6 err. in %	soft, CPWT6 err. in %	hard, PWT6 err. in %	Soft, PWT6 err. in %
0.15	1	1	1×600	3.01(3.11)	0.60	5.49(5.51)	1.24
		2	2×600	2.87(3.05)	0.23	2.87(3.05)	0.23
		3	3×600	2.69(2.77)	0.35	4.62(6.65)	2.59
		4	4×600	1.73(2.38)	0.14	1.73(2.38)	0.13
0.15	2	1	1×752	2.79(2.77)	1.1	6.78(9.44)	5.32
		2	2×752	2.68(2.68)	0.42	2.13(2.61)	0.42
		4	4×752	0.86(1.64)	0.34	0.86(1.64)	0.34
1.2	2	1	1×1344	78.30(8.83)	147.72	82.52(126.89)	147.72
		2	2×1344	34.31(6.34)	73.8	34.30(6.33)	124.73
		4	4×1344	1.47(1.07)	1.44	1.47(1.07)	1.44
1.2	4	1	1×5896	22.58(1.51)	21.41	10.80(16.47)	21.93
		2	2×5896	1.48(1.57)	1.64	1.48(1.57)	1.64
		4	4×5896	1.02(0.95)	0.96	1.35(0.95)	0.96

3.3.2 The sound-hard elliptical cylinder

We consider now a sound-hard elliptical cylinder with a major and minor semi-axis respectively equal to $a = 1$ and $b = 0.25$ along the x- and y-directions. The obstacle is

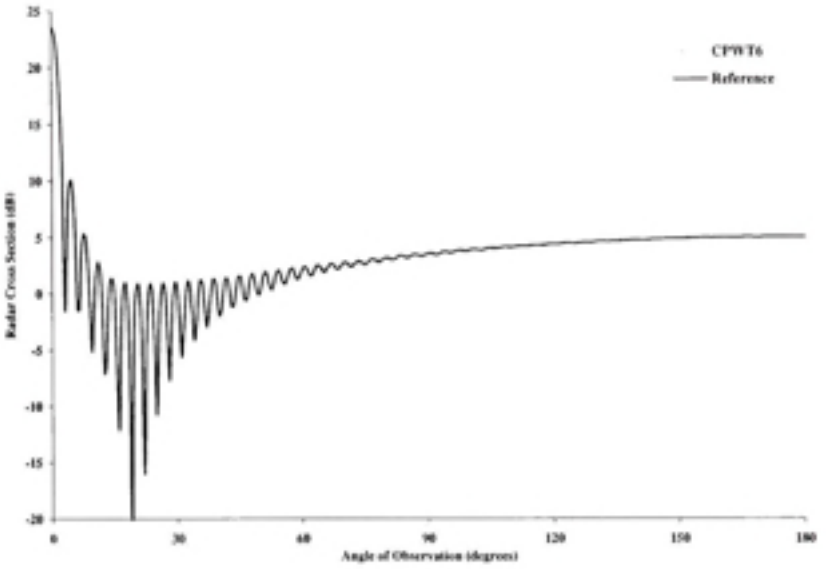

Figure 3.2 ***Radar Cross Section of the sound-hard circular cylinder at*** $ka = 60$, $\theta^{inc} = 0$ ***degree,*** $m = 0.15$, $n_\lambda = 1$ ***and*** $n_q = 2$ ***using the Padé-type ABC.***

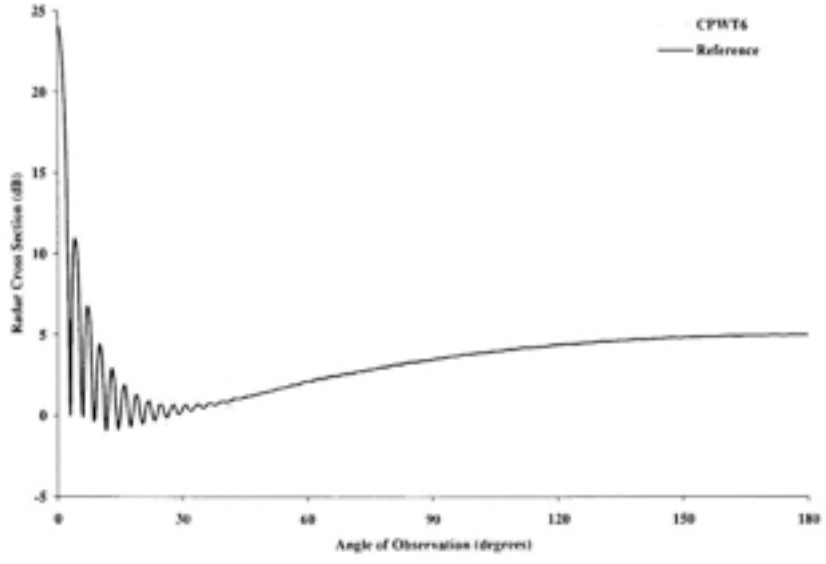

Figure 3.3 ***Radar Cross Section of the sound-soft circular cylinder at*** $ka = 60$, $\theta^{inc} = 0$ ***degree,*** $m = 0.15$, $n_\lambda = 1$ ***and*** $n_q = 2$ ***using the Padé-type ABC.***

centered at the origin. The wave number is set to $ka = 60$ and the direction of the incident plane wave is $\mathbf{d} = (\frac{\sqrt{2}}{2}, \frac{\sqrt{2}}{2})^T$. The reference solution is computed by the (CHIEF) integral equation method (Kirkup,1998) using a mesh resolution of $n_\lambda = 80$ elements per wavelength to ensure a high accuracy. The fictitious boundary Σ is an ellipse with major (respectively minor) semi-axis equal to $a' = a + m\lambda$ (respectively $b' = b + m\lambda$).(Fig.2.3)

We report in Tables 3.5 and 3.6 the relative error with respect to the reference solution of the trace on Γ_h of the scattered field. On this new example different points must be noticed :

- An important accuracy improvement is again obtained when using the CPWT6 and PWT6 FEM. Moreover, the CPWT6 method generally leads to a better accuracy. Using the PWT6 FEM requires an even value of n_q to get a satisfactory precision. Finally, increasing n_q gives a higher accuracy.
- The fictitious boundary can be set very close to the scatterer but, to obtain a good accuracy for low discretization densities, the CPWT6 or PWT6 FEM must be used with $n_q \geq 2$. Of course, a limited accuracy is obtained for a fixed distance m and, as expected, increasing m yields an improved solution.

We see on this example that we can get a small error approximation if we combine the CPWT6 (or PWT6) FEM with the Padé-type ABC. We must notice at this point that using a low-order ABC for high wave number would have the effect of leading to large computational domains and much more pollution. This is why the two following points must be used in conjunction : 1) to use a high-order accurate ABC for large wave numbers in order to have a small size computational domain and therefore also less pollution and 2) to consider a suitable approximation method like the CPWT6 FEM to reduce the pollution effect.

To see the impact on the RCS computation, we present some results on Figures 3.4 and 3.5 obtained for different mesh resolutions and values of n_q for the CPWT6 and T6 FEM. We

see that a much better accuracy is obtained for the CPWT6 approach using for example the discretization corresponding to 3×120 dof . This is again confirmed on Figure 3.6 where the fictitious boundary is placed at a larger distance to improve the accuracy.

Table 3.5

Sound-hard elliptical cylinder : RMS error on Γ_h for the T6 FEM at $ka = 60$, $\theta^{inc} = 45$ degrees

m	n_λ	#dof	Err. on Γ_h (%)
0.15	1	272	66.89
	2	524	18.58
	4	996	4.43
	8	1992	4.43
1.2	2	944	29.56
	3	2172	5.27
	4	3824	2.33
	8	15336	1.49
	16	18352	1.47

Table 3.6

Sound-hard elliptical cylinder : RMS error on Γ_h for the CPWT6 and PWT6 FEM at $ka = 60, \theta^{inc} = 45$ degrees

m	n_λ	n_q	#dof	CPWT6 Err. on Γ_h in %	PWT6 Err. on Γ_h in %
0.15	0.5	1	1×120	14.84	71.13
		2	2×120	12.55	12.55
		3	3×120	7.54	28.37
		4	4×120	7.51	7.51
0.15	1	1	1×240	8.59	23.95
		2	2×240	5.30	5.30
		3	3×240	5.07	7.00
		4	4×240	5.03	5.03
0.15	2	1	1×524	6.08	11.82
		2	2×524	4.74	4.74
		3	3×524	4.74	4.88
		4	4×524	4.74	4.74
0.15	4	1	1×996	6.05	4.85
		2	2×996	4.64	4.64
		3	3×996	4.64	4.80
		4	4×996	4.64	4.64
1.2	1	3	3×264	20.22	97.66
		4	4×264	4.66	4.66
		5	5×264	2.44	15.28
		6	6×264	1.69	1.69
		7	7×264	1.64	4.69
		8	8×264	1.63	1.63
1.2	2	1	1×944	12.00	122.26
		2	2×944	11.94	12.62
		3	3×944	2.42	7.01
		4	4×944	1.52	1.52
		5	5×944	1.50	1.69
1.2	4	1	1×3824	3.36	24.34
		2	2×3824	1.94	1.94
		3	3×3824	1.47	1.49

3.3.3 The submarine-like shaped scatterer

To consider a more realistic case, we choose the submarine-like shaped scatterer shown on Fig.3.7. We set its dimensions as follows : the total length is $L = 11m$, its thickness is $D = 1m$, the height and length of the tower are respectively $l = 1m$ and $2l = 2m$.

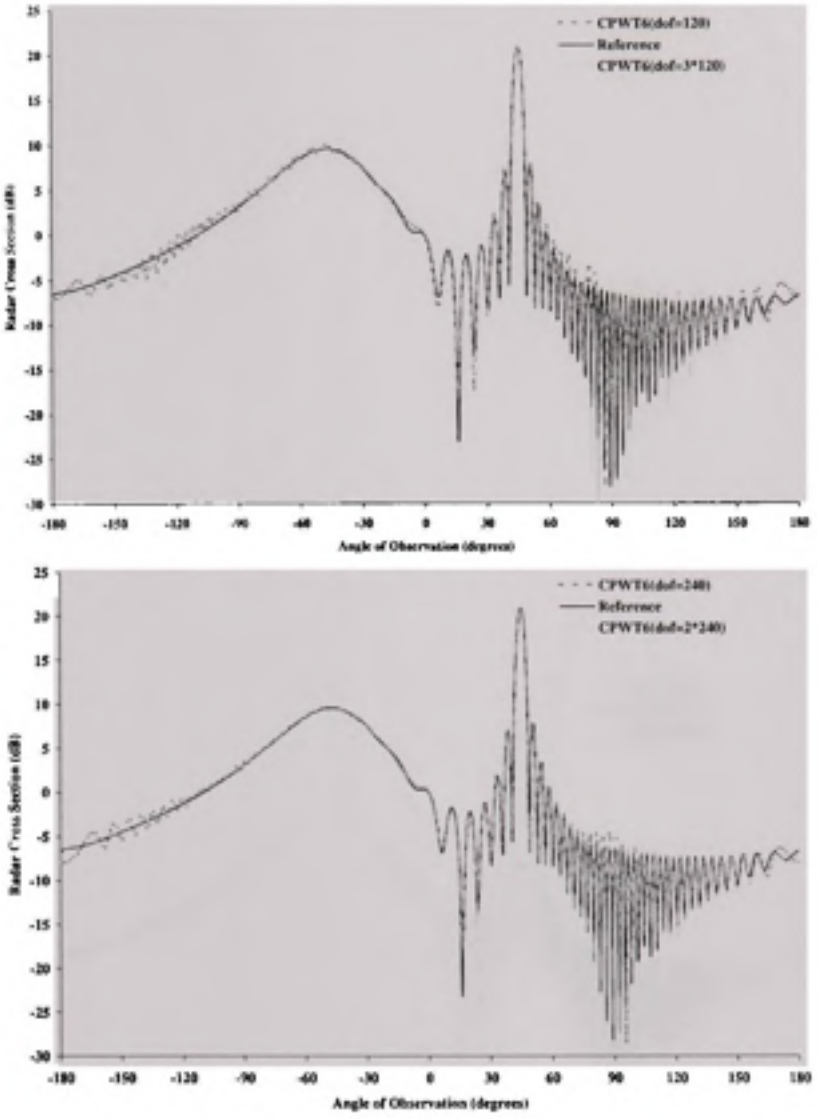

Figure 3.4 ***Comparison of the computed RCS of the sound-hard elliptical cylinder at*** $ka = 60$, ***for*** $\theta^{inc} = 45$ ***degrees and*** $m = 0.15$. ***We use the CPWT6 FEM for different values of*** n_q.

We perform several acoustic scattering computations at for $kD = 20$ for an incidence vector $\mathbf{d} = -(\frac{\sqrt{2}}{2}, \frac{\sqrt{2}}{2})^T$. We place an elliptical fictitious boundary Σ (Fig. 3.7) with a major semi-axis (resp. a minor semi-axis) equal to $a' = L/2 + m\lambda$ (respectively $b' =$

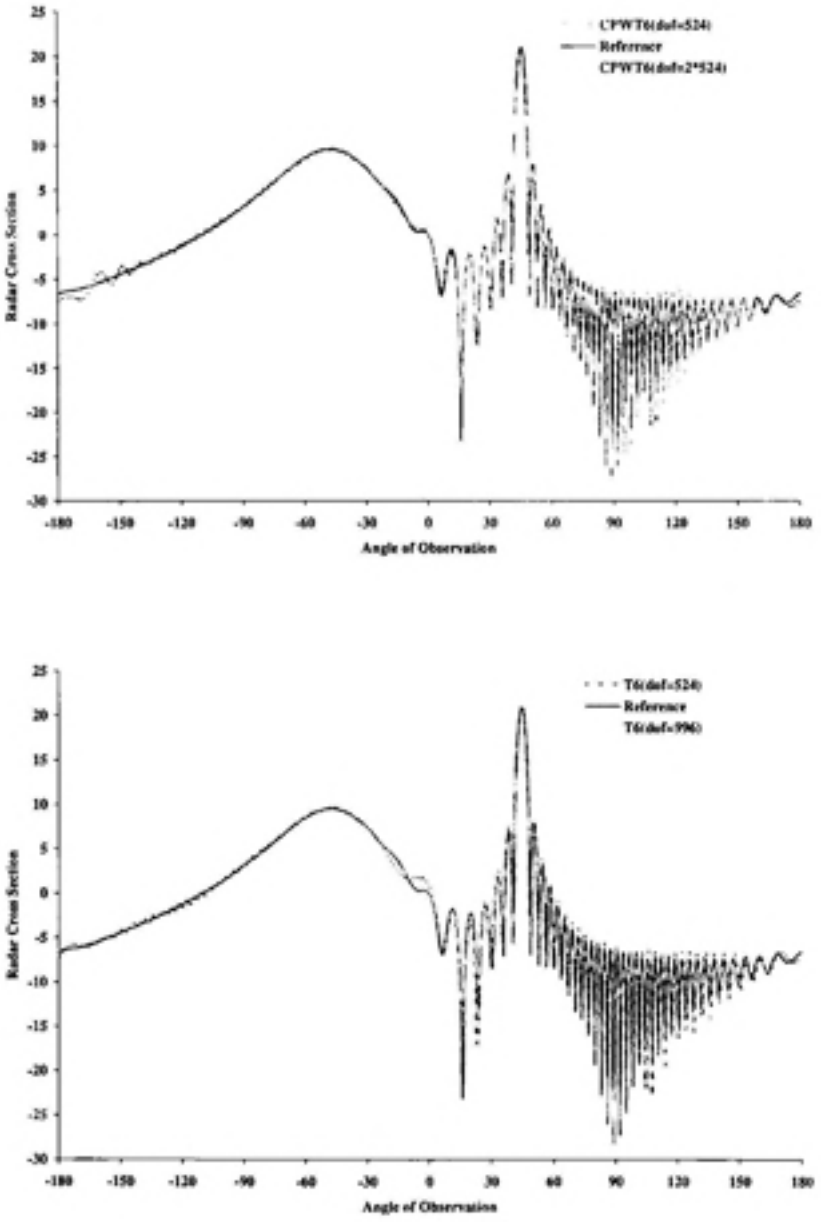

Figure 3.5 ***Comparison of the computed RCS of the sound-hard elliptical cylinder at*** $ka = 60$, ***for*** $\theta^{inc} = 45$ ***degrees and*** $m = 0.15$. ***We again increase the mesh resolution and compare it to the T6 FEM.***

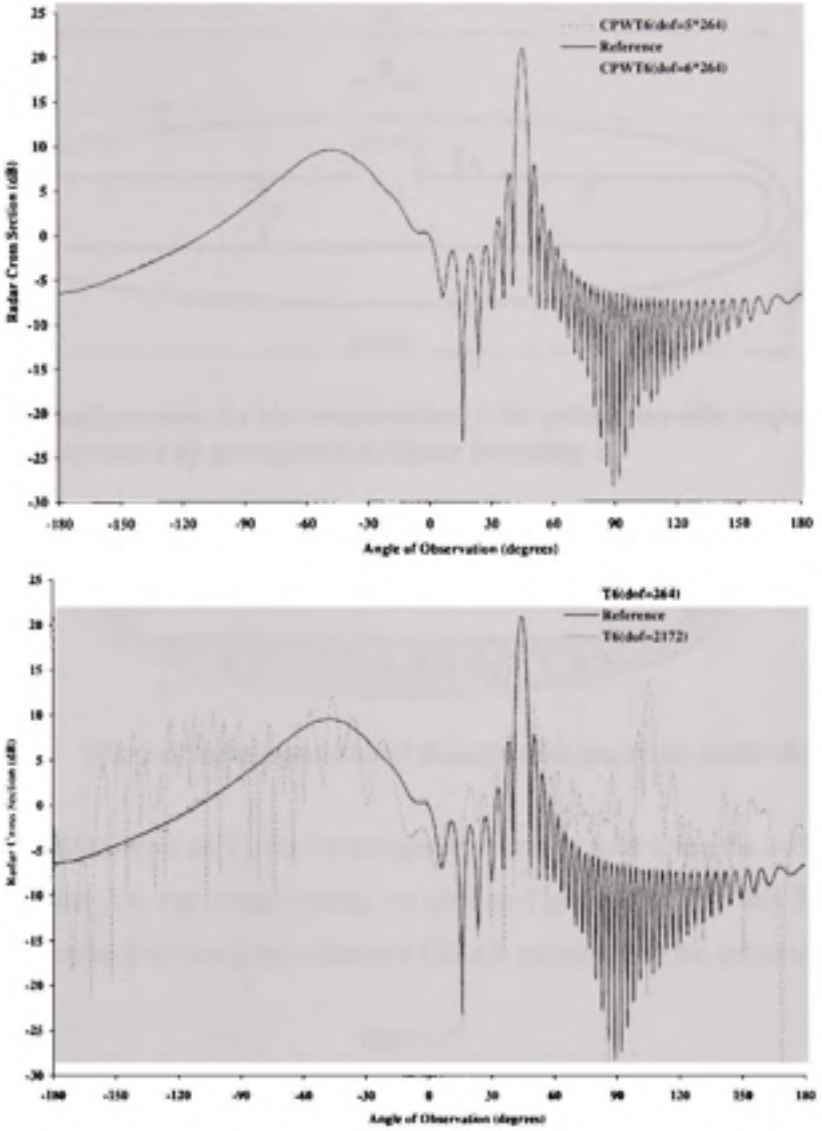

Figure 3.6 ***Comparison of the computed RCS of the sound-hard elliptical cylinder at*** $ka = 60$***, for*** $\theta^{inc} = 45$ ***degrees and*** $m = 1.2$.

$D/2 + l + m\lambda$) which circumscribe the submarine. The computational domain bounded by Σ and Γ is meshed with quadratic finite elements (Fig.3.8). The reference solution is obtained again with the CHIEF integral equation method (Kirkup,1998) for a mesh resolution corresponding to $n_\lambda = 40$ elements per wavelength to ensure a high accuracy.

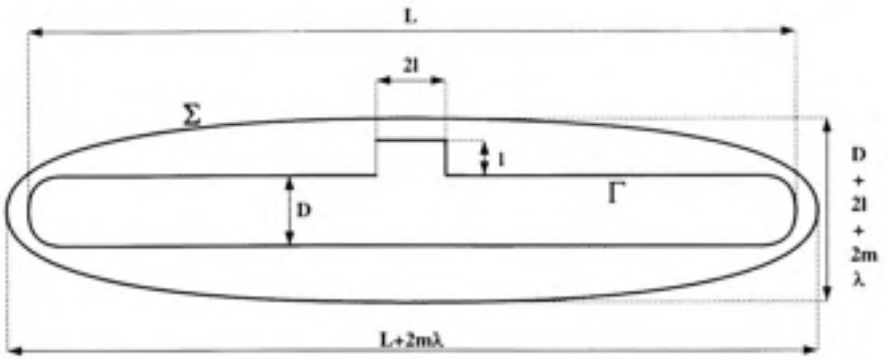

Figure 3.7 ***Configuration for the computations : the submarine-like shaped scatterer is enclosed by an elliptical fictitious boundary*** Σ.

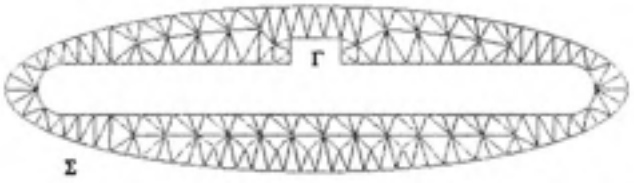

Figure 3.8 ***Mesh of the computational domain with quadratic finite elements.***

We report the RMS error on Γ_h for the computed scattered field using the different FEM in Tables 3.7 and 3.8. For completeness, we plot on Figures 3.9, 3.10 and 3.11 the bi-static RCS computed by using the reference CHIEF solution and the solutions obtained

Table 3.7

Sound-hard submarine-like scatterer : RMS error on the computational domain Γ_h for the T6 finite element method for $kD = 20$ and $\theta^{inc} = 225$ degrees

m	n_λ	#dof	Err. on Γ_h in %
1	2	2582	26.7
	4	10102	5.25
	6	22410	3.82
	8	38544	3.13
2	2	3942	27.95
	4	15493	4.04
	6	34037	2.46
	8	60622	1.85

Table 3.8

Sound-hard submarine-like scatterer : RMS error on the computational domain Γ_h for CPWT6 and PWT6 finite elements for $kD = 20$ and $\theta^{inc} = 225$ degrees

m	n_λ	n_φ	#dof	CPWT6 Err. on Γ_h in %	PWT6 Err. on Γ_h in %
1	1	4	4 × 701	14.83	14.83
		5	5 × 701	4.67	14.18
		6	6 × 701	3.99	3.99
		7	7 × 701	3.82	7.51
		8	8 × 701	3.82	3.82
1	2	1	1 × 2582	48.30	104.85
		2	2 × 2582	27.85	27.85
		3	3 × 2582	4.50	6.10
		4	4 × 2582	3.30	3.30
		5	5 × 2582	3.23	3.84
1	4	1	1 × 10102	17.63	30.46
		2	2 × 10102	4.30	4.30
		3	3 × 10102	3.09	3.18
2	1	4	4 × 1041	14.34	14.34
		5	5 × 1041	3.15	46.66
		6	6 × 1041	2.80	2.80
		8	8 × 1041	2.44	2.44
2	2	1	1 × 3942	45.18	105.16
		2	2 × 3942	25.95	25.95
		3	3 × 3942	2.58	13.30
		4	4 × 3942	2.04	2.04
		5	5 × 3942	2.04	3.25
2	4	1	1 × 15493	17.00	44.37
		2	2 × 15493	2.99	2.99
		3	3 × 15493	1.88	2.60

using the T6 and CPWT6 FEM for different mesh resolutions and positions of the ABC. From the reported results, we can notice that to obtain a suitable accuracy for engineering calculations :

- We have to increase the number of directions in the CPWT6 and PWT6 FEM when the mesh resolution is low in order to control the pollution error. Indeed, a number of directions $n_\varphi = 6$ seems to be sufficient for a mesh resolution of $n_\lambda = 1$. This can be further decreased to only two directions per node if the mesh resolution consists

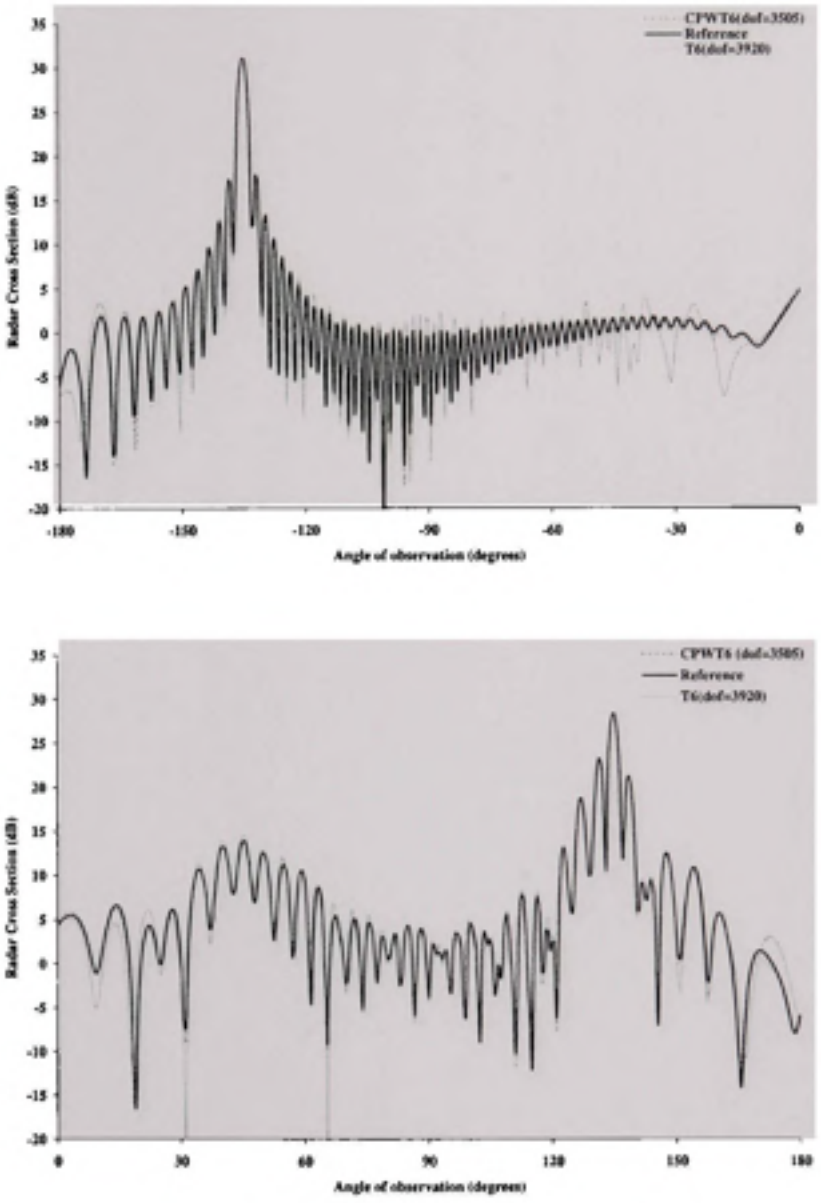

Figure 3.9 ***Comparison of the RCS of the sound-hard submarine-like scatterer for*** $kD = 20$, $m = 1.0$ ***and*** $\theta^{inc} = 225$ ***degrees using the Padé-type ABC with the T6 and the CPWT6 finite elements (setting*** $n_\lambda = 1$ ***and*** $n_q = 5$ ***for the CPWT6 FEM and*** $n_\lambda = 2.5$ ***for the T6 FEM).***

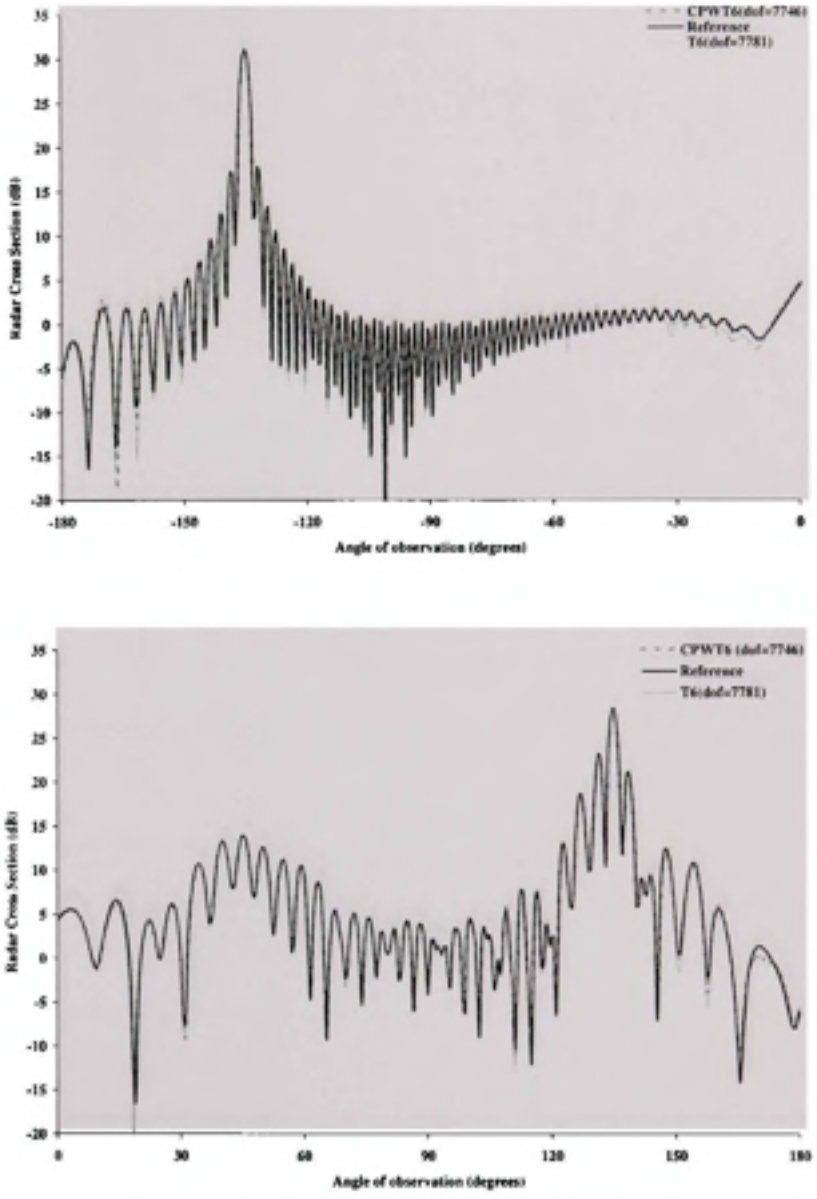

Figure 3.10 ***Comparison of the RCS of the sound-hard submarine-like scatterer for*** $kD = 20$, $m = 1.0$ ***and*** $\theta^{inc} = 225$ ***degrees using the Padé-type ABC with the T6 and CPWT6 finite elements (setting now*** $n_\lambda = 2$ ***and*** $n_q = 3$ ***for the CPWT6 FEM and*** $n_\lambda = 3.5$ ***for the T6 FEM).***

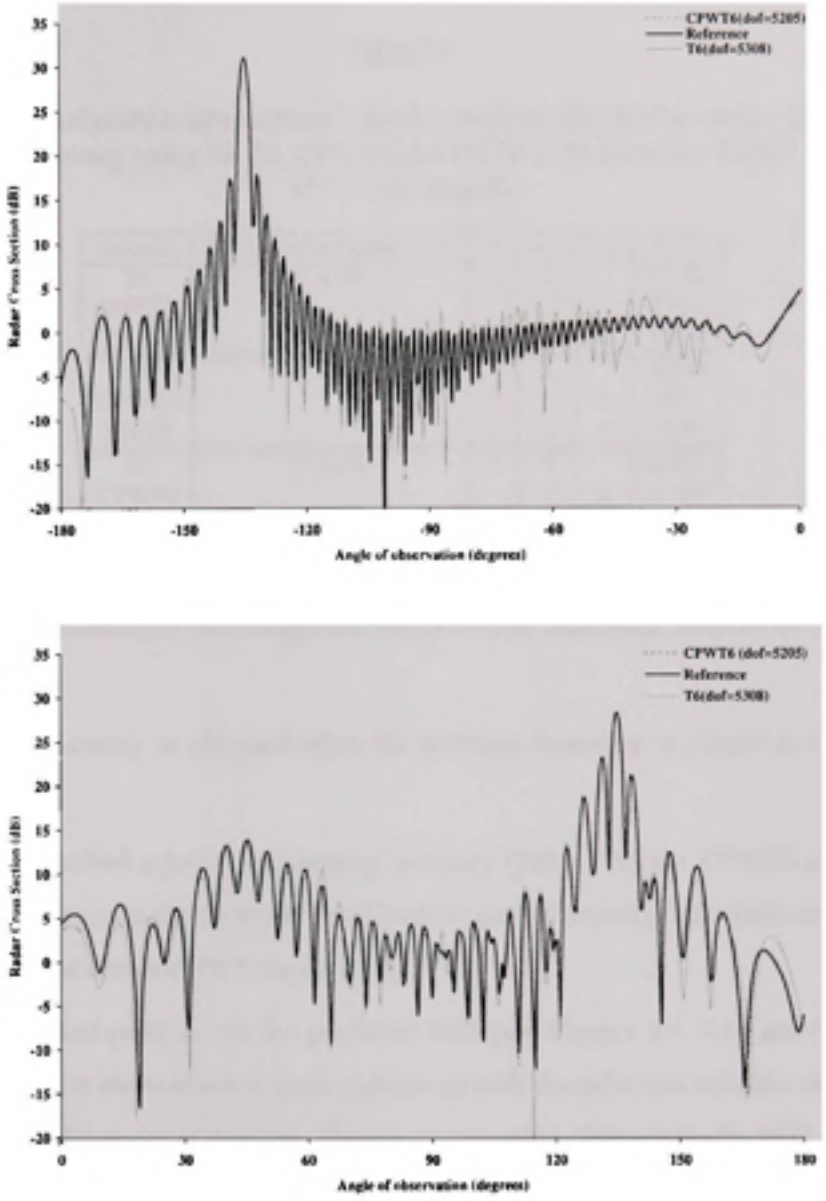

Figure 3.11 ***Comparison of the RCS of the sound-hard submarine-like scatterer for*** $kD = 20$, $m = 2.0$ ***and*** $\theta^{inc} = 225$ ***degrees using the Padé-type ABC with the T6 and CPWT6 FEM (*** $n_\lambda = 1$ ***and*** $n_q = 5$ ***for the CPWT6 and*** $n_\lambda = 2.3$ ***for the T6 FEM).***

Table 3.9

Sound-hard submarine-like scatterer : mesh resolution and #dof needed to achieve a prescribed accuracy using the T6, CPWT6 and PWT6 finite elements for $kD = 20$ and $\theta^{inc} = 225$ degrees

element	prescribed accuracy in %	m	n_λ	n_q	#dof
T6	$\leq 5.5\%$	1	4		10102
CPWT6			1	5	3505
PWT6			1	6	4206
T6	$\leq 3.2\%$	1	8		38544
CPWT6		2	1	5	5205
PWT6		2	1	6	6246
T6	$\leq 2.1\%$	2	8		60622
CPWT6			2	4	15768
PWT6			2	4	15768

of four elements per wavelength but the cost is an increasing number of degrees of freedom.

- A better accuracy is obtained when the fictitious boundary is placed at $m = 2$ as expected.
- For a prescribed *a priori* engineering accuracy (Table 3.9), the CPWT6 and PWT6 FEM require only coarse meshes and leads to small systems of equations in comparison with the classical T6 finite element.

Another important point is that the predicted RCS (see Figures 3.9, 3.10 and 3.11) with the CPWT6 finite element are in good agreement with the reference solution even with a small number of degrees of freedom. The situation is quite different for the RCS computed by the T6 finite element solution since a correct agreement with the reference RCS is lost when the mesh resolution is less than three elements per wavelength. These last computations on a more realistic test-case shows that it is finally important for efficiency and accuracy reasons to combine both a high-order ABC and a suitable finite element method like the CPWT6 FEM for high frequencies.

3.4 Conlusion

We have conducted in this paper a numerical study to analyze the performance of coupling a high-order artificial boundary condition and conjugate and unconjugate plane wave finite element methods for solving two-dimensional high-frequency scattering problems. It is shown that small computational domains in terms of wavelength are needed to achieve a satisfactory accuracy on the trace of the wavefield and radar cross section. In particular, the method leads to a reduction of the effect of pollution into the global numerical method. The superiority of the conjugate finite element method is shown compared to a classical quadratic Lagrange finite element method and the unconjugate plane wave version. The performance is analyzed in detail for three numerical examples and in particular for a submarine-like scatterer. In a forthcoming work, we will focus on the extension to three-dimensional scattering problems.

BIBLIOGRAPHIE

Antoine, Xavier, Barucq Hélène, et Bendali Abderrahmane. 1999. ≪Bayliss-Turkel like radiation condition on surfaces of arbitrary shape≫. *Journal of Mathematical Analysis and Applications*, vol.229, n°3, p.184-211.

Antoine, Xavier, Darbas Marion et Lu Ya Yan. 2005. ≪An improved On-Surface Radiation Condition for acoustic scattering in the high-frequency spectrum≫. *Comptes Rendus de l'Academie des Sciences. Serie 1, Mathematique*, vol.340, n°10, (Mai), p. 769-774.

Antoine Xavier, Darbas Marion et Lu Ya Yan. 2006. ≪An Improved Surface Radiation Condition for High-Frequency Acoustic Scattering Problems≫. *Computer Methods in Applied Mechanics and Engineering*, vol.195, n°33-36, (Juillet), p.4060-4074.

Antoine, Xavier. 2007. ≪Advances in the On-Surface Radiation Condition Method : Theory, Numerics and Applications≫. In *Computational Methods in Acoustics*, Saxe-Coburg, pp. 169-194. (to appear)

Astley, R.J. 2000. ≪Infinite element for wave problems : a review of current formulations and an assessment of accuracy≫. *International Journal for Numerical Methods in Engineering*, vol.49, n°7, p.951-976.

Babuška, Ivo, Sauter Stefan A. 1997. ≪Is the pollution effect of the FEM avoidable for the Helmholtz equation considering high wave numbers≫. *Society for Industrial and Applied Mathematics : Journal of Numerical Analysis*, vol.34, n°6, (Décembre), p.2392-2423.

Bayliss, Alvin and Turkel Eli. 1980. ≪Radiation boundary conditions for wave-like equations≫. *Communications on Pure and Applied Mathematics*, vol.33, n°6, p.707-725.

Bayliss, Alvin, Gunzburger Max and Turkel Eli. 1982. ≪Boundary conditions for the numerical solution of elliptic equations in exterior regions≫. *Society for Industrial and Applied Mathematics : Journal of Applied Mathematics*, vol.42, n°2, p.430-451.

Bendali, Abderrahmane and Fares M'Barek. 2007. *Boundary Integral Equations in Acoustic Scattering*. Coll. ≪ Rapport interne du Laboratoire MIP≫, Internal Report 07-05, Toulouse (France), Laboratoire de Mathématiques pour l'Industrie et la Physique, 33 p.

Bérenger, Jean-Pierre. 1994. ≪A perfectly matched layer for the absorption of electromagneticwaves≫. *Journal of Computational Physics*, vol.114, n°2, (Octobre), p.185-200.

Bettess, Peter, Shirron Joseph, Laghrouche Omar, Peseux Bernard, Sugimoto Rie ND Trevelyan John. 2003. ≪A numerical integration scheme for special finite elements for the Helmholtz equation≫. *International Journal for Numerical Methods in Engineering*, vol.56, n°4, p. 531-552.

Bruno, Oscar O. 2007. ≪New high-order integral methods in computational electromagnetism≫. *Computer Modeling in Engineering & Sciences*, vol.5, n°4, p.319-330.

Burton, A.J. AND Miller G.F. 1971. ≪The Application of Integral Equation Methods to the Numerical Solution of Some Exterior Boundary-Value Problems. *Proceedings of the Royal Society of London. Series A, Mathematical and Physical Sciences*, vol.323, n°1553, A discussion on numerical analysis of partial differential equations, (Juin), p.201-210.

Chew, Weng Cho, Jin Jiang-Ming, Michielssen Eric AND Song Jiming. 2001. *Fast and Efficient Algorithms in Computational Electromagnetics*. 1st ed. Norwood : Artech House Antennas and Propagation Library, 993 p.

Djellouli, Rabia, Farhat Charbel, Macedo Antonini and Tezaur Radek. 2000. ≪Finite element solution of two-dimensional acoustic scattering problems using arbitrarily shaped convex artificial boundaries≫. *Journal of Computational Acoustics*, vol.8, n°1, (Mars), p.81-99.

Tezaur, Radek, Macedo Antonini, Farhat Charbel and Djellouli Rabia. 2000. ≪Three dimensional finite element calculations in acoustic scattering using arbitrarily shaped convex artificial boundaries≫. *International Journal for Numerical Methods in Engineering*, vol.53, n°3, p.1461-1476.

Colton, David et Kress Rainer. 1983. *Integral Equation Methods in Scattering Theory*. 1st ed. ≪Pure and Applied Mathematics≫. New York, USA : John Wiley and Sons Inc., 286p.

Darve, Eric. 2000. ≪The fast multipole method : numerical implementation≫. *Journal of Computational Physics*, vol.160,, n°1, p.195-240.

Enquist, Bjorn et Majda Andrew. 1977. ≪Absorbing boundary conditions for the numerical simulation of waves≫. *Mathematics of Computation*, vol.31, n°139, (Juillet), p.629-651.

Farhat, Charbel, Tezaur Radek and Djellouli Rabia. 2002. ≪On the solution of three-dimensional inverse obstacle acoustic scattering problems by a regularized Newton method≫. *Inverse Problems*, vol.18, n°5, p.1229-1246.

Gerdes, Klaus. 2000. ≪A review of infinite element methods for exterior Helmholtz problems≫. *Journal of Computational Acoustics*, vol.8, n°1, (Mars), p. 43-62.

Guddati, Murthy N. and Lim Keng-Wit. 2005. ≪Continued fraction absorbing boundary conditions for convex polygonal domains≫. *International Journal for Numerical Methods in Engineering*, vol.66, n°6 , p.949-977.

Givoli, Dan. 1999. ≪Exact representation on artificial interfaces and applications in mechanics≫.*Applied Mechanics Reviews*, vol.52, n°9, p.333-349.

Givoli, Dan. 2004.≪High-order local non-reflecting boundary conditions : a review≫.*Wave Motion*, vol.39, p.319-326.

Hagstrom, Thomas. 1999. ≪Radiation boundary conditions for the numerical simulation of waves≫. *Acta Numerica*, p.47-106.

Ihlenburg, Franck, 1998. *Finite Element Analysis of Acoustic Scattering*. 1st ed. Coll. ≪Applied Mathematical Sciences≫, vol.132. New York : Springer-Verlag New York, Inc., 224 p.

Kechroud, Riyad, Antoine Xavier and Soulaïmani Azzeddine. 2005. ≪Numerical accuracy of a Padé-type non-reflecting boundary condition for the finite element solution of acoustic scattering problems at high-frequency≫. *International Journal for Numerical Methods in Engineering*, vol.64, n°10, p.1275-1302.

Kechroud, Riyad, Soulaïmani Azzeddine, Antoine Xavier. 2006. ≪Padé absorbing boundary conditions for finite element solution of high frequency scattering problems≫. In *IEEE International Symposium on Industrial Electronics, ISIE 2006*.(Montréal, Juillet 9-12 2006), p.2626-2630. Montréal : IEEE.

Kirkup, Stephen. 1998. The Boundary Element Method in Acoustics : A Development in Fortran. Coll. ≪Integral Equation Methods in Engineering≪. nouvelle ed. Hebden Bridge : Integrated Sound Software, 158 p. The code is available at : http ://www.boundary-element-method.com/.

Kriegsmann, Gregory A., Taflove Allen and Umashankar Korada R. 1987. ≪A new formulation of electromagnetic wave scattering using the on-surface radiation condition method≫. *Institute of Electrical and Electronics Engineers : Transactions on Antennas and Propagation*, vol.35, n°2, p.153-161.

Laghrouche, Omar and Bettess Peter. 2002. ≪ Short wave modelling using special finite elements≫. *Journal of Computational Physics*, vol.8, n°1, (Mars), p.189-210.

Laghrouche, Omar, Bettess Peter and Astley R. J. ≪Modelling of short wave diffraction problems using approximating systems of plane waves≫. *International Jourani of Numerical Methods in Engineering*, vol.54, n°54, p.1501-1533.

Lindmann, E.F., 1985. ≪Free-space boundary conditions for the time dependent wave equation≫. *Journal of Computational Physics*, vol.18, p.16-78.

Milinazzo, Fausto A., Zala Cedric A. and Brooke Gary H. 1997. ≪Rational square-root approximations for parabolic equation algorithms≫. *The Journal of the Acoustical Society of America*, vol.101, n°2, p.760-766.

Molinet, Frédéric, Andronov Ivan V. and Bouche Daniel. 2005. *Asymptotic and Hybrid Methods in Electromagnetics*. 1st ed. Coll. ≪IEE Electromagnetic Waves Series≫. London (England) :The Institution of Electrical Engineers, 249p.

Nédélec, Jean-claude. 2001. *Acoustic and Electromagnetic Equations, Integral Representations for Harmonic Problems*. Coll. ≪Applied Mathematical Sciences≫, vol.144, New York : Springer-Verlag, Inc., 318 p.

Ortiz, P. and Sanchez E. 2001. ≪An improved partition of unity finite element model for diffraction problems≫. *International Journal of Numerical Methods in Engineering*, vol.50, n°12, p.2727-2740. Volume 50,

Rokhlin, V. ≪Rapid solution of integral equations of scattering theory in two dimensions≫. *Journal of Computational Physics*, vol.86, n°12, (Février), p.414-439.

Thompson, Lonny L. 2006. ≪A review of finite element methods for time-harmonic acoustics≫. *Journal of the Acoustical Society of America*, vol.119, n°3, p.1315-1330.

Turkel, Eli. 1998. ≪Absorbing PML boundary layers for wave-like equations≫. *Applied Numerical Mathematics*, vol.27, n°4, (Août), p.533-557.

Turkel, Eli. 2007.*Boundary Conditions and Iterative Schemes for the Helmholtz Equation in Unbounded Regions*. In *Computational Methods in Acoustics*, Saxe-Coburg Editors. (to appear)

Tsynkov, Simon V. 1998. ≪Numerical solution of problems on unbounded domains. A review≫. *Applied Numerical Mathematics*, vol.27, n°4, (Août) p.465-532.

Zienkiewicz, Olgierd C. 2000. ≪Achievements and some unsolved problems of the finite element method≫. *International Journal for Numerical Methods in Engineering*, vol.47, n°1-3, p.9-28.

Résumé

Nous avons effectué dans ce chapitre une étude numérique des performances d'une méthode de couplage éléments finis à base d'ondes planes (conjugués ou non-conjugués) dans la résolution des problèmes bidimensionnels de diffraction acoustique où les fréquences en jeu sont relativement élevées.

Nous avons montré á travers différentes expériences numériques outre la réduction de la taille du domaine de calcul (en termes de longueur d'onde) sans perte de précision pratique, que la méthodologie proposée permet également une réduction des effets de pollution numérique. Les éléments finis conjugués à base d'ondes planes se sont avérés équivalents en termes de précision à leurs homologues non-conjugués lorsque le nombre d'ondes planes par noeud choisi est paire. Pour une précision donnée, ces deux types d'éléments conduisent à la résolution de systèmes de taille relativement réduite en comparaison avec ceux obtenus en optant pour des éléments finis quadratiques standards et ce grâce à un choix judicieux du nombre d'éléments par longueur d'onde et du nombre d'ondes planes par noeud.

CONCLUSION GÉNÉRALE

Dans cette thèse, nous nous sommes intéressés à la résolution des problèmes de diffraction acoustique hautes fréquences en milieu infini par la méthode des éléments finis. Ces problèmes sont gouvernés en régime harmonique par l'équation de Helmholtz. La perte du caractère elliptique de cette équation et sa solution fortement oscillante à mesure que le nombre d'onde augmente rend sa résolution numérique difficile à cause du nombre d'éléments finis par longueur d'onde et du problème de pollution inhérent à cette méthode. De plus, dans la pratique, le domaine de calcul est borné par l'introduction d'une frontière artificielle convexe sur laquelle est imposée des conditions absorbantes locales. Ces conditions induisent des réflexions parasites non-physiques qui affectent la précision et obligent à la placer à plusieurs longueurs d'ondes de l'obstacle ce qui aggrave la dispersion numérique. Une précision pratique n'est atteinte qu'au prix de la résolution itérative de systèmes d'équations indéfinis de plusieurs millions de degré de liberté lorsque les fréquences sont élevées ou/et l'obstacle est de forme allongée tel qu'un sous-marin.

Trois problématiques sont examinées dans cette thèse à savoir :

a. La résolution itérative du système discret de Helmholtz par une méthode de projection dans l'espace de Krylov préconditionnée par des préconditionneurs algébriques ;

b. Les conditions absorbantes locales ;

c. Et les moyens implicite et explicite pour réduire la pollution ou dispersion numérique dans les schémas MEF.

Contributions

Dans une première phase, nous proposons la résolution itérative des systèmes discrets de Helmholtz par une version complexe du solveur GMRES préconditionné avec des versions complexes de ILU0, ILUT et ILUTC. Une stagnation de ce solveur est constatée si

le nombre d'onde est élevé même si le paramètre de remplissage lfil est augmenté. Des remèdes utilisant des préconditionneurs calculés à partir de nombres d'onde moins élevés ou un lfil peu élevé sont proposés. Une autre solution pratique pour éviter la stagnation consiste à utiliser un ILUT déflaté (calculé en utilisant un nombre d'onde complexe).

Dans une deuxième phase, nous développons et validons une méthodologie originale de résolution itérative des problèmes de diffraction acoustique en milieu infini mettant en jeu des fréquences élevées et/ou des obstacles allongés tel qu'un sous-marin. La méthodologie développée est basée sur un couplage éléments finis de type Lagrange, GLS et à base d'ondes planes avec de nouvelles conditions absorbantes généralisées basées sur les approximants complexes de Padé. Sa validation est démontrée pour différents problèmes hautes fréquences de diffraction acoustique mettant en jeu différentes formes d'obstacles (notamment un sous-marin) et de frontières artificielles. La précision pratique de cette méthodologie est préservée en champ proche et en champ lointain et ce même si la frontière artificielle est placée près de l'obstacle. Ainsi, l'image radar ou sonar (section équivalente radar) peut être obtenue à faible coût. L'étude numérique menée nous a permis de fixer les paramètres optimaux caractérisant ces nouvelles conditions absorbantes de type Padé. Comparativement aux conditions généralisées d'ordre deux de Bayliss-Gunzburger-Turkel, cette condition permet pour une précision pratique donnée de réduire :

- les réflexions parasites dues à l'introduction de la frontière artificielle ;
- la taille du domaine de calcul ;
- la pollution numérique ;
- la taille des systèmes d'équations à résoudre ;
- le temps de calcul. Le coût associé à la résolution des systèmes périphériques n'est pas prohibitive.

En somme, des problèmes de fréquences plus élevées peuvent être solutionnées pour des ressources de calcul données.

Dans la méthodologie proposée, le phénomène de pollution ou de dispersion numérique est contré également explicitement via différents schémas éléments finis. Les éléments linéaires de Lagrange permettent de réduire la pollution en augmentant le nombre d'éléments par longueur d'onde. Les éléments linéaires stabilisés par GLS permettent de relaxer cette contrainte via un choix adéquat du paramètre de stabilisation τ. Une nouvelle méthode de calcul de ce paramètre est proposée et mise en œuvre. Une résolution itérative à l'aide de GMRES préconditionné par un ILUT déflaté est choisie pour solutionner les systèmes d'équations relativement larges obtenus avec ces deux schémas. Pour traiter des problèmes de diffraction où les fréquences en jeu sont plus élevées tout en réduisant la taille des systèmes d'équations à résoudre, le recours aux éléments finis quadratiques de Lagrange s'avère nécessaire. Ces éléments permettent en effet de réduire le nombre d'éléments par longueur d'onde comparativement aux éléments linéaires standards et stabilisés.

Enrichis avec des ondes planes, ces éléments quadratiques condui- sent, pour une précision pratique donnée, à des systèmes d'équations de taille encore plus réduite (comparativement aux éléments finis quadratiques de Lagrange) grâce à un choix judicieux des nombres d'éléments par longueur et d'ondes planes par nœud. Les éléments finis avec ondes planes conjuguées sont en outre équivalents à leurs homologues non-conjugués du point de vue précision lorsque le nombre de directions par noeud est pair. Par contre, les éléments conjugués sont plus précis lorsque ce nombre est impair. Des solveurs directs peuvent être utilisés dans ce cas étant donné la taille relativement réduite des systèmes d'équations à résoudre.

Cependant, dans le cas des problèmes de diffraction 3D, il est évident que le recours au solveur itératif du type ILUT-GMRES s'impose. Les méthodes directes restent chers dans ce cas en termes de mémoire et temps de calcul. La technique de résolution ILUT-GMRES est déjà adoptée à partir de la version 3.3 dans le code commercial ComsolMultiphysics®. En outre, les importants résultats du chapitre I sont cités dans plusieurs références à titre

d'exemple (Erlangga et *al.*,2004) et en particulier dans les revues de littérature récentes de Thompson (Thompson,2006) et de Harari (Harari,2006).

La validation de la méthodologie proposée en 3D est déjà amorcée par (Kechroud et *al.*,2006) et des résultats probants sont obtenus dans le cas des obstacles de formes sphéroïdales. Dans les annexes, nous rapportons quelques aspects de la mise en œuvre en 3D.

Perspectives

Comme suite à ce travail, nous proposons les axes suivants :

- Une étude numérique exhaustive de cette méthodologie pour les problèmes 3D de diffraction acoustique.
- Utilisation des techniques d'intégration et de résolution parallèles adaptées notamment lorsqu'il est question des éléments finis à base d'ondes planes ceci afin de réduire les temps de calcul et résoudre des problèmes à fréquences plus élevées.
- La résolution des problèmes inverses de diffraction 2D et 3D. Une étape importante de la résolution de ces problèmes est justement la résolution des problèmes directs correspondants.
- Et, le traitement des problèmes 3D de vibro-acoustique pour de moyennes fréquences où la méthode populaire d'analyse statistique de l'énergie n'est plus fiable .

ANNEXE A

ON THE THREE-DIMENSIONAL SCATTERING PROBLEM

A.1 The three-dimensional scattering problem

Define $\Omega^- \subset \mathbb{R}^3$ as a three-dimensional impenetrable bounded domain with boundary $\Gamma := \partial\Omega^-$. The associated homogeneous exterior domain of propagation, which is the complementary set of the scatterer Ω^- in $\mathbb{R}^3$, is denoted by Ω^e. Then, the scattering of an incident time-harmonic acoustic wavefield u^{inc} by Ω^- can be formulated as the following exterior Boundary Value Problem (BVP) find the scattered field u solution to :

$$\begin{cases} \Delta u + k^2 u = 0, \text{ in } \Omega^e, \\ \partial_{\mathbf{n}_\Gamma} u = -\partial_{\mathbf{n}_\Gamma} u^{inc} \text{ or } u = -u^{inc}, \text{on } \Gamma, \\ \lim\limits_{r\to\infty} r(\partial_r u - iku) = 0. \end{cases} \tag{A.1}$$

If $\mathbf{a}$ and $\mathbf{b}$ are two complex-valued vector fields (and $\overline{z}$ denotes the complex conjugate of a complex number $z \in \mathbb{C}$), their inner product is defined by $\mathbf{a} \cdot \mathbf{b} = \sum_{j=1}^{3} a_j \overline{b_j}$, and the associated norm $\|\cdot\|$ is $\|\mathbf{a}\|^2 = \mathbf{a} \cdot \mathbf{a}$. Let $\mathbf{x} = (x_1, x_2, x_3) \in \mathbb{R}^3$, then the gradient ∇ of a complex-valued scalar field f and the divergence div of $\mathbf{a}$ are defined respectively by $\nabla f = (\partial_{x_1} f, \partial_{x_2} f, \partial_{x_3} f)^T$ and $\text{div}\, \mathbf{a} = \sum_{j=1}^{3} \partial_{x_j} a_j$, designating by $\mathbf{a}^T$ the transposed of $\mathbf{a}$. Under these notations, the Laplace operator Δ is classically defined by $\Delta = \text{div}\, \nabla$. We consider that the incident wave u^{inc} is plane $u^{inc}(\mathbf{x}) = e^{ik\mathbf{d}\cdot\mathbf{x}}$. The wave number k is related to the wavelength λ by the relation $k = 2\pi/\lambda$. The direction of incidence $\mathbf{d}$ is given through the relation $\mathbf{d} = (\cos(\theta^{inc})\cos(\phi^{inc}), \sin(\theta^{inc})\cos(\phi^{inc}), \sin(\phi^{inc})^T$, where θ^{inc} et ϕ^{inc} are the scattering angles. If we define by $\mathbf{n}_\Gamma$ the outwardly directed unit normal to Ω^e at the boundary Γ, then, the sound-hard or Neumann (respectively sound-soft or Dirichlet) boundary condition on Γ corresponds to the second (respectively third) equation of (A.1). Finally, the last equation is the Sommerfeld radiation condition which allows only outgoing waves at infinity, setting $r = \|\mathbf{x}\|$. This thereby guarantees the uniqueness of the

solution to the BVP (A.1).

A.1.1 Bounding the domain by using a Padé-type ABC

It is well-known that the BVP (A.1) cannot be solved by usual domain based methods like the Finite Element Method (FEM) or the Finite Difference Method (FDM) if the infinite domain Ω^e is not truncated *via* a fictitious boundary Σ enclosing Ω^-. This implies that the considered domain of computation is now the one, denoted by Ω, delimited by Γ and Σ. To avoid in the best case or at least to minimize the reflection at the nonphysical boundary Σ, one must impose a suitable boundary condition at Σ. This condition takes different denominations like non-reflecting, artificial or absorbing boundary condition. Generally, this condition is given through the Dirichlet-to-Neumann (DtN) operator or an approximation of this operator. More precisely, if M is an approximation of the DtN operator, we get the following new approximate BVP with an Artificial Boundary Condition (ABC) :

$$\begin{cases} \Delta u + k^2 u = 0, \text{in } \Omega, \\ \partial_{\mathbf{n}_\Gamma} u = -\partial_{\mathbf{n}_\Gamma} u^{inc} \text{ or } u = -u^{inc}, \text{ on } \Gamma \\ \partial_{\mathbf{n}_\Sigma} u = -Mu, \text{ on } \Sigma. \end{cases} \tag{A.2}$$

For high-frequency acoustic scattering, an alternative to the BGT2-like ABC is the Padé-type ABC scattering. This condition is expressed through a square-root operator which can be efficiently computed by paraxial approximation techniques. More specifically, this operator is given by the relation :

$$\begin{aligned} -Mu = ik\sqrt{1+\frac{\Delta_\Sigma}{k^2}}u - (\mathcal{H} + \frac{i}{2k}(1+i\frac{2\mathcal{H}}{k})^{-1}(\mathcal{K}-\mathcal{H}^2) + \frac{\Delta_\Sigma}{4k^2})u \\ -\text{div}_\Sigma(\frac{1}{2ik}((\mathbb{I}+\frac{i\mathcal{R}}{k})^{-1} - \mathbb{I})\nabla_\Sigma)u. \end{aligned} \tag{A.3}$$

In this expression, Δ_Σ is the Laplace-Beltrami differential operator, $\mathcal{H}$ and $\mathcal{K}$ are respectively the mean curvature and the Gauss curvature at a point of Σ,$\mathcal{R}$ is the self-adjoint

operator that maps the tangent plane to Σ, ∇_Σ and div $_\Sigma$ are respectively the surface gradient and divergence on Σ.

The modified regularized square-root operator used in (A.3) is replaced and approximated by :

$$\sqrt{1+\text{div}_\Sigma(\frac{1}{k_\epsilon^2}\nabla_\Sigma)}u \approx C_0 u + \sum_{j=1}^{N} \frac{A_j \text{div}_\Sigma(\frac{1}{k_\epsilon^2}\nabla_\Sigma))}{1+B_j \text{div}_\Sigma(\frac{1}{k_\epsilon^2}\nabla_\Sigma)} u \tag{A.4}$$

where $k_\epsilon = k + i\epsilon$. A possible choice of the damping parameter ϵ is $\epsilon = 0.4k^{1/3}\mathcal{H}^{2/3}$. In (A.4), the complex coefficients C_0, A_j and B_j are given by :

$$\begin{aligned} C_0 &= e^{i\frac{\alpha}{2}} R_N(e^{-i\alpha}-1), \\ A_j &= \frac{e^{-\frac{i\alpha}{2}} a_j}{(1+b_j(e^{-i\alpha}-1))^2}, \\ B_j &= \frac{e^{-i\alpha} b_j}{(1+b_j(e^{-i\alpha}-1))^2}. \end{aligned} \tag{A.5}$$

The angle of rotation is α and (a_j, b_j), for $j = 1, ..., N$, are the standard real Padé coefficients given by :

$$a_j = \frac{2}{2N+1}\sin^2(\frac{j\pi}{2N+1}) \, , b_j = \cos^2(\frac{j\pi}{2N+1}), \tag{A.6}$$

denoting by R_N the Padé approximant of order N :

$$\sqrt{1+z} \approx R_N(z) = 1 + \sum_{j=1}^{N} \frac{a_j z}{1+b_j z}. \tag{A.7}$$

In view of an efficient numerical treatment, the approximation of the Padé-type ABC (A.3)-(A.7) is represented by using Lindman's auxiliary functions trick :

$$\begin{aligned} -Mu &= ik(u + \sum_{j=1}^{N} A_j \varphi_j) - (\mathcal{H} + \frac{i}{2k}(1+i\frac{2\mathcal{H}}{k})^{-1}(\mathcal{K}-\mathcal{H}^2) + \frac{\Delta_\Sigma}{4k^2})u \\ -\text{div}_\Sigma(&\frac{1}{2ik}((\mathbb{I}+\frac{i\mathcal{R}}{k})^{-1}-\mathbb{I})\nabla_\Sigma)u., \text{ on } \Sigma, \end{aligned} \tag{A.8}$$

where the functions φ_j, $j = 1, .., N$, defined on Σ, are solutions of the following differential equations :

$$(1 + B_j \text{div}_\Sigma(\frac{1}{k_\epsilon^2}\nabla_\Sigma)\varphi_j = \text{div}_\Sigma(\frac{1}{k_\epsilon^2}\nabla_\Sigma)u. \tag{A.9}$$

A.1.2 Variational formulation with Padé-type ABC

Let us introduce V as the Sobolev space $H^1(\Omega)$ for a Neumann boundary condition or $H_0^1(\Omega)$ for a Dirichlet boundary condition. Let us define the product spaces $W_N := H^1(\Sigma) \times ... \times H^1(\Sigma)$, N times, and $X_N := V \times W_N$. Under these notations, a variational formulation of (A.2) with the Padé-type ABC (A.3)-(A.7) is find $(u, \varphi_1, ..., \varphi_N)$ in X_N such that :

$$\begin{cases} \mathcal{A}(u, v) + \sum_{j=1}^{N} \mathcal{B}_j(\varphi_j, v) = b(v), \\ \mathcal{C}(u, \psi_j) + \mathcal{D}_j(\varphi_j, \psi_j) = 0, \end{cases} \tag{A.10}$$

with $j = 1, ..., N$, and for test-functions $(v, \psi_1, ..., \psi_N) \in X_N$. The symmetrical bilinear form $\mathcal{A}$ acts from $V \times V$ into $\mathbb{C}$ and is defined by :

$$\begin{aligned} \mathcal{A}(u, v) = &\int_\Omega \left\{\nabla u \cdot \nabla v - k^2 uv\right\} d\Omega - ik \int_\Sigma uv d\Sigma + \int_\Sigma \mathcal{H} uv d\Sigma \\ &+ \frac{1}{2ik} \int_\Sigma (1 + i\frac{2\mathcal{H}}{k})(\mathcal{K} - \mathcal{H}^2) uv d\Sigma - \frac{1}{4k^2} \int_\Sigma \Delta_\Sigma \mathcal{H} uv d\Sigma \\ &- \frac{1}{2ik} \int_\Sigma ((\mathbb{I} + i\frac{\mathcal{R}}{k})^{-1} - \mathbb{I}) \nabla_\Sigma u \nabla_\Sigma v d\Sigma. \end{aligned} \tag{A.11}$$

Moreover, the bilinear forms $\{\mathcal{B}\}_{j=1,...,N}$, $\mathcal{C}$ and $\{\mathcal{D}\}_{j=1,...,N}$ are defined from $H^1(\Sigma) \times H^1(\Sigma)$ into $\mathbb{C}$ by :

$$\begin{aligned} \mathcal{B}_j(\varphi_j, v) &= -ikA_j \int_\Sigma \varphi_j v d\Sigma, \\ \mathcal{C}(u, \psi_j) &= \int_\Sigma \frac{1}{k^2} \nabla_\Sigma u \nabla_\Sigma \psi_j d\Sigma, \\ \mathcal{D}_j(\varphi_j, \psi_j) &= \int_\Sigma \varphi_j \psi_j d\Sigma - B_j \int_\Sigma \frac{1}{k_\epsilon^2} \nabla_\Sigma \varphi_j \nabla_\Sigma \psi_j d\Sigma. \end{aligned} \tag{A.12}$$

The definition of the linear form b which follows from the nature of the boundary condition on Γ.

The variational formulation (A.10) is an unconjugated formulation with bilinear operators. The following alternative conjugated formulation with sesquilinear operators can be obtained if the weighting functions v and ψ_j are substituted respectively by $\overline{v}$ and $\overline{\psi_j}$:

$$\begin{cases} \mathcal{A}(u,\overline{v}) + \sum_{j=1}^{N} \mathcal{B}_j(\varphi_j,\overline{v}) = b(\overline{v}), \\ \mathcal{C}(u,\overline{\psi_j}) + \mathcal{D}_j(\varphi_j,\overline{\psi_j}) = 0, \end{cases} \tag{A.13}$$

for $j = 1, ..., N$, and $\forall (v, \psi_1, ..., \psi_N) \in X_N$.

A.2 Finite element approximation

To discretize the variational formulations, the computational domain Ω is partitioned into tetrahedral finite elements resulting in a covering Ω_h. The unknown scattered field u within each finite element can be approximated by using standard polynomial shape functions $N_j,\ j = 1, .., \#nodes$, as follows :

$$u = \sum_{j=1}^{\#nodes} N_j u_j, \tag{A.14}$$

denoting by $u_j,\ j = 1, .., \#nodes$, the nodal values of u at the interpolation points.

Another way of building interpolating finite element functions, called *plane wave finite element functions* , is to approximate the unknown field u within each tetrahedral finite element by using the standard polynomial shape functions $N_j,\ j = 1, .., \#nodes$, each function being enriched by n_q radiating plane waves $e^{ik\mathbf{d}_q\cdot(\mathbf{x}-\mathbf{x}_j)}$ centered at the j-th nodes and for n_q equally spaced directions of propagation The resulting approximation of the wavefield, solution to (A.10), is seek through the following expansion on each triangle :

$$u = \sum_{j=1}^{\#nodes} \sum_{q=1}^{n_q} N_j e^{ik\mathbf{d}_q\cdot(\mathbf{x}-\mathbf{x}_j)} u_{jq} \tag{A.15}$$

The finite element discretization of the variational problems (A.10) and (A.13) and using basis functions (A.14) or (A.15) leads to a linear system of coupled equations of the generic form :

$$\begin{pmatrix} \mathbf{A}_h & \mathbf{B}_h \\ \mathbf{C}_h & \mathbf{D}_h \end{pmatrix} \begin{pmatrix} \mathbf{u}_h \\ \boldsymbol{\varphi}_h \end{pmatrix} = \begin{pmatrix} \mathbf{b}_h \\ \mathbf{0} \end{pmatrix}. \tag{A.16}$$

The solution $(\mathbf{u}_h, \boldsymbol{\varphi}_h)$ is composed from the approximate wavefield $\mathbf{u}_h$ in $\mathbb{C}^{n_h}$, where n_h is the number of degrees of freedom of the finite element method for the covered domain Ω_h, h being the largest finite element size, and $\boldsymbol{\varphi}_h$ is in $\mathbb{C}^{Nn_{\Sigma_h}}$, designating by n_{Σ_h} the number of discretization points of the interpolated boundary $\Sigma_h := \partial\Omega_h$. We classically introduce $n_\lambda := h/\lambda$ as the density of discretization points per wavelength which is often used in scattering problems to measure the thickness of the mesh. The complex linear system (A.16) is sparse, globally non-symmetric, non-Hermitian and non-diagonally dominant. Its size is equal to #dof, where #dof designates the total number of degrees of freedom involved in the numerical solution. In the case of the unconjugated formulation, all sub-matrices $\mathbf{A}_h$, $\mathbf{B}_h$, $\mathbf{C}_h$ and $\mathbf{D}_h$ are however symmetric.

A.2.1 Implementation of the Padé non-reflecting boundary condition

We describe a numerical procedure for constructing the mass- and stiffness-like element-level matrices that arise from the above integral quantity. This procedure is applicable to any finite element discretization. We assume that the practical artificial boundary Σ is a triangulated surface. We evaluate the curvatures and the operator $\mathcal{R}$ analytically in order to minimize the effect of the error in the approximation of these quantities on the performance of the Padé-Type absorbing conditions.

The mean curvature $\mathcal{H}$ and Gauss curvature $\mathcal{K}$ at a point of the surface Σ are given by :

$$\begin{aligned} \mathcal{H} &= \frac{1}{2}(\kappa_1 + \kappa_2) \\ \mathcal{K} &= \kappa_1 \kappa_2 \end{aligned} \tag{A.17}$$

where κ_1 and κ_2 are the principal curvatures at that point of the surface. In 2D, $\mathcal{H} = \frac{\kappa_1}{2}$ and $\mathcal{K} = 0$ since $\kappa_2 = 0$

If Σ is parameterized as follows :

$$\mathbf{x} = (x(u,v), y(u,v), z(u,v)) \tag{A.18}$$

then the principal curvatures κ_1 and κ_1 can be determined by computing the eigenvalues of the matrix $\mathcal{R}$ relatively to the base $(\tau_1, \tau_2, \mathbf{n})$

$$\mathcal{R} = -\begin{pmatrix} \mathbf{x}_{,uu} & \mathbf{x}_{,uv} \\ \mathbf{x}_{,vu} & \mathbf{x}_{,vv} \end{pmatrix} \begin{pmatrix} \mathbf{x}_{,u} \cdot \mathbf{x}_{,u} & \mathbf{x}_{,u} \cdot \mathbf{x}_{,v} \\ \mathbf{x}_{,v} \cdot \mathbf{x}_{,u} & \mathbf{x}_{,v} \cdot \mathbf{x}_{,v} \end{pmatrix}^{-1} \tag{A.19}$$

where $\mathbf{n}$ is the outward unit normal at a point of the surface defined by :

$$\mathbf{n} = \frac{\mathbf{x}_{,u} \times \mathbf{x}_{,v}}{\|\mathbf{x}_{,u} \times \mathbf{x}_{,v}\|} \tag{A.20}$$

The vectors τ_1 and τ_2 are defined by :

$$\begin{aligned} \tau_1 &= \mathbf{x}_{,u} \\ \tau_2 &= \mathbf{x}_{,v} \end{aligned} \tag{A.21}$$

For a sphere of radius R, the principal curvatures are both equal to $\frac{1}{R}$, and therefore $\mathcal{H} = \frac{1}{R}$ and $\mathcal{K} = \frac{1}{R^2}$. Furthermore, the matrix $\mathcal{R} = \frac{1}{R}\mathbb{I}$. Simple expressions for $\mathcal{H}$ and $\mathcal{K}$ can also be found for other surfaces of revolution (Do Carmo,1999). If the curvatures cannot be computed analytically, they may be approximated by the method described in the reference (Haman,1993).

Each point with coordinates x,y and z belonging to a given surface finite element can represented by :

$$\begin{aligned} x &= \sum_{i=1}^{\#nodes} N_i(\xi,\eta)x_i \\ y &= \sum_{i=1}^{\#nodes} N_i(\xi,\eta)y_i \\ z &= \sum_{i=1}^{\#nodes} N_i(\xi,\eta)z_i \end{aligned} \tag{A.22}$$

where x_i, y_i and z_i (i=1,#dof)are the nodes coordinates and N_i (i=1,#dof) the corresponding shape functions.

Let us define the matrix **G** as follows :

$$\mathbf{G} = \begin{pmatrix} \mathbf{x}_{,\xi} \cdot \mathbf{x}_{,\xi} & \mathbf{x}_{,\xi} \cdot \mathbf{x}_{,\eta} \\ \mathbf{x}_{,\eta} \cdot \mathbf{x}_{,\xi} & \mathbf{x}_{,\eta} \cdot \mathbf{x}_{,\eta} \end{pmatrix} \tag{A.23}$$

Then the surface gradient of an interpolation function $\underline{N}(\xi,\eta)$ is given in the base $(\mathbf{e}_1, \mathbf{e}_2)$ by :

$$\nabla_\Sigma \underline{N} = G^{-1} \begin{pmatrix} \underline{N}_{,\xi} \\ \underline{N}_{,\eta} \end{pmatrix} \tag{A.24}$$

with the vectors $\mathbf{e}_1$ and $\mathbf{e}_2$ defined by :

$$\begin{aligned} \mathbf{e}_1 &= \mathbf{x}_{,\xi} \\ \mathbf{e}_2 &= \mathbf{x}_{,\eta} \end{aligned} \tag{A.25}$$

For 2D problems, the expression is more simpler. Indeed, the surface gradient of the interpolation function $\underline{N}(\xi)$, in the base $\mathbf{e}_1$ is given by :

$$\nabla_\Sigma \underline{N} = (\mathbf{e}_1 \cdot \mathbf{e}_1)^{-1} \underline{N}_{,\xi} \mathbf{e}_1 \tag{A.26}$$

with $\mathbf{e}_1 = \mathbf{x}(\xi)_{,\xi}$

The elementary surface mass and stiffness are then defined by :

$$\mathbf{M}_{\Sigma} = \int_{\Sigma_e} \underline{N}_i \underline{N}_j d\Sigma \tag{A.27}$$

$$\mathbf{K}_{\Sigma} = \int_{\Sigma_e} \nabla_{\Sigma} \underline{N}_i \nabla_{\Sigma} \underline{N}_j d\Sigma \tag{A.28}$$

where $\underline{N}_i, i = 1, .., \#dof$ per node and $\underline{N}_j, j = 1, .., \#dof$ per node are the interpolation functions.

The matrix of transformation from the base $(\mathbf{e}_1, \mathbf{e}_2)$ to the base (τ_1, τ_2) is given by :

$$\mathbf{P}_{(\mathbf{e}_1,\mathbf{e}_2)\to(\tau_1,\tau_2)} = \begin{pmatrix} \mathbf{e}_1 \cdot \tau_1 & \mathbf{e}_1 \cdot \tau_2 \\ \mathbf{e}_2 \cdot \tau_1 & \mathbf{e}_2 \cdot \tau_2 \end{pmatrix} \tag{A.29}$$

The elementary matrix involving the curvature operator can then be evaluated thanks to :

$$\int_{\Sigma_e} \mathbf{P}_{(\tau_1,\tau_2)\to(\mathbf{e}_1,\mathbf{e}_2)} (\mathbb{I} + i\frac{\mathcal{R}}{k})^{-1} \mathbf{P}_{(\mathbf{e}_1,\mathbf{e}_2)\to(\tau_1,\tau_2)} \nabla_{\Sigma} \underline{N}_i \nabla_{\Sigma} \underline{N}_j d\Sigma \tag{A.30}$$

A.3 Numerical study

Based on the numerical experiments presented by Kechroud *et al.* in (Kechroud et *al.*,2005), we set the parameters of the Padé-type ABC to $N = 2$ and $\theta = \pi/6$. The ABC location is measured by a parameter m which is the distance in terms of wavelengths between the boundary Γ_h of the scatterer Ω_h and the fictitious boundary Σ_h.

To measure the accuracy of the different finite element methods and formulations, we compute the relative Root-Mean Square (RMS) error (in percents %) between the reference solution and the approximate solution onto the computational domain Ω_h (respectively, Γ_h) in the $L^2(\Omega_h)$-norm (respectively, $L^2(\Gamma_h)$-norm). The reference solution is computed analytically.

The sphere

The first test-case is the scattering problem of a plane wave of incidence $\mathbf{d} = (0, 0, 1)^T$ by a circular cylinder of radius $a = 1$. The artificial bounday is placed at a distance $b = a + m\lambda$. The results reported in table A.1 show that the Padé-type ABCs leads to a better accuracy in comparaison with the BGT-2 ABCS even when the artificial boundary is close to the scatterer.

Table A.1

Sphere : RMS error for different mesh resolutions of the linear FEM with BGT2 and Padé-Type ABC positions.

n_λ	m	BGT2 in Ω	BGT2 on Γ	Padé in Ω	Padé on Γ	# nodes in Ω	# elements in Ω	# elements on Γ	# nodes on Γ
5		37.28	37.68	25.65	26.01	3131	10383	2824	1414
10	1/63.6	37.28	37.68	12.96	13.05	9845	30025	9760	4882
15		37.28	37.68	10.67	10.87	20116	61328	20216	10110
5		15.26	16.12	17.25	18.76	2708	8225	2856	1430
10	0.125	15.26	16.12	8.02	8.63	13021	50137	10088	5046
15		14.96	15.44	6.50	6.05	34684	147695	21512	10758
5		18.24	16.91	15.04	17.04	3813	14195	3256	1630
10	0.25	10.25	9.98	4.15	5.10	21038	94569	11504	5754
15		8.96	9.40	3.10	3.78	63784	313602	24664	12334
5		19.63	21.84	17.77	19.93	6705	28670	4480	2240
10	0.5	7.60	8.37	5.25	5.29	43269	218914	15496	7750
15		5.23	5.84	2.68	2.44	136164	727325	32904	16454

ANNEXE B

POIDS ET POINTS D'INTÉGRATION

B.1 Points et poids d'intégration de Gauss en 1D

B.1.1 Abscisses des points d'intégration de Gauss en 1D

La formule de Rodriguez permet de retrouver les polynômes de Legendre d'ordre $n \geq 1$:

$$P_n(\xi) = \frac{1}{(2n)n!}\frac{d^n(\xi^2-1)^n}{dn} \tag{B.1}$$

A titre d'exemple, les polynômes de Legendre correspondant à n=0,1,...,4 sont donnés par :

$$\begin{aligned} P_0(\xi) &= 1 \\ P_1(\xi) &= \xi \\ P_2(\xi) &= \xi^2 - \frac{1}{3} \\ P_3(\xi) &= \xi^3 - \frac{3}{5}\xi \\ P_4(\xi) &= \xi^4 - \frac{6}{7}\xi^2 + \frac{3}{35} \end{aligned} \tag{B.2}$$

Les n abscisses $(\xi_1, ..., \xi_n)$ des points de Gauss dans l'intervalle [-1,1] sont les racines du polynôme de Legendre de degré $n \geq 1$ et sont donc les n solutions de l'équation :

$$P_n(\xi) = 0 \tag{B.3}$$

À titre d'exemple, pour n=1, il y a qu'un seul point dont l'abscisse correspond à $\xi_1 = 0$ et pour n=2, il y a deux points dont les abscisses correspondent repectivement à $\xi_1 = -\frac{\sqrt{3}}{3}$

et $\xi_1 = \frac{\sqrt{3}}{3}$

B.1.2 Poids des points d'intégration de Gauss en 1D

Si $(\xi_1, ..., \xi_n)$ sont les racines du polynôme de Legendre de degré n, alors les poids des points de Gauss $(w_1, ..., w_n)$ sont définis par :

$$w_i = \int_{-1}^{1} \prod_{j=1, j\neq i}^{n} \frac{x - \xi_j}{\xi_i - \xi_j} \mathrm{dx} \tag{B.4}$$

Ainsi, pour n=1, le poids du point de Gauss d'abscisse $\xi_1 = 0$ est $w_1 = 2$ alors que pour n=2, les poids des deux points de Gauss d'abscisses $\xi_1 = -\frac{\sqrt{3}}{3}$ et $\xi_1 = \frac{\sqrt{3}}{3}$ sont égaux à $w_1 = w_1 = 1$.

Pour générer les points et les poids correspondants à $n = 27$, nous avons utilisé le programme Matlab ≪Multi-Dimensional Gauss Points and Weights≫ développé par Brent Lewis. Ce programme est disponible à l'adresse web suivante
http ://www.mathworks.com/matlabcentral/fileexchange/ loadCategory.do ?objectType= categoryobjectId=16objectName=integration

B.2 Points et Poids d'intégration de Gauss en 2D

Nous faisons appel à la méthode ≪produit≫ qui consiste à utiliser dans chaque direction ξ et η une intégration à une dimension. Encore une fois, le programme Matalab de Brent Lewis est utilisé pour générer les poids et les coordonnées des points de Gauss pour un élément de référence carré définie par $-1 \leq \xi \leq 1$ et $-1 \leq \eta \leq 1$.

À partir des points et des poids de Gauss générés sur un élément de référence carré, nous générons les points et poids de Gauss pour un élément de référence triangulaire en utili-

sant les transformations géométriques de Gauss-Radau qui transforme les points (ξ, η) de l'élément carré en les points $(\overline{\xi}, \overline{\eta})$ de l'élément triangulaire :

$$\begin{aligned} \overline{\xi} &= \frac{1+\xi}{2} \\ \overline{\eta} &= \frac{1-\xi}{2}\frac{1+\eta}{2} \end{aligned} \tag{B.5}$$

avec $0 \leq \overline{\xi} \leq 1, 0 \leq \overline{\eta}) \leq (1 - \overline{\xi})$

Les poids correspondant aux points de Gauss avec $(\overline{\xi}, \overline{\eta})$ peuvent être calculés grâce à :

$$\overline{w} = \frac{w}{2}\frac{1-\xi}{2} \tag{B.6}$$

B.3 Points et poids d'intégration de Gauss en 3D

Une démarche similaire à celle en 2D peut être utilisé en 3D. Ainsi, dans chaque direction ξ, η et ζ une intégration à une dimension est utlisée. Le programme Matlab de Brent Lewis est utilisé pour générer les poids et les coordonnées des points de Gauss pour un élémenet de référence cubique défini par $-1 \leq \xi \leq 1$, $-1 \leq \eta \leq 1$ et $-1 \leq \zeta \leq 1$. À partir des points et des poids de Gauss générés sur un élément de référence cubique, sont générés les points et les poids de Gauss pour un élément de référence tétrahédrique en utilisant les transformations géométriques qui transforme les points (ξ, η, ζ) de l'élément cubique en les points $(\overline{\xi}, \overline{\eta}, \overline{\zeta})$ de l'élément tétrahédrique :

$$\begin{aligned} \overline{\xi} &= \frac{1+\xi}{2} \\ \overline{\eta} &= \frac{1-\xi}{2}\frac{1+\eta}{2} \\ \overline{\zeta} &= \frac{1-\xi}{2}\frac{1-\zeta}{2} \end{aligned} \tag{B.7}$$

avec $0 \leq \overline{\xi} \leq 1, 0 \leq \overline{\eta} \leq (1 - \overline{\xi}, 0 \leq \overline{\zeta} \leq (1 - \overline{\xi} - \overline{\eta})$

Les poids correspondants aux points de Gauss $(\overline{\xi}, \overline{\eta}, \overline{\zeta})$ peuvent être calculés grâce à :

$$\overline{w} = \frac{w}{2}\frac{1-\xi}{2}\frac{1-\eta}{2} \tag{B.8}$$

ANNEXE C

MÉTHODE GMRES ET SES PRÉCONDITIONNEURS

C.1 Méthode GMRES pour systèmes à nombres complexes

Pour la résolution des systèmes d'équations, nous avons utlisé une version double précision pour systemes d'équations à nombres complexes de la méthode GMRES. Le programme en language fortran est disponible à l'adresse web suivante
http ://www.ann.jussieu.fr/ koutchmy/spectrales/doc/syslin.html

C.2 Préconditionneurs algébriques ILU0, ILUT et ILUTC

Les préconditionneurs ILU0, ILUT et ILUTC font partie de la librairie SPARSKIT développée par Youcef Saad. Celle-ci est disponible à l'adresse web suivante
http ://www-users.cs.umn.edu/ saad/software/SPARSKIT/sparskit.html

Ces préconditionneurs développées pour les systemes d'équations à nombres réels ont été modifiés pour prendre en charge des systèmes à nombres complexes.

C.3 Préconditionneurs déflatés

La discrétisation de l'équation de Helmholtz $\Delta u + k^2 u = 0$ par la méthode des éléments finis conduit à un systeme matricielle du type $(\mathbf{A})\{\mathbf{u}\} = \{\mathbf{b}\}$ avec $(\mathbf{A}) = (\mathbf{R}) - k^2(\mathbf{M})$ où $\mathbf{R}$ est la matrice rigidité et $\mathbf{M}$ la matrice masse. Les préconditionneurs algébriques ILU, ILU0 et ILUTC sont construits à partir de la matrice $\mathbf{A}$ alors que les préconditionneurs déflatés sont construits à partir de la matrice $\mathbf{R} - \alpha k_2 \mathbf{M}$ avec α un nombre complexe de déflation que nous déterminons par expérimentation numérique. Dans la pratique, nous avons opté pour $\alpha = \sqrt{2}/2(1+i)$ où i est le nombre complexe défini par $i^2 = -1$. Les auteurs (Erlangga et *al.*,2004) proposent un coefficient optimal $\alpha = 1 - i0.5$.

BIBLIOGRAPHIE GÉNÉRALE

Antoine, Xavier, Barucq Hélène, et Bendali Abderrahmane. 1999. ≪Bayliss-Turkel like radiation condition on surfaces of arbitrary shape≫. *Journal of Mathematical Analysis and Applications*, vol.229, n°3, p.184-211.

Antoine, Xavier. 2001. ≪Fast Approximate computation of a time-harmonic scattered field using the on-surface radiation condition method≫. *Institute of Mathematics and its Applications (IMA) : Journal of Applied Mathematics*, vol.66, n°1, p.83-110.

Antoine, Xavier. 2002. ≪An Algorithm Coupling the OSRC and FEM for the Computation of an Approximate Scattered Acoustic Field by a Non-convex Body≫.*International Journal for Numerical Methods in Engineering*,vol.54, n°7, p.1021-1041.

Antoine, Xavier et Darbas Marion. 2005. ≪Alternative Integral Equations for the Iterative Solution of Acoustic Scattering Problems≫.*Quaterly Journal of Mechanics and Applied Mathematics*, vol.58, n°1, p.107-128.

Antoine, Xavier, Darbas Marion et Lu Ya Yan. 2005. ≪An improved On-Surface Radiation Condition for acoustic scattering in the high-frequency spectrum≫. *Comptes Rendus de l'Academie des Sciences. Serie I, Mathematique*, vol.340, n°10, (Mai), p. 769-774.

Antoine, Xavier, Darbas Marion et Lu Ya Yan. 2006. ≪An Improved Surface Radiation Condition for High-Frequency Acoustic Scattering Problems≫. *Computer Methods in Applied Mechanics and Engineering*, vol.195, n°33-36, (Juillet), p.4060-4074.

Antoine, Xavier. 2007. ≪Advances in the On-Surface Radiation Condition Method : Theory, Numerics and Applications≫. In *Computational Methods in Acoustics*, Saxe-Coburg, pp. 169-194. (to appear)

Astley, R.J. 2000. ≪Infinite element for wave problems : a review of current formulations and an assessment of accuracy≫. *International Journal for Numerical Methods in Engineering*, vol.49, n°7, p.951-976.

Bendali, Abderrahmane et Fares M'Barek. 2007. *Boundary Integral Equations in Acoustic Scattering*. Coll. ≪ Rapport interne du Laboratoire MIP≫, Internal Report 07-05, Toulouse (France), Laboratoire de Mathématiques pour l'Industrie et la Physique, 33 p.

Babuška, Ivo, Sauter Stefan A. 1997. ≪Is the pollution effect of the FEM avoidable for the Helmholtz equation considering high wave numbers≫. *Society for Industrial and Applied Mathematics : Journal of Numerical Analysis*, vol.34, n°6, (Décembre), p.2392-2423.

Bayliss, Alvin et Turkel Eli. 1980. ≪Radiation boundary conditions for wave-like equations≫. *Communications on Pure and Applied Mathematics*, vol.33, n°6, p.707-725.

Bayliss, Alvin, Gunzburger Max et Turkel Eli. 1982. ≪Boundary conditions for the numerical solution of elliptic equations in exterior regions≫. *Society for Industrial and Applied Mathematics : Journal of Applied Mathematics*, vol.42, n°2, p.430-451.

Bérenger, Jean-Pierre. 1994. ≪A perfectly matched layer for the absorption of electromagneticwaves≫. *Journal of Computational Physics*, vol.114, n°2, (Octobre), p.185-200.

Bettess, Peter, Shirron Joseph, Laghrouche Omar, Peseux Bernard, Sugimoto Rie et Trevelyan John. 2003. ≪A numerical integration scheme for special finite elements for the Helmholtz equation≫. *International Journal for Numerical Methods in Engineering*, vol.56, n°4, p. 531-552.

Bowman, John J., Senior Thomas B.A. et Uslenghi Piergiorgio L.E. 1969. *Electromagnetic and acoustic scattering by simple shape*, 1st ed. Amsterdam, The Netherlands : North-Holland Publishing Co. 728p.

Bruno, Oscar P. et Kunyansky Leonid A. 2001.≪Surface scattering in three dimensions : an accelerated high-order solver≫.*Royal Society of London Proceedings Series A. Proceedings : Mathematical, Physical and Engineering Sciences*, vol.457, Vol.457, n°2016, (Decembre), p.2921-2934.

Bruno, Oscar P. et Kunyansky Leonid A. 2001. ≪A fast, high-order algorithm for the solution of surface scattering problems : basic implementation, tests, and applications≫. *Journal of Computational Physics*. vol.169, n°1, p.80-110.

Bruno, Oscar P. 2007. ≪New high-order integral methods in computational electromagnetism≫. *Computer Modeling in Engineering & Sciences*, vol.5, n°4, p.319-330.

Burton, A.J. et Miller G.F. 1971. ≪The application of integral equation methods to the numerical solution of some exterior boundary-Value problems≫. *Proceedings of the Royal Society of London. Series A, Mathematical and Physical Sciences*, vol.323 , n°1553, A Discussion on Numerical Analysis of Partial Differential Equations, (Juin), p. 201-220.

Chew, Weng Cho, Jin Jiang-Ming, Michielssen Eric et Song Jiming. 2001. *Fast and Efficient Algorithms in Computational Electromagnetics*. 1st ed. Norwood : Artech House Antennas and Propagation Library, 993 p.

Colton, David et Kress Rainer. 1983. *Integral Equation Methods in Scattering Theory*. 1st ed. ≪Pure and Applied Mathematics≫. New York, USA : John Wiley and Sons Inc., 286p.

Colton, David et Kress Rainer. 1992. *Inverse acoustic in electromagnetic scattering theory*. 2nd ed. ≪Applied Mathematics Sciences≫. vol.93, Berlin, Germany : Springer, 305 p.

Darbas, Marion. 2004.≪Préconditionneurs analytiques de type Caldéron pour les formulations intégrales des problèmes de diffraction d'ondes≫. Thèse de doctorat en mathématiques appliquées, Toulouse (France), Instiut national des sciences appliquées, Université Paul Sabatier, 253 p.

Darve, Eric. 2000. ≪The fast multipole method : numerical implementation≫. *Journal of Computational Physics*, vol.160,, n°1, p.195-240.

Djellouli, Rabia, Farhat Charbel, Macedo Antonini et Tezaur Radek. 2000. ≪Finite element solution of two-dimensional acoustic scattering problems using arbitrarily shaped convex artificial boundaries≫. *Journal of Computational Acoustics*, vol.8, n°1, (Mars), p.81-99.

Djellouli, Rabia, Farhat Charbel, et Tezaur Radek. 2001. ≪A fast method for solving acoustic scattering problems in frequency bands≫. *Journal of Computational Physics*, vol.168, n°2,(Avril), p.412-432.

Do Carmo, M.P. 1976. *Differential Geometry of Curves and Surfaces*. 1st ed. Englewood CliLs. New Jersey : Prentice-Hall. 503p.

Elman, H.C. et O'Leary D.P. 1998. ≪Efficient iterative solution of the three-dimensional Helmholtz equation≫. *Journal of Computational Physics*, vol.142, n°,p.163-181.

Enquist, Bjorn et Majda Andrew. 1977. ≪Absorbing boundary conditions for the numerical simulation of waves≫. *Mathematics of Computation*, vol.31, n°139, (Juillet), p.629-651.

Erlangga, Y.A., Vuik C., et Oosterlee C.W. 2004. ≪On a class of preconditioners for solving the Helmholtz equation≫. *Applied Numerical Mathematics*, vol.50, n°3-4, pp.409-425.

Farhat, Charbel, Radek Tezaur et Rabia Djellouli. 2002. ≪On the solution of three-dimensional inverse obstacle acoustic scattering problems by a regularized Newton method≫. *Inverse Problems*, vol.18, n°5, p.1229-1246.

Farhat, Charbel and Hetmaniuk Ulrich. 2002.≪A fictitious domain decomposition method for the solution of partially axisymmetric acoustic scattering problems. Part I : Dirichlet boundary conditions acoustic scattering problems≫. *International Journal for Numerical Methods in Engineering*, vol.54 (2002), n°9, p.1309-1332.

Gander, Martin J. and Nataf Frédéric. 2001. ≪AILU for Helmholtz problems : A new preconditioner based on the analytic parabolic factorization ≫. *Journal of Computational Acoustics*, vol.9, n°4, pp. 1499-1509.

Gary, Cohen C. 2002. *Higher-order Numerical Methods for transient wave equations*. ≪Scientific Computation≫.1st ed. Berlin, Germany : Springer-Verlag, 348 p.

Gerdes, Klaus. 2000. ≪A review of infinite element methods for exterior Helmholtz problems≫. *Journal of Computational Acoustics*, vol.8, n°1, (Mars), p. 43-62.

Gillman, Adrianna. 2006. ≪On the numerical performance of a mixed-hybrid type solution methodology for solving high-frequency Helmholtz problems≫. Thèse de Maitrise en sciences mathématiques, Northridge (Californie), Université de l'état de Californie, 41 p.

Gillman, Adrianna, Djellouli Rabia and Amara Mohamed. 2007. ≪A mixed hybrid formulation based on oscillated finite element polynomials for solving Helmholtz problems≫. *Journal of Computational and Applied Mathematics*, vol.204, n°2, (Juillet) , p.515-525.

Givoli,Dan. 1999. ≪Exact representation on artificial interfaces and applications in mechanics≫.*Applied Mechanics Reviews*, vol.52, n°9, p.333-349.

Givoli,Dan. 2004. ≪High-order local non-reflecting boundary conditions : a review≫.*Wave Motion*, vol.39, p.319-326.

Guddati, Murty N. and Tassoulas John L. 2000.≪Continued-fraction absorbing boundary conditions for the wave equation≫. *Journal of Computational Acoustics*, vol.8, n°1, p.139-156.

Guddati, Murthy N. and Lim Keng-Wit. 2005. ≪Continued fraction absorbing boundary conditions for convex polygonal domains≫. *International Journal for Numerical Methods in Engineering*, vol.66, n°6 , p.949-977.

Hagstrom, Thomas. 1999. ≪Radiation boundary conditions for the numerical simulation of waves≫. *Acta Numerica*, p.47-106.

Hamann, B. 1993. ≪Curvature approximation for triangulated surfaces≫. *Computing Supplement*. vol.8. p. 139-153.

Harari, Isaac. 1991. ≪ Computational methods for problems of acoustics with particular reference to exterior domains≫. Thèse de doctorat, Stanford (États-Unis) Université de Stanford, 216 p.

Harari, Isaac and Hughes Thomas J.R. 1992. ≪A cost comparison of boundary element and finite element methods for problems of time-harmonic acoustics≫. *Computer Methods in Applied Mechanics and Engineering*, vol.97, n°1,(Mars), p. 77-102.

Harari, Isaac and Turkel Eli. 1995. ≪Accurate finite difference methods for time-harmonic wave propagation≫. *Journal of Computational physics*, vol.119, n°2, p.252-270.

Harrari, Isaac, Grosch Karl, Hughes Thomas J.R., Malhotra Manish, Pinsky Peter M., Stewart Jean R., and Thompson Lonny L. 1996. ≪Recent developpments in finite element methods for structural acoustics≫. *Archives of Computional Methods in Engineering*, vol.3, n°2-3, p.131-109.

Harari, Isaac and Nogueira Carnot L. 2002. ≪Reducing dispersion of linear triangular elements for the Helmholtz equation≫. *Journal of Engineering Mechanics*, vol.128, n°3, (Mars), p. 351-358.

Harari, Isaac and Magoulès Frédéric. 2004. ≪Numerical investigations of stabilized finite element computations for acoustics≫. *Wave Motion*, vol.39, n°4, p. 339-349. (2004).

Harari, Isaac and Djellouli Rabia. 2004. ≪Analytical study of the effect of wave number on the performance of local absorbing boundary conditions for acoustic scattering≫. *Applied Numerical Mathematics*, vol.50, n°4, (Juillet), p.15-47.

Harari, Isaac. 2006. ≪A survey of finite element methods for time-harmonic acoustics Computer Methods in Applied Mechanics and Engineering≫. *Computer Methods in Applied Mechanics and Engineering*, vol. 195, n°13-16, (Fevrier), p. 1594-1607.

Hetmaniuk, Ulrich and Farhat Charbel. 2003. ≪A fictitious domain decomposition method for the solution of partially axisymmetric acoustic scattering problems. Part 2 : Neumann boundary conditions≫. *International Journal for Numerical Methods in Engineering*, vol.58, n°1, p.63-81.

Ihlenburg, Franck and Babuška Ivo. 1995. ≪Finite element solution of the helmholtz equation with high wavenumber Part I : the h-version of the fem.≫. *Computers and Mathematics with Applications*, vol.30, n°9, (Novembre), p.9-37.

Ihlenburg, Franck and Babuška Ivo. 1997. ≪Finite element solution of the Helmholtz equation with high wave Number Part II : The h-p Version of the FEM.≫. *Society for Industrial and Applied Mathematics : Journal on Numerical Analysis*, vol.34, n°1, p.315-358.

Ihlenburg, Franck, 1998. *Finite Element Analysis of Acoustic Scattering*. 1st ed. Coll. ≪Applied Mathematical Sciences≫, vol.132. New York : Springer-Verlag New York, Inc., 224 p.

Karniadakis, George EM and Sherwin Spencer J. 1999. *Spectral/hp elemrnt mthods for CFD*. ≪Numerical Mathematics and Scientific Computation≫. 1st ed. New York, USA : Oxford university Press, 390 p.

Kechroud, Riyad, Soulaïmani Azzeddine, Saad Yousef and Gowda Shivaraju. 2004. ≪Preconditioning techniques for the solution of the Helmholtz equation by the finite element method≫. *Mathematics and Computer in Simulation*, vol.65, n°4-5, p.303-321.

Kechroud, Riyad, Antoine Xavier and Soulaïmani Azzeddine. 2005. ≪Numerical accuracy of a Padé-type non-reflecting boundary condition for the finite element solution of acoustic scattering problems at high-frequency≫. *International Journal for Numerical Methods in Engineering*, vol.64, n°10, p.1275-1302.

Kechroud, Riyad, Soulaïmani Azzeddine, Antoine Xavier. 2006. ≪Padé absorbing boundary conditions for finite element solution of high frequency scattering problems≫. In *IEEE International Symposium on Industrial Electronics, ISIE 2006*.(Montréal, Juillet 9-12 2006), p.2626-2630. Montréal : IEEE.

Keller, Joseph B. and Givoli Dan. 1989. ≪Exact non reflecting boundary conditions≫. *Journal of Computational Physics*, vol.82, n°1, (Mai), p.172-192.

Kirkup, Stephen. 1998. The Boundary Element Method in Acoustics : A Development in Fortran. Coll. ≪Integral Equation Methods in Engineering≪. nouvelle ed. Hebden Bridge : Integrated Sound Software, 158 p. The code is available at : http ://www.boundary-element-method.com/.

Kriegsmann, Gregory A., Taflove Allen and Umashankar Korada R. 1987. ≪A new formulation of electromagnetic wave scattering using the on-surface radiation condition method≫. *Institute of Electrical and Electronics Engineers : Transactions on Antennas and Propagation*, vol.35, n°2, p.153-161.

Laghrouche, Omar, Bettess Peter. 2002. ≪ Short wave modelling using special finite elements≫. *Journal of Computational Physics*, vol.8, n°1, (Mars), p.189-210.

Laghrouche, Omar, Bettess Peter, Astley R. J. ≪Modelling of short wave diffraction problems using approximating systems of plane waves≫. *International Jourani of Numerical Methods in Engineering*, vol.54, n°54, p.1501-1533.

Li, Na, Saad Youcef and Chow Edmond. 2002. *Crout versions of ILU for general sparse matrices*. Coll. ≪Minnesota Supercomputer Institute Technical Report≫, UMSI-2002-021, Minneapolis (MN) : University of Minnesota, Minneapolis, 17p.

Lindmann, E.F., 1985. ≪Free-space boundary conditions for the time dependent wave equation≫. *Journal of Computational Physics*, vol.18, p.16-78.

Leigh, Little Yousef Saad and Laurent Smoch. 2003. ≪Block LU preconditioners for symmetric and nonsymmetric saddle point problems≪. *Society for Industrial and Applied Mathematics : Journal of Scientifique Computing*, vol.25, n°2, p.729-748.

Mardochée, Magolu M.M. 2001. ≪Incomplete factorization based preconditionings for solving the helmholtz equation≫. *International Journal for Numerical Methods in Engineering* , vol.50, n°5, p.1077-1101.

Mehdizadeh, Omid Z. and Paraschivoiu Marius. 2003. ≪Investigation of a two-dimensional spectral element method for Helmholtz's equation≫. *Journal of Computational Physics*, vol.189, n°1, (Juillet), p.111-129.

Milinazzo, Fausto A., Zala Cedric A., Brooke Gary H. 1997. ≪Rational square-root approximations for parabolic equation algorithms≫. *The Journal of the Acoustical Society of America*, vol.101, n°2, p.760-766.

Mittra, R., Ramahi 0., Khebir A., Gordon R. and Kouki A. 1989. ≪A review of absorbing boundary conditions for two and three-dimensional electomagnetic scattering problems ≫. *Institute of Electrical and Electronics Engineers : Transactions on Magnetics*, vol.25, n°4, p.3034-3039.

Molinet, Frédéric, Andronov Ivan V. and Bouche Daniel. 2005. *Asymptotic and Hybrid Methods in Electromagnetics*. 1st ed. Coll. ≪IEE Electromagnetic Waves Series≫. London (England) :The Institution of Electrical Engineers, 249p.

Nédélec, Jean-Claude. 2001. *Acoustic and Electromagnetic Equations, Integral Representations for Harmonic Problems*. Coll. ≪Applied Mathematical Sciences≫, vol.144, New York : Springer-Verlag, Inc., 318 p.

Oberai, A. Assad and Pinsky M. Peter. 2000. ≪A numerical comparaison of finite element methods for the helmholtz equation≫. *Journal of Computational Acoustics*, vol.8, n°1, p.211-221.

Ortiz, P. and E. Sanchez. 2001. ≪An improved partition of unity finite element model for diffraction problems≫. *International Journal of Numerical Methods in Engineering*, vol.50, n°12, p.2727-2740. Volume 50,

Rokhlin, V. *Rapid solution of integral equations of scattering theory in two dimensions*. ≪Journal of Computational Physics≫, vol.86, n°12, (Fevrier), p.414-439.

Saad, Yousef and Schultz Martin H. 1986. ≪GMRES : A Generalized minimal residual algorithm for solving nonsymmetric linear aystems ≫. *Society for Industrial and Applied Mathematics : Journal on Scientific and Statistical Computing*, vol.7, n°3, p.856-869.

Saad,Yousef. 1994. ≪ILUT : a dual threshold incomplete ILU factorization≫.*Numerical Linear Algebra with Applications*, vol.1, n°4 , p.387-402.

Saad, Yousef. 1996. *Iterative Methods for Sparse Linear Systems*. 1st ed. Boston, USA : PWS Publishing Co., 447 p.

Schenck, Harry A. 1968. ≪Improved integral formulation for acoustic radiation problems≫. *The Journal of the Acoustical Society of America*, vol.44, n°1, p.41-58.

Shirron, Joseph J. and Babuška Ivo. 1998. ≪A comparison of approximate boundary conditions and infinite element methods for exterior Helmholtz problems≫. *Computer Methods in Applied Mechanics and Engineering*, vol.164, n°1-2, (October), p.121-139.

Taylor, Michael E. 1981. *Pseudodifferential Operators*. 1st ed. Princeton, NJ : Princeton University Press. 451 p.

Tezaur, Radek, Macedo Antonini, Farhat Charbel and Djellouli Rabia. 2000. ≪Three dimensional finite element calculations in acoustic scattering using arbitrarily shaped convex artificial boundaries≫. *International Journal for Numerical Methods in Engineering*, vol.53, n°3, p.1461-1476.

Turkel, Eli. 1998. ≪Absorbing PML boundary layers for wave-like equations≫. *Applied Numerical Mathematics*, vol.27, n°4, (Août), p.533-557.

Turkel, Eli. 2007.*Boundary Conditions and Iterative Schemes for the Helmholtz Equation in Unbounded Regions*. In *Computational Methods in Acoustics*,Saxe-Coburg Editors. (to appear)

Thompson, Lonny L., Ianculescu Cristian and Huan R. 2000. ≪Exact radiation conditions on spheroidal boundaries with sparse iterative methods for efficient computation of exterior acoustics≫. In *Seventh International Congress on Sound and Vibration*. (Garmisch-Partenkirchen, Germany 4-7 July 2000),p.2101-2108, Berlin : Springer.

Thompson, Lonny L., Huan R. and He D. 2001. ≪Accurate radiation boundary conditions for the two-dimensional wave equation on unbounded domains≫. *Computer Methods in Applied Mechanics and Engineering*, vol. 191, n°3, (Novembre), p.311-351.

Thompson, Lonny L. 2006. ≪A review of finite element methods for time-harmonic acoustics≫. *Journal of the Acoustical Society of America*, vol.119, n°3, p.1315-1330.

Tsynkov, Simon V. 1998. ≪Numerical solution of problems on unbounded domains. A review≪. *Applied Numerical Mathematics*, vol.27, n°4, (Août) p.465-532.

Vacus, Olivier. 2005. ≪Mathematical analysis of absorbing boundary conditions for the wave equation : the corner problem≫. *Mathematics of Computation*, vol.74, n°249, p.177-200.

Zebic, Anabelle. 1992. *Equation de helmholtz : étude numérique de quelques preconditionneurs pour la méthode gmres*. Coll. ≪Rapport Technique de l'INRIA≫, RR-1802, Rocquencourt (France) : Institut National de Recherche en Infoormatique and en Automatique, 66p.

Zienkiewicz, Olgierd C. 2000. ≪Achievements and some unsolved problems of the finite element method≫. *International Journal for Numerical Methods in Engineering*, vol.47, n°1-3, p.9-28.